DDC
Copy

①

84 05 01 075

AN EVALUATION OF THE MODIFIED SACHS
AND LEDSHAM-PIKE SCALING OF A
NUCLEAR AIR BLAST

DISSERTATION

DS/PH/83-1   Michael L. Crawford
                Captain   USAF

DTIC
ELECTE
SELECTED
MAY 1 1984
A

REPORT DOCUMENTATION PAGE

READ INSTRUCTIONS
BEFORE COMPLETING FORM

1. REPORT NUMBER	2. GOVT ACCESSION NO.	3. RECIPIENT'S CATALOG NUMBER
DS/PH/83-1	AD-A140653	

4. TITLE (and Subtitle)	5. TYPE OF REPORT & PERIOD COVERED
AN EVALUATION OF THE MODIFIED SACHS AND LEDSHAM-PIKE SCALING OF A NUCLEAR AIR BLAST	PhD Dissertation
	6. PERFORMING ORG. REPORT NUMBER

7. AUTHOR(s)	8. CONTRACT OR GRANT NUMBER(s)
MICHAEL L. CRAWFORD	

9. PERFORMING ORGANIZATION NAME AND ADDRESS	10. PROGRAM ELEMENT, PROJECT, TASK AREA & WORK UNIT NUMBERS
Air Force Institute of Technology Wright-Patterson Air Force Base, OH 45433	

11. CONTROLLING OFFICE NAME AND ADDRESS	12. REPORT DATE
	Jan 83
	13. NUMBER OF PAGES
	131

14. MONITORING AGENCY NAME & ADDRESS(if different from Controlling Office)	15. SECURITY CLASS. (of this report)
	UNCLASSIFIED
	15a. DECLASSIFICATION DOWNGRADING SCHEDULE

16. DISTRIBUTION STATEMENT (of this Report)

APPROVED FOR PUBLIC RELEASE, DISTRIBUTION UNLIMITED

17. DISTRIBUTION STATEMENT (of the abstract entered in Block 20, if different from Report)

18. SUPPLEMENTARY NOTES

Approved for public release: IAW AFR 190-17.

LYNN E. WOLAVER
Dean for Research and Professional Development
Air Force Institute of Technology (ATC)
Wright-Patterson AFB OH 45433

9 SEP 1983

19. KEY WORDS (Continue on reverse side if necessary and identify by block number)

NUCLEAR AIR BLAST
FINITE DIFFERENCE METHODS
SHOCK DYNAMICS
OVERPRESSURE
SCALING

20. ABSTRACT (Continue on reverse side if necessary and identify by block number)

The accuracy of modified Sachs and Ledsham-Pike scaling of peak shock hydrodynamic variables from a nuclear burst in air is evaluated. The modified Sachs shock positions, dynamic pressures, and overpressures and the Ledsham-Pike overpressures are compared to a fully two dimensional flux-corrected transport finite difference solution. Modified Sachs and Ledsham-Pike overpressures are found to be essentially identical, and their values compare with the numerical results more favorably in the ascending directions than in the descending directions.
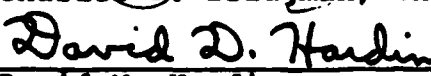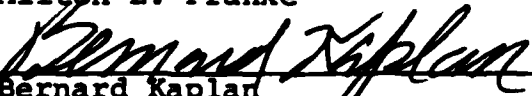
DD FORM 1473 1 JAN 73   EDITION OF 1 NOV 65 IS OBSOLETE

DS/PH/83-1

AN EVALUATION OF THE MODIFIED SACHS

AND LEDSHAM-PIKE SCALING OF A

NUCLEAR AIR BLAST

by

Michael L. Crawford
Captain   USAF

Approved:

Charles J Bridgman   24 May 83
Charles J. Bridgman, Chairman

David D. Hardin   4/14/83
David M. Hardin

George H Nickel   4/21/83
George H. Nickel

Milton E Franke   31 May, 83
Milton E. Franke

Bernard Kaplan   24 May 83
Bernard Kaplan

Michael R. Stamm   3 JUNE '83
Michael R. Stamm

Accepted:

J S Przemieniecki   6 June 1983
J. S. Przemieniecki, Dean
School of Engineering

Acknowledgements

Although the work presented here is the result of my research alone (and I alone must take full responsibility for it), there are several people without whose influence this work would not have been completed. I thank Dr. John Slaughter and Maj. Dan Rubera of the Defense Nuclear Agency for providing computer money; Lts. Bob Connell and Tom Lutton of the Air Force Weapons Laboratory for working overtime to help me finish the computer work; Profs. George Nickel and David Hardin for demanding a complete product; and particularly my advisor, Prof. C.J. Bridgman, for recommending the topic, guiding me through the research, and pushing me toward the conclusion.

I wish to thank especially my wife, Dell. Without her encouragement and understanding, as well as many sacrifices on her part, I could not have made it through the past three years. This dissertation is dedicated to her.

i

Table Of Contents

List of Tables and Illustrations

iv

Abstract

The accuracy of modified Sachs and Ledsham-Pike scaling of peak shock hydrodynamic variables from a nuclear burst in air is evaluated. The modified Sachs and Ledsham-Pike methods are corrections applied to the similarity transform which is used to compute shock overpressures and related variables for infinite homogeneous atmospheric ambient conditions. This similarity transform no longer applies when the burst and target are located at different altitudes, and the modified Sachs and Ledsham-Pike corrections are applied to account for these varying ambient conditions. In this dissertation, the modified Sachs shock positions, dynamic pressures, and overpressures and the Ledsham-Pike overpressures are compared to a fully two dimensional flux-corrected transport finite difference solution. The flux-corrected transport method maintains a sharp and steady shock with no oscillations. The numerical calculations include a real atmospheric model, the Doan and Nickel equation of state of air, and radiation energy losses. It is found that the modified Sachs and Ledsham-Pike overpressures are essentially identical, and that their overpressures compare with the numerical results more favorably in the ascending directions than in the descending directions. A new Ledsham-Pike correction factor is presented for the descending directions.

Chapter I. Introduction

When a nuclear weapon is detonated in the atmosphere the immediate effect is the liberation of a large amount of energy in a small volume. Between seventy and eighty percent of the weapon's yield appears in the form of X-rays (see Glasstone and Dolan, 1977), and since the mean free path of these X-rays in air is a few meters, they are absorbed within several meters of the burst point. The air becomes ionized, and the resulting plasma, which includes bomb debris, is called the fireball. Initially, the radiation energy from the weapon is greater than that required to completely ionize the fireball's constituent atoms. The X-rays then stream through the plasma and are absorbed at the fireball's boundary, ionizing successive layers of air near the boundary. The fireball thus grows until the radiation energy from the weapon can no longer reach the surface of the fireball. This point is called "burn-out". The fireball continues to grow diffusively after burn-out by X-ray re-emission and re-absorption, but the growth rate continuously slows down. At some time during the diffusive growth phase of the fireball, the potential shock wave speed from the blast is greater than the rate of growth of the fireball. At this time the shock wave emerges from the fireball, and this phenomenon is called "hydrodynamic separation".

After hydrodynamic separation, the shock wave propagates outward, and its motion, as well as the motion of the fluid

1

behind the shock front, is governed by the partial differential equations of hydrodynamics. These are continuity equations expressing the conservation of mass, momentum, and energy (see Zel´dovich and Raizer, 1966; or Harlow and Amsden, 1971), and in one dimension they can be written

$$\frac{\partial \vec{U}}{\partial t} + \frac{1}{r^\nu}\frac{\partial}{\partial r}\left[r^\nu \vec{F}(\vec{U}) \right] + \vec{S} = 0 \qquad (I-1)$$

where

$$\vec{U} = \begin{bmatrix} \rho \\ \rho v \\ E \end{bmatrix} \qquad (I-2)$$

$$\vec{F}(\vec{U}) = \begin{bmatrix} \rho v \\ \rho v^2 \\ E v \end{bmatrix} \qquad (I-3)$$

$$\vec{S} = \begin{bmatrix} 0 \\ \frac{\partial P}{\partial r} \\ \frac{1}{r^\nu}\frac{\partial}{\partial r}(r^\nu P v) \end{bmatrix} \qquad (I-4)$$

and $\nu = 0$, 1, 2 for Cartesian, cylindrical and spherical geometry respectively. For a complete evaluation of the hydrodynamics variables as functions of time and space, the three equations represented by (I-1), together with an appropriate equation of

2

state, must be simultaneously solved for the mass density ρ, momentum density ρv, energy density E, and pressure p. In the most general case, the complete multidimensional hydrodynamics equations would be solved with initial conditions appropriate for each atmospheric condition of interest. These extremely expensive repeated calculations can be (and are) avoided by a scaling method which uses a single complete solution of the one-dimensional equations (I-1) for a given yield in a uniform homogeneous atmosphere, and then transforming this solution to another yield and atmosphere. The similarity transformation which allows this procedure is known as Sachs scaling, and it is used extensively by the nuclear survivability and vulnerability analysts. The "given" complete solution is usually for a one-kiloton burst in a standard temperature and pressure, sea level (but no ground effects) atmosphere. Since this solution is widely used in the nuclear effects community, the Air Force Weapons Laboratory (AFWL) has prepared a compendium of one-dimensional numerical solutions and experimental measurements, all scaled to the one kiloton yield and standard sea level conditions (Needham and Havens, 1975). This averaged survey of results has become known as the AFWL 1 kt standard.

With the AFWL 1 kt standard as the known solution, the Sachs scaling laws can be used to transform all the flow variables to any other yield and homogeneous atmosphere; however, the similarity transformation gives no information about the case when the burst is at one altitude and the target is at another altitude. In this case, the shock travels through a variable density and

3

pressure atmosphere and these spatially variable external conditions have a pronounced effect on the shock values over intermediate and large distances (several kilometers). To account for these effects, a procedure known as modified Sachs scaling is used. This procedure is defined in the next section and has no theoretical basis, but when compared to measured data, it has been found to give "reasonably reliable" answers (Moulton, 1960). A second correction procedure is available, but has received little attention. It is the Ledsham-Pike correction, and is used to correct overpressures values only (Ledsham and Pike, 1951). The Ledsham-Pike correction factor has a theoretical basis, but its values must be experimentally measured or computed from a fully two-dimensional solution of the equations of hydrodynamics.

This dissertation is a critical evaluation of the modified Sachs and Ledsham-Pike correction techniques. They are evaluated for one set of initial and external conditions by comparing their results to a two-dimensional finite difference solution which uses the method of flux-corrected transport. The particular case chosen for comparison was a one megaton burst at 15 kilometers altitude. The next section is a discussion of the Sachs and modified Sachs scaling methods and the Ledsham-Pike correction factor. It is followed by a description of the numerical calculations required for the comparison including a discussion of finite differences and flux-corrected transport. The fourth section compares the scaling law predictions to the numerical results, and this is followed by the conclusions.

Chapter II. Scaling Laws

To predict shock densities, velocities and pressures for different initial conditions (yields) and ambient or atmospheric conditions requires a solution of the partial differential equations of hydrodynamics or experimental measurement of the properties for each set of conditions. Fortunately, we can use similarity theory to develop scaling relationships to avoid such a costly procedure. The fundamental principle underlying these relationships is that the same conservation laws govern the fluid flow and shock wave mechanics for all explosions. For distances far enough removed from the explosion that the mechanism by which the explosion energy is transfered to the air is not important, the only governing parameters are total explosion energy and the ambient conditions of the air. Thus, explosions in air obey principles of similitude:

> "Two phenomena are similar, if the characteristics of one can be obtained from the assigned characterictics of the other by a simple conversion, which is analogous to the transformation from one system of units of measurement to another." (Sedov, 1959)

The transformation functions, or similarity ratios, are called scaling factors, and are generally derived from the hydrodynamics equations when they are reformulated as relations between

nondimensional quantities. (Dimensional quantities depend on the units of measurement used in their numerical definition - nondimensional quantities do not depend on the measurement scale and their numerical values are the same in all systems.)

One of the earliest scaling laws for high explosive detonations was proposed by Hilliar in 1919 (see Moulton et al, 1971). Since the energy available in a charge is directly proportional to the mass, and the cube root of the mass is directly proportional to the characteristic length of the volume containing the mass, Hilliar concluded that the scaling factors for radius and time for two similar explosions of different yields but in identical air media must be the cube root of the ratio of the two explosives' masses (or energies). Thus, for example, the peak pressure p_2 of a TNT explosion of weight w_2 at radius r_2 is

$$P_2(r_2) = P_1(r_1) \qquad (\text{II-1})$$

where

$$r_1 = r_2 \left(\frac{w_1}{w_2}\right)^{\frac{1}{3}} \qquad (\text{II-2})$$

and p_1 is the peak pressure of a "reference" explosion.

Sachs and Modified Sachs Scaling

Hilliar's yield scaling laws developed for high explosive shock waves apply to nuclear explosions in an infinite homogeneous atmosphere when the weight of the nuclear explosion is defined by the "TNT equivalent" (or when explosive energy is used instead); however, there is a critically important condition associated with nuclear explosions, which Hilliar's scaling laws do not address. Since nuclear explosive shock waves travel many times further than those generated from high explosives or TNT, and since nuclear weapons may be used at high altitude against flying targets, more general scaling laws which include the effects of a variable atmosphere were needed. One such set of scaling laws were provided by Sachs in 1944, and the Sachs scaling laws are the most widely used similarity transformations for shock waves traveling in a nonhomogeneous atmosphere (see Glasstone and Dolan, 1977).

Sachs assumed that the total energy in the blast wave is independent of the external conditions, and the only effect of a change in external atmospheric conditions is to change the scale of pressure, distance and time. His result was a generalized similarity transformation in which the shock pressure and density as a function of distance and time for a blast with one set external conditions can be obtained from that for a different blast with another set of external conditions:

7

"If the atmospheric pressure and temperatures are
changed to $P' = \pi P$ and $T' = \theta T$, then, according
to the law of similitude, the new blast pressure
$p'(R', t')$ at distance $R' = xR$ and $t' = \tau t$ is
given by

$$P'(R', t') = \pi P(R, t)$$

where x and τ are constants which determine
the change in scale of distance and time." (Sachs, 1944)

The distance and time scale factors x and τ were determined by
Sachs purely from dimensional reasoning. Since velocity has
dimensions of length divided by time, the velocity in the primed
system must be related to the velocity in the unprimed system by

$$u'(R', t') = \frac{x}{\tau} \vec{u}(R, t) \qquad \text{(II-3)}$$

and since density is proportional to p/T through the ideal gas
law, the two densities are related by

$$\rho'(R', t') = \frac{\pi}{\theta} \rho(R, t) \qquad \text{(II-4)}$$

When these are substituted into the continuity equation

$$\frac{\partial \rho}{\partial t} + \text{div}(\rho \vec{u}) = 0 \qquad \text{(II-5)}$$

and the equation of motion

8

$$\rho \frac{\partial \vec{u}}{\partial t} + \text{grad } P = 0 \qquad \text{(II-6)}$$

the corresponding equations in the primed system are produced:

$$\frac{\Theta}{\pi} \tau \frac{\partial \rho'}{\partial t} + \frac{\Theta}{\pi} \tau \text{ div}' \rho' \vec{u}' = 0 \qquad \text{(II-7)}$$

$$\frac{\Theta}{\pi} \frac{\tau^2}{x} \frac{\partial \vec{u}'}{\partial t} + \frac{x}{\pi} \text{grad}' P' = 0 \qquad \text{(II-8)}$$

where div´ and grad´ imply differentation with respect to R´. Equations (II-7) and (II-8) must express solutions of the hydrodynamics equations (II-5) and (II-6). Equation (II-7) already has the required form of (II-5), but (II-8) has the form of (II-6) only if

$$\frac{x}{\tau} = \sqrt{\Theta} \qquad \text{(II-9)}$$

This is one of the relations between x and τ ; the other was derived by Sachs from a dimensional analysis of the energy equation. It was assumed that the total energy in the blast wave was the total energy of the air behind the shock front minus the energy of the same volume of air at atmospheric conditions. Integrating each term in the energy equation ($p + \frac{1}{2}\rho u^2 + \rho \int C_v \ dT$) over the volume behind the shock front indicates the following dimensional relationship between the energies in the primed and unprimed system:

9

$$E'(t') = \pi \chi^2 E(t) \tag{II-10}$$

Now, invoking the assumption that the total energy is independent of the external conditions, if the mass (or equivalently yield) is increased by a factor m from the unprimed to the primed system, it follows that

$$m = \pi \chi^3 \tag{II-11}$$

Thus the two scale factors x and τ are given by

$$\chi = \left(\frac{m}{\pi}\right)^{\frac{1}{3}} \tag{II-12}$$

$$\tau = \left(\frac{m}{\pi}\right)^{\frac{1}{3}} \left(\frac{1}{\Theta}\right)^{\frac{1}{2}} \tag{II-13}$$

The Sachs scaling factors, and indeed the entire Sachs similarity transformation, can be obtained in a slightly different manner by transforming both the dependent and independent variables in the hydrodynamics equations (see Bridgman, 1980). The transformed dependent variables density, velocity, energy and pressure represent dimensionless ratios of the value of each variable to some reference value, and the new independent variables are determined so that they are scaled so as to eliminate the dimensioned constants in each equation. This process of normalization of the differential equations leads to the same scaling laws as Sachs', but it has the advantage of explicity

10

demonstrating that a solution to the resultant normalized equations can be used for any set of constants (initial and boundary conditions).

The Sachs scaling laws may be used to produce values for peak pressure (static, dynamic or total), range, and time of arrival for a blast of yield Y in a homogeneous atmosphere of ambient pressure P_a and ambient temperature T_a if the values are known for some "reference" blast of yield Y* and ambient conditions P_a^* and T_a^* as follows:

$$P = P^* \; \frac{P_a}{P_a^*} \tag{II-14}$$

$$r = r^* \left(\frac{P_a^*}{P_a}\right)^{\frac{1}{3}} \left(\frac{Y}{Y^*}\right)^{\frac{1}{3}} \tag{II-15}$$

$$t = t^* \left(\frac{P_a^*}{P_a}\right)^{\frac{1}{3}} \left(\frac{Y}{Y^*}\right)^{\frac{1}{3}} \left(\frac{T_a^*}{T_a}\right)^{\frac{1}{2}} \tag{II-16}$$

It can be easily shown (Bridgman, 1980) that the density and velocity are given by

$$\rho = \rho^* \; \frac{\rho_a}{\rho_a^*} \tag{II-17}$$

$$u = u^* \frac{c_0}{c_0^*} \qquad\qquad \text{(II-18)}$$

where c_0 is the speed of sound in the undisturbed air. The "reference" yield and atmosphere is usually that of a one kiloton burst in a standard (STP) atmosphere (see Glasstone and Dolan, 1977).

Sachs scaling predicts the solution of one explosion in an infinite homogeneous atmosphere, given a solution for the shock variables of another explosion in the same or another infinite homogeneous atmosphere. It gives no information, however, in the case of a blast wave moving through a real, spatially varying atmosphere which must be considered in the case of nuclear burst at one altitude when the target is at a substantially different altitude. To account for the variable atmospheric effects on the shock values, the nuclear weapons effects community has adopted the following procedure, called modified Sachs scaling: instead of using the ambient pressure, temperature and density at the burst altitude in the Sachs scaling laws, the corresponding values at the target altitude are used. Modified Sachs scaling has no rigorous, theoretical basis, but it is very simple to implement and can readily produce results in lieu of a step-by-step analysis of a blast wave propagating through a real, varying two dimensional atmosphere.

Ledsham-Pike Alpha Correction

Several investigators have studied the nonhomogeneous atmos-
pheric effects analytically (Bach, Kuhl, and Oppenheim, 1975;
Laumbach and Probstein, 1969; Sachdev, 1972; Hayes 1968a and
1968b). Although these studies differ in the assumptions made,
most assume an exponential density variation in the atmopshere
and all neglect ambient pressure. They define various nondimen-
sional parameters consistent with their formulation of the hydro-
dynamics equations and they reduce the partial differential equa-
tions to ordinary differential equations, which are then solved
numerically. None of these studies has been used by the Air
Force for nuclear survivability analysis because of the restric-
tive assumptions made and because they still rely on an approxi-
mate numerical solution. An earlier study, however, has been
used in survivability/ vulnerability analysis (see Sharp and Das-
sow, 1970). This study proposed a simple correction to the over-
pressure values calculated or measured for homogeneous atmospher-
ic conditions to approximately account for homogeneous effects.

Ledsham and Pike (1951) assumed that all fluid motion at the
shock front was purely radial and that each part of the shock
front behaved as though the atmosphere were spherically symmetric
with respect to the radial direction concerned. Following the
procedures of Brinkley and Kirkwood (1947), they nondimensional-
ized the Lagragian form of the hydrodynamics equations, and made
several assumptions based on experimental evidence. Ledsham and

13

Pike's primary conclusion was that overpressure Δp at a location where the ambient pressure is P_a can be approximated if the overpressure $\Delta p'$ is known at the same range, but coaltitude with the burst by

$$\Delta P = \Delta P' \left(\frac{P_a}{P_a'}\right)^{\alpha} \qquad \text{(II-19)}$$

where P_a' is the ambient pressure at the burst altitude and α is the correction factor. The α factor was calculated by Ledsham and Pike as a function of distance by simultaneously solving their normalized differential equations for 10, 20 and 40 kilotons of TNT exploded on the ground. (Thus the α values were calculated only for the ascending portion of the shock wave). The values were recomputed for a one kiloton burst (no ground reflection) in a standard atmosphere by Alexander. These values are shown graphically in figure (II-1), and were taken from Sharp and Dassow (1970).

The modified Sachs and Ledsham-Pike correction methods produce approximate values of the shock variables (only overpressure for Ledsham-Pike), and for their reliable use as predictive tools they must be checked for accuracy. Lutzky and Lehto (1968) performed one-dimensional finite difference calculations of nuclear shock waves traveling in a spherically symmetric atmosphere with exponentially varying pressure and density and with an ideal gas. They considered downward propagating shocks only and found a maximum error in modified Sachs overpressure of about 20%. The remainder of this dissertation is a second evaluation of the

14
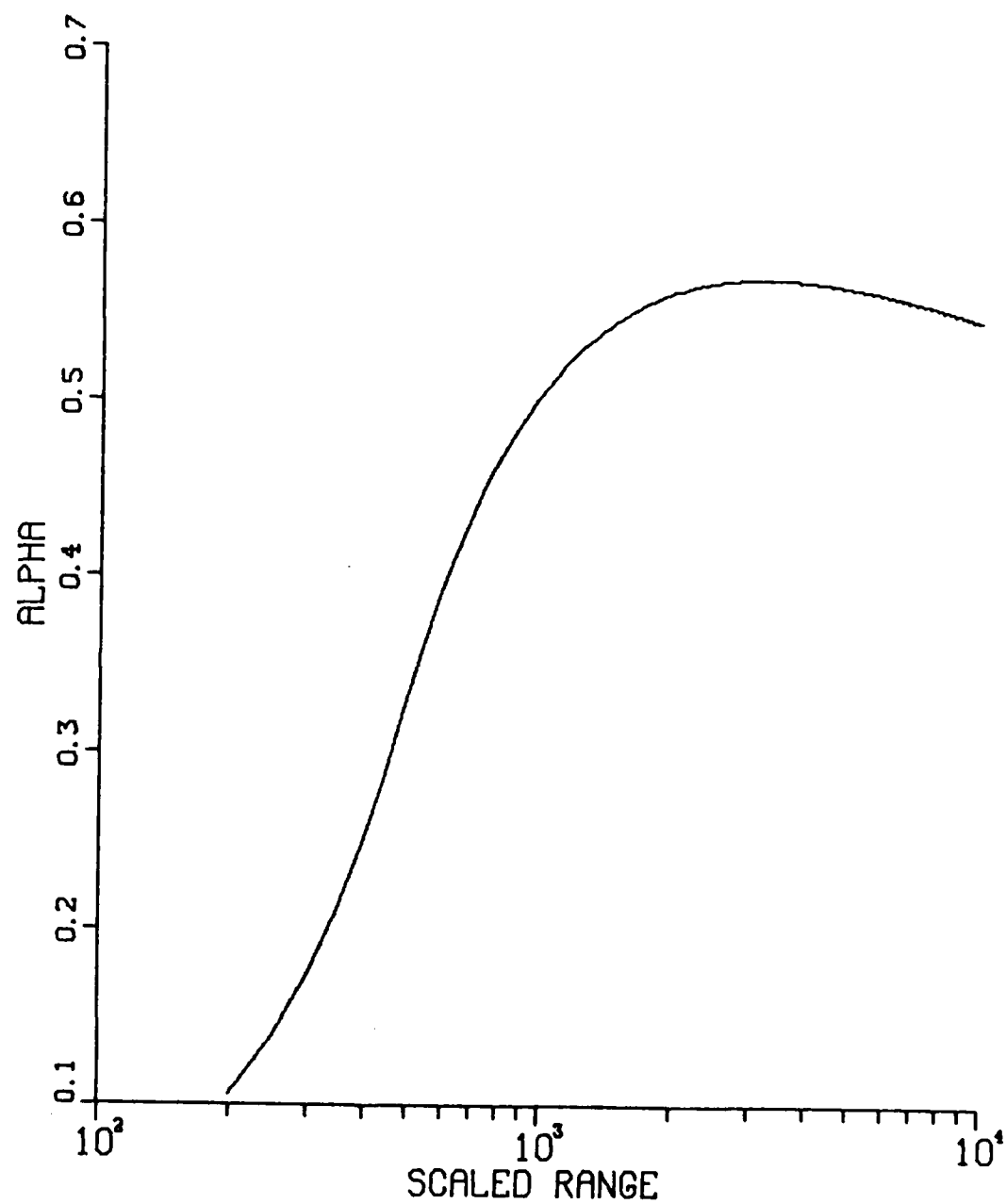
Figure II-1. Ledsham-Pike alpha correction factor vs 1 kt standard range.

modified Sachs and Ledsham-Pike techniques, which uses a fully two-dimensional finite difference calculation. The 2-D solution has the advantage that both the upward and downward directions can be checked, as well as all directions in between and in addition, a spherically symmetric atmosphere need not be assumed since a real, horizontally stratified atmosphere can be modeled. Furthermore, the effects of a rising fireball are included inherently in the solution. A variable γ ideal gas (γ is the ratio of specific heats and is a function of density and internal energy) and a variable gravitational acceleration (a function of altitude) are used. Energy loss from the fireball due to thermal radiation is also included.

The particular set of burst conditions chosen for comparison with modified Sachs and Ledsham-Pike scaling, was a one megaton burst at 15 kilometers altitude. (This choice of burst conditions ensures that the shock wave does not reflect from the ground before low overpressure is reached, yet it exercises a considerable amount of atmosphere before low overpressure. We consider low overpressure as 15 kpascals. The 1 Mt results are not proposed as being superior to 1 kt scaling - rather the results of scaling to large distances are being compared to approximate finite difference results.) Prior to the 2-D calculations however, a series of one-dimensional calculations were performed. To check the reliability of the finite difference equations, a steady state flow through a shock and an unsteady flow in a shock tube were simulated. Then, a 1-D calculation of a one kiloton burst in a standard atmosphere was performed followed by

16

a 1-D one megaton burst at 15 kilometers (uniform atmosphere).
This final 1-D calculation was used as the "seed" for the modi-
fied Sachs and Ledsham-Pike scaling and these results were com-
pared to the 2-D calculation. The 1-D one kiloton and one mega-
ton calculations, as well as the 2-D calculations are discussed
in the next chapter.

17

Chapter III. Numerical Calculations

Finite Differences and Flux-Corrected Transport

This chapter presents the results of one-and two- dimensional finite difference calculations of shock waves resulting from nuclear explosions in the atmosphere. The numerical method of finite differences is used to solve the hyperbolic system of partial differential equations of hydrodynamics (I-1) in one-dimensional spherical form and in two-dimensional cylindrical form. The technique of flux-corrected transport, and in particular the SHASTA (an acronym for SHarp And Smooth Transport Algorithm) finite difference scheme is used.

The origin of finite difference methods for numerically solving partial differential equations can be traced to a famous paper by Courant, Friedrichs, and Lewy (1928). The method has since been put to use in many fields of applied science, and one of the most successful applications has been in the field of fluid dynamics. In this study, we are interested in fluid flows that are characterized by internal discontinuities, or shock waves. One possible solution technique is "shock fitting", in which we apply special boundary conditions at the shock front provided by the Rankine-Hugoniot equations (Zel'dovich and Raizer, 1966) and then solve for the smooth flow behind the shock

using one of the excellent fourth order difference schemes available (see, for example, Roberts and Weiss, 1966). However, since the shock surface is itself moving through the fluid, and its motion is not known in advance but is governed by the differential equations, serious difficulties arise immediately.

A slightly different approach was proposed by von Neumann and Richtmyer (1950) which results in an approximate method of fluid dynamics calculations and which takes care of shocks automatically. Rather than incorporate the Rankine-Hugoniot jump conditions into the calculations, von Neumann and Richtmyer introduced an artificial dissipation into the equations. Like viscosity or heat conduction, this dissipation spatially smoothes the shock, so that the discontinuity is replaced by a thin layer where the flow quantities (density, velocity and pressure) change rapidly, but continuously. This artificial dissipative term is called the von Neumann- Richtmyer pseudo-viscous pressure, and allows the differential equations to be solved over the entire region of interest - including the shock front.

The effect of pseudo-viscosity on the calculated fluid properties is dissipation, and by definition this causes the properties (density, momentum, energy and pressure) to be attenuated with subsequent time steps. To prevent the dissipation and attenuation from controlling the results or unacceptably influencing the results, especially after thousands of time steps, we require strict control of the artificial viscosity term. It can be shown that any difference scheme that attenuates any Fourier

19

component of the solution can be thought of as containing viscous terms, even though no such terms are explicitly written into the equations. This concept was exploited by Lax and Wendroff (1960), and has been widely used to calculate fluid flows containing shock waves. A major difficulty with the Lax-Wendroff , and other difference schemes using psuedo-viscosity, is not only are they dissipative, which they must be to allow the discontinuity to be smeared over a finite region, but they are also dispersive (i.e., different Fourier components of the solution travel with different speeds). A distinguishing, and unwanted, feature of such schemes is the appearance of non-physical oscillations in the solution which unpredictably influence the peak shock values (see Richtmyer and Morton, 1967). .

In an effort to eliminate or at least minimize these oscillations, Boris and Book (1973) developed a new class of finite difference techniques called flux-corrected transport. Like the pseudo-viscosity techniques, FCT treats all grid points identically; however, there are no added artificial viscosity terms and no special knowledge about the solution is required. An FCT scheme handles steep gradient problems by invoking a physical property of the continuity equations which Boris and Book call "positivity":

"An operator Ω is said to be positive if ρ_j >C,

all j, implies $\Omega \rho_j$ >C also." (Book, Boris and Hain, 1975)

In this definition, ρ_j is an element of the vector (I-2) and C is

20

a constant. The thing that separates FCT from other schemes is the application of a flux limiter to the antidiffusive fluxes, such that the antidiffusion operation is positive. These new ideas are discussed more fully in Appendix A.

An FCT algorithm contains three individual operations which when combined carry the fluid properties (density, momentum density, and energy density) through successive time steps, and when these finite difference operations are combined they are both conservative and positive. The transport operation advects the fluid through the mesh (assuming an Eulerian mesh) and is the same finite difference operation as conventional schemes without artificial viscosity terms or other special terms included to handle shocks. The diffusion operation is analogous to the viscosity terms in conventional schemes; however, the magnitude of the dissipation in FCT is purposely much larger than in schemes with pseudo-viscosity. By adding a large amount of diffusion in regions near sharp gradients, the dispersively generated ripples are overwhelmed. (Some FCT schemes, such as SHASTA described later, combine the transport and diffusion operations into one). The final operation in an FCT algorithm is antidiffusion. In this step, equal and opposite fluxes are applied to exactly cancel the added diffusion almost everywhere. The antidiffusive fluxes are limited term-by-term so as to maintain positivity, and the effect is that small amounts of diffusion are retained near sharp gradients to eliminate the oscillations.

SHASTA is a one-dimensional, explicit, Eulerian FCT algorithm written by Boris and Book primarily from a geometrical

21

interpretation of the coninuity equation. It can be generalized to include source terms and thus allow solution of all three equations (I-1) with the same algorithm. With minor adjustments of the flux terms, it can be used for Cartesian, cylindrical or spherical meshes in one dimension (with angular symmetry). By alternating between 1-D subroutines in a time-step splitting procedure, SHASTA can be used for multidimensional calculations. A more complete description, including a derivation of the SHASTA finite difference equations, and an outline of the time-step splitting procedure, is given in Appendix A.

One-Dimensional Calculations

To establish a data base for the modified Sachs and Ledsham-Pike scaling of one-dimensional results to compare to the numerically calculated two-dimensional results, a series of one-dimensional calculations were performed using a SHASTA flux-corrected transport code. A one-dimensional calculation of a one kiloton nuclear explosion in a standard uniform atmosphere was done, followed by the one-dimensional uniform atmosphere analogue of the two-dimensional test case (a one megaton burst at 15 kilometers altitude). These one-dimensional results were then scaled, using Sachs scaling, to a common reference for a test of consistency. The common reference used was the one kiloton burst in a standard atmosphere, and this allowed the one-dimensional

22

results to be compared to the AFWL one kiloton standard.

The first step in any finite difference analysis is the generation of a grid of node points. For the two one-dimensional calculations, the regions over which the differential equations apply was divided into discrete finite difference one-dimensional spherical Eulerian meshes. These are illustrated in figures III-1 and III-2 for the one kiloton and one megaton simulations. Since we are primarily interested in the peak shock values, and since the peak values would be constantly eroded by a coarse grid (large distances between node points), the meshes were controlled so that the shock wave was continually maintained in the region with the smallest mesh point spacing. When the shock wave approached the edge of the mesh (the criterion used was when the peak pressure occurred within 10 node points of the last one) the entire region was conservatively rezoned, by proportionately expanding all zones so that the shock was replaced to the same relative position in the mesh as when the calculations began. In this manner, the shock remained in the region of finest zone sizes although all zones were intermitently expanded. The number of times the mesh was rezoned depended upon the size of the mesh, the length of the time steps, and the number of time steps taken.

The initial conditions at the shock front and behind were taken from the AFWL one kiloton standard (Needham, et al, 1975), where for the one megaton calculation, these values were scaled using Sachs scaling. Using the AFWL one kiloton standard eliminates any device-dependent considerations such as energy

partitioning. The initial pressure, density, and velocity profiles for the one kiloton yield are shown in figures III-3 - III-5 and in figures III-6 - III-8 for the one megaton yield. In the unshocked region, ahead of the shock wave, the initial densities and pressures were taken from the 1976 U.S. Standard Atmosphere, and the velocities were zero. The boundary condition at the origin was that of symmetry:

$$\frac{\partial}{\partial r}\bigg|_{r=0} = 0 \qquad\qquad\text{(III-1)}$$

and no boundary condition (other than the external ambient conditions) was needed at the other boundary since there are no velocities or source terms there (the finite difference equations can be solved in such a cell with no change in density, momentum or energy.)

The Doan and Nickel (1963) equation of state of air was used to calculate.he ratio of specific heats. This method is a "semi-physical fit" generated from tabulated values, and handles densities from 10 to 100 times normal density and temperatures from 0.0025 to 1.5 electron volts.

The rate of radiation energy loss from the fireball was calculated using a model developed by McNamara, Jordano, and Lewis (1977). While the detailed radiation transport process may not be important at late times after bomb initiation, the total
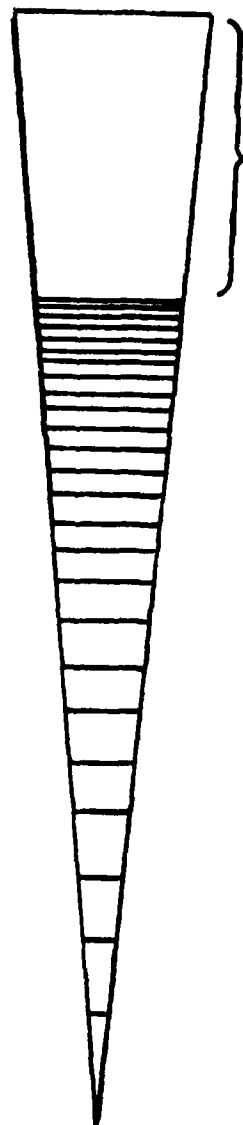
Figure III-2. One dimensional 1 Mt mesh. The burst point is located at the origin of the spherically symmetric mesh. The mesh contains a total of 200 node points, but the spacing in the area indicated by the bracket is too small for resolution with the scale used in the figure.
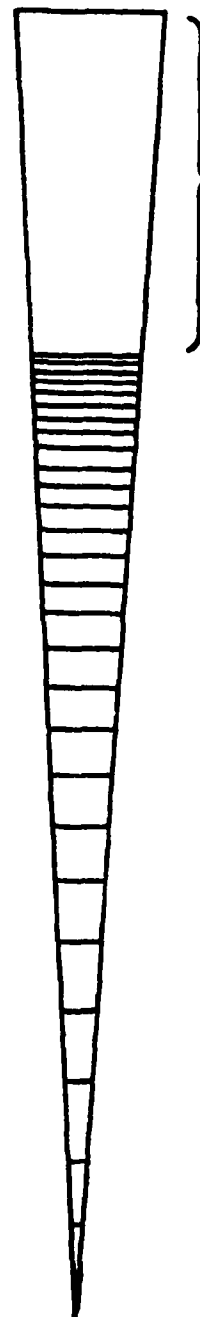
Figure III-1. One dimensional 1 kt mesh. The burst point is at the origin of the spherically symmetric mesh. The mesh contains a total of 100 node points, but the spacing is too small for resolution at the area indicated by the bracket.

25
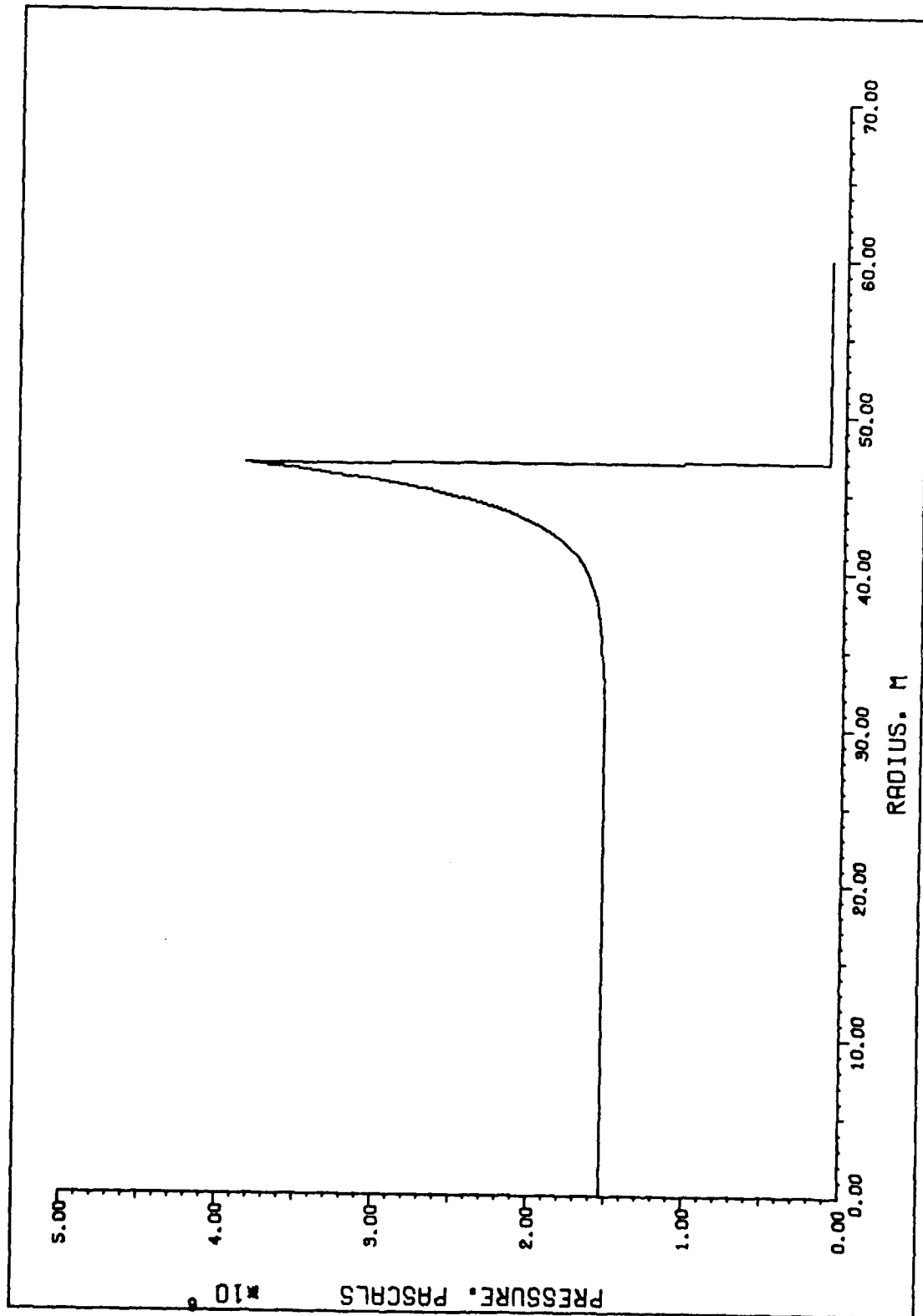
Figure III-3. Initial pressure profile for the 1-D 1 kt calcula-
tion.
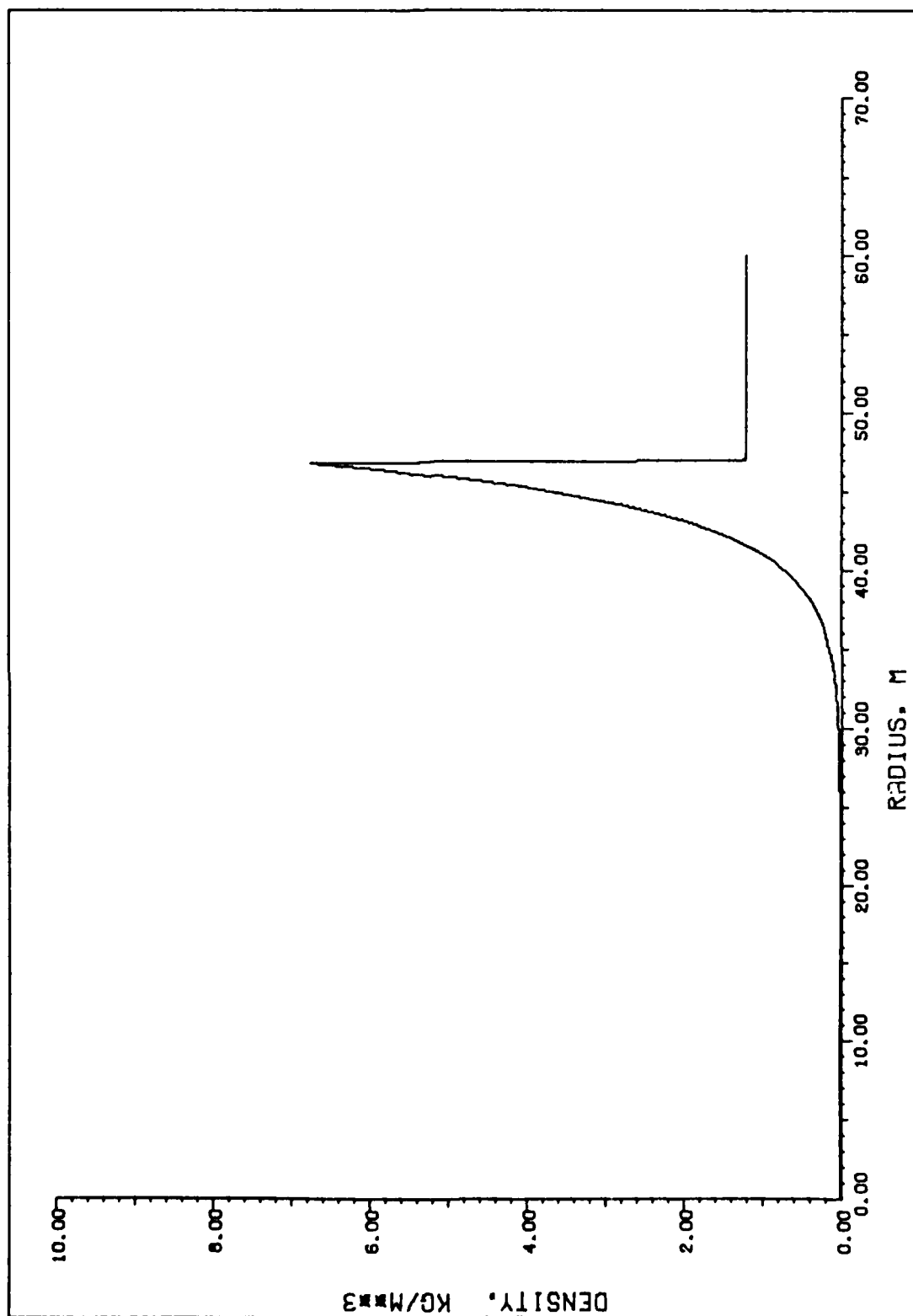
Figure III-4. Initial density profile for the 1-D 1 kt calculation.
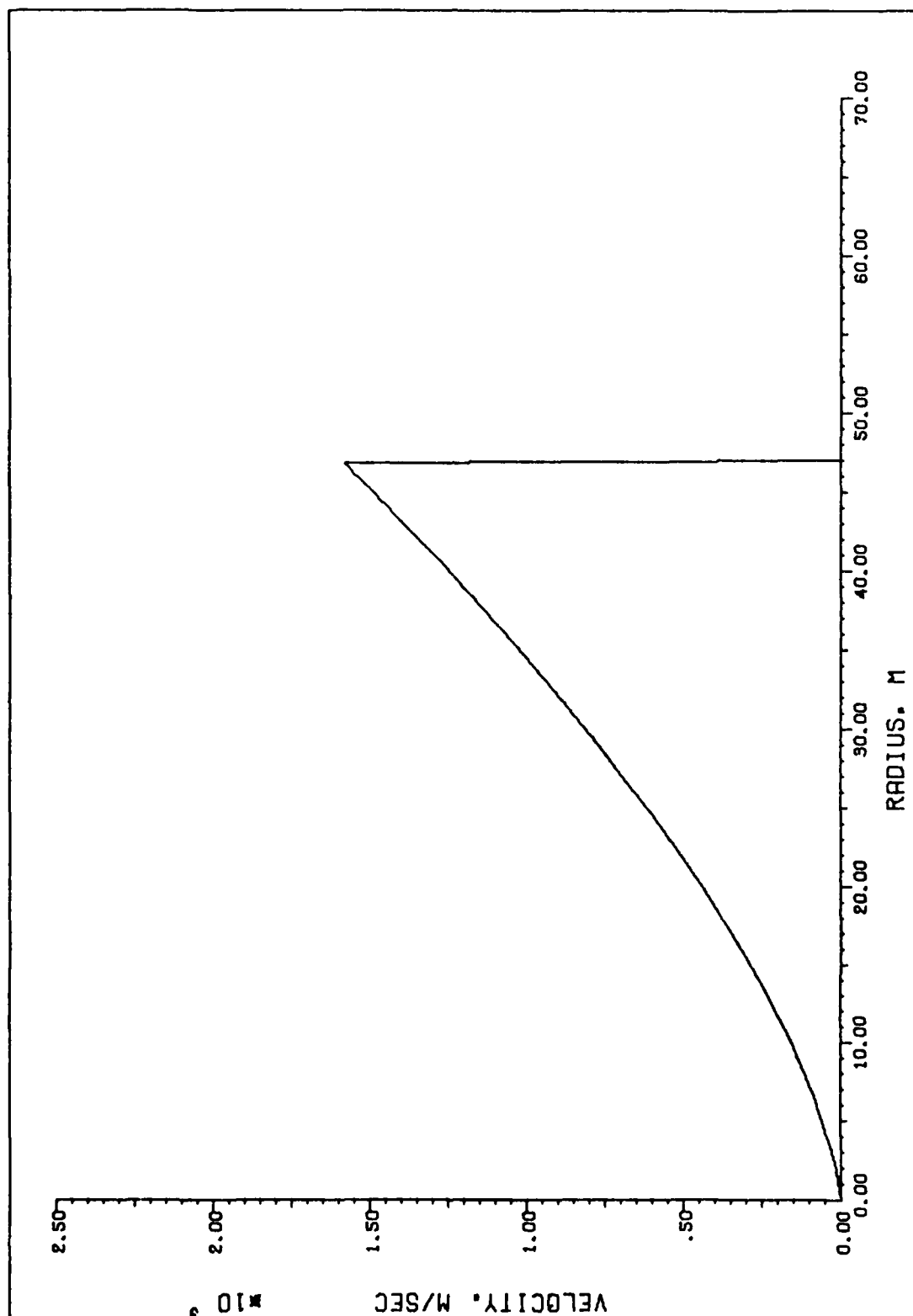
Figure III-5. Initial velocity profile for the 1-D 1 kt calcula-
tion.
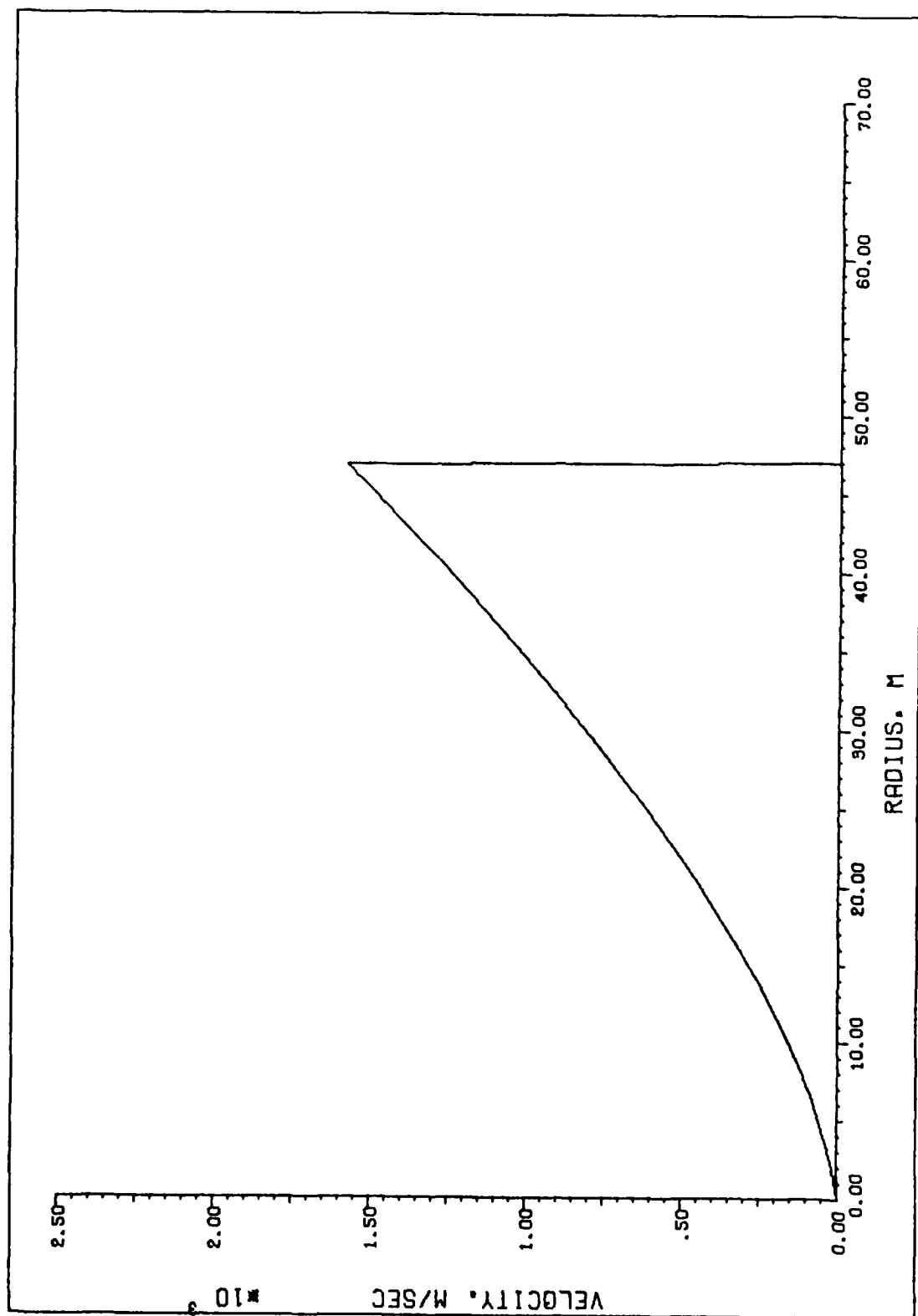
Figure III-5. Initial velocity profile for the 1-D 1 kt calcula-
tion.
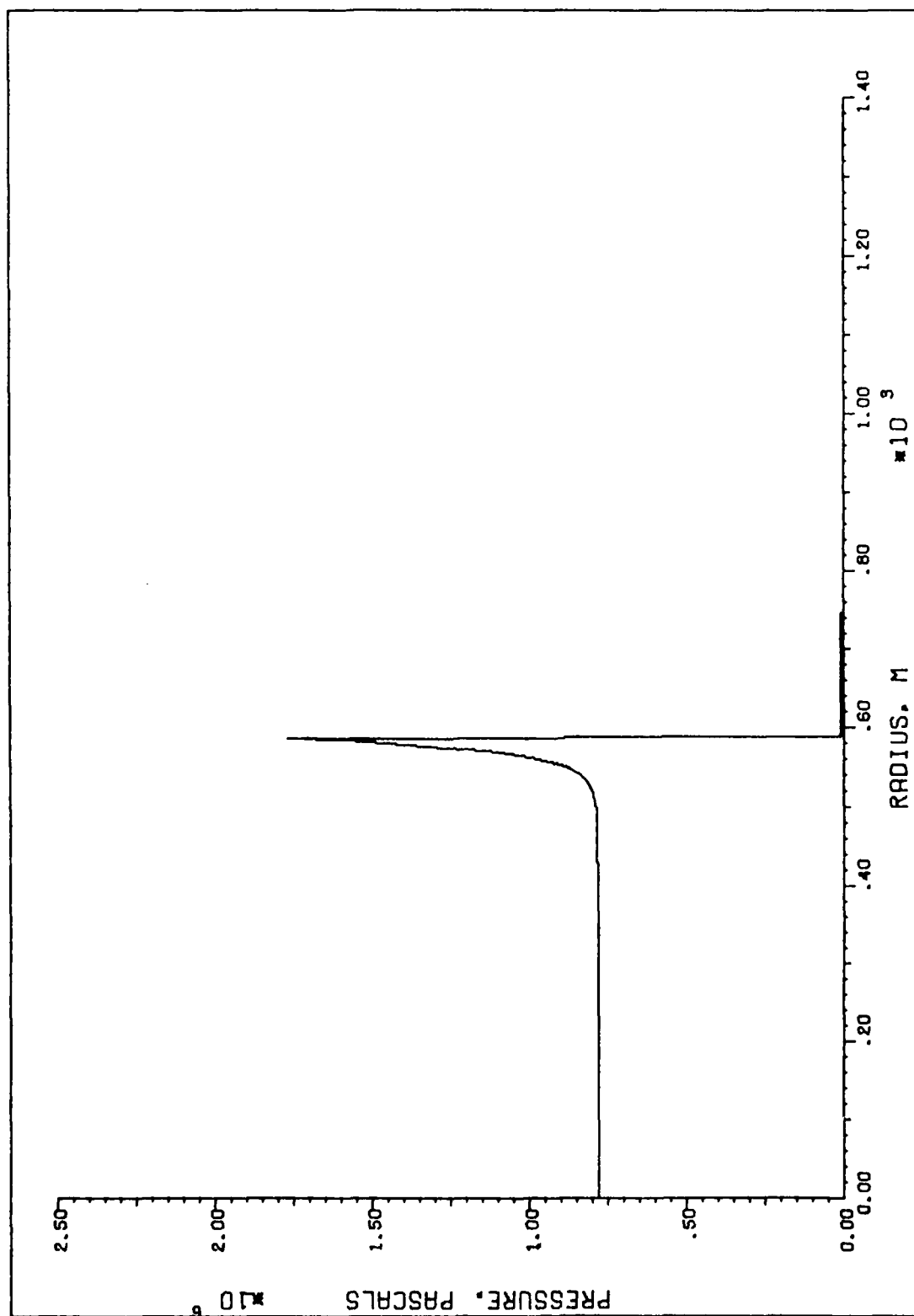
Figure III-6. Initial pressure profile for 1-D 1 Mt calculation.
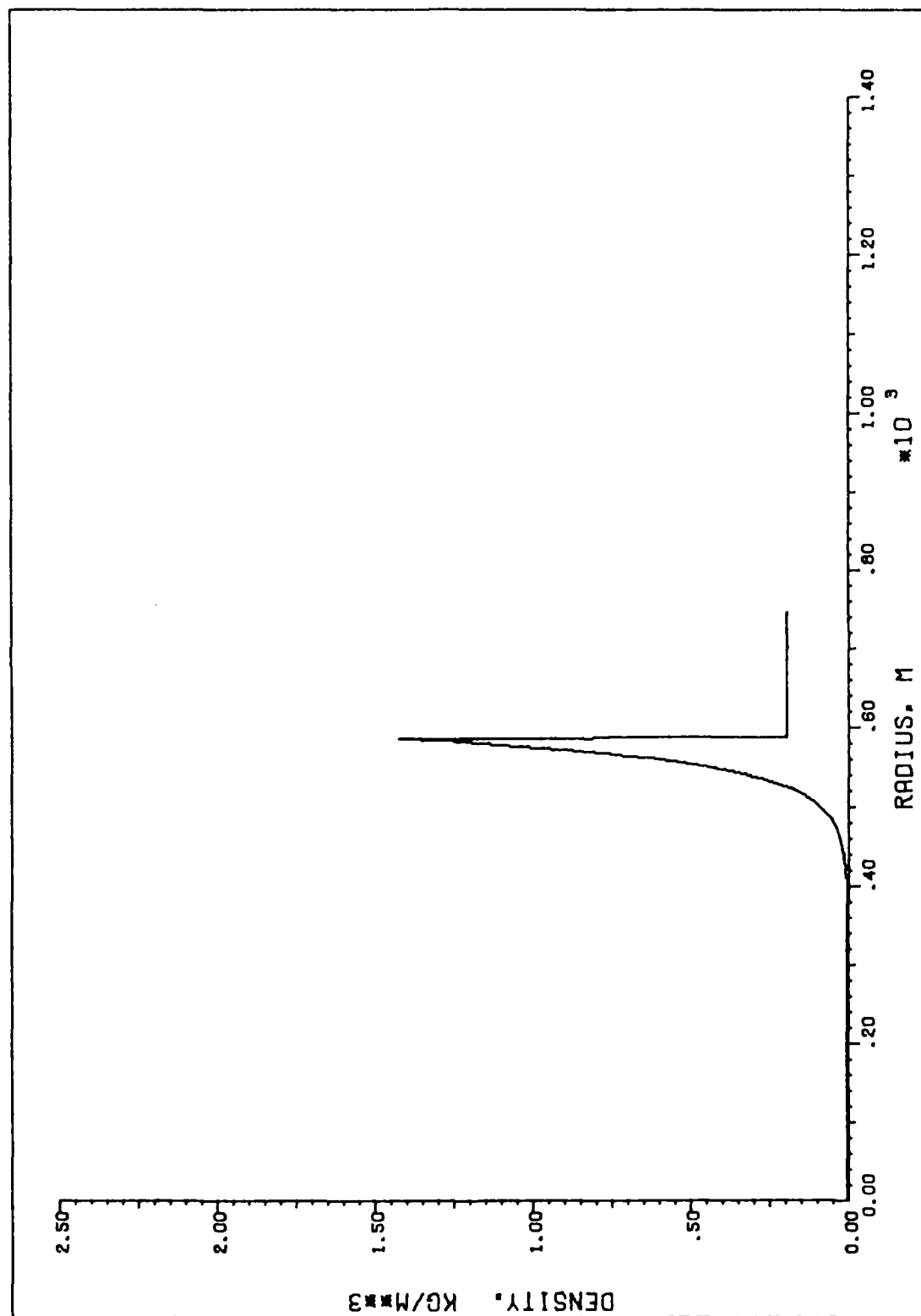
Figure III-7. Initial density profile for the 1-D 1 Mt calculation.
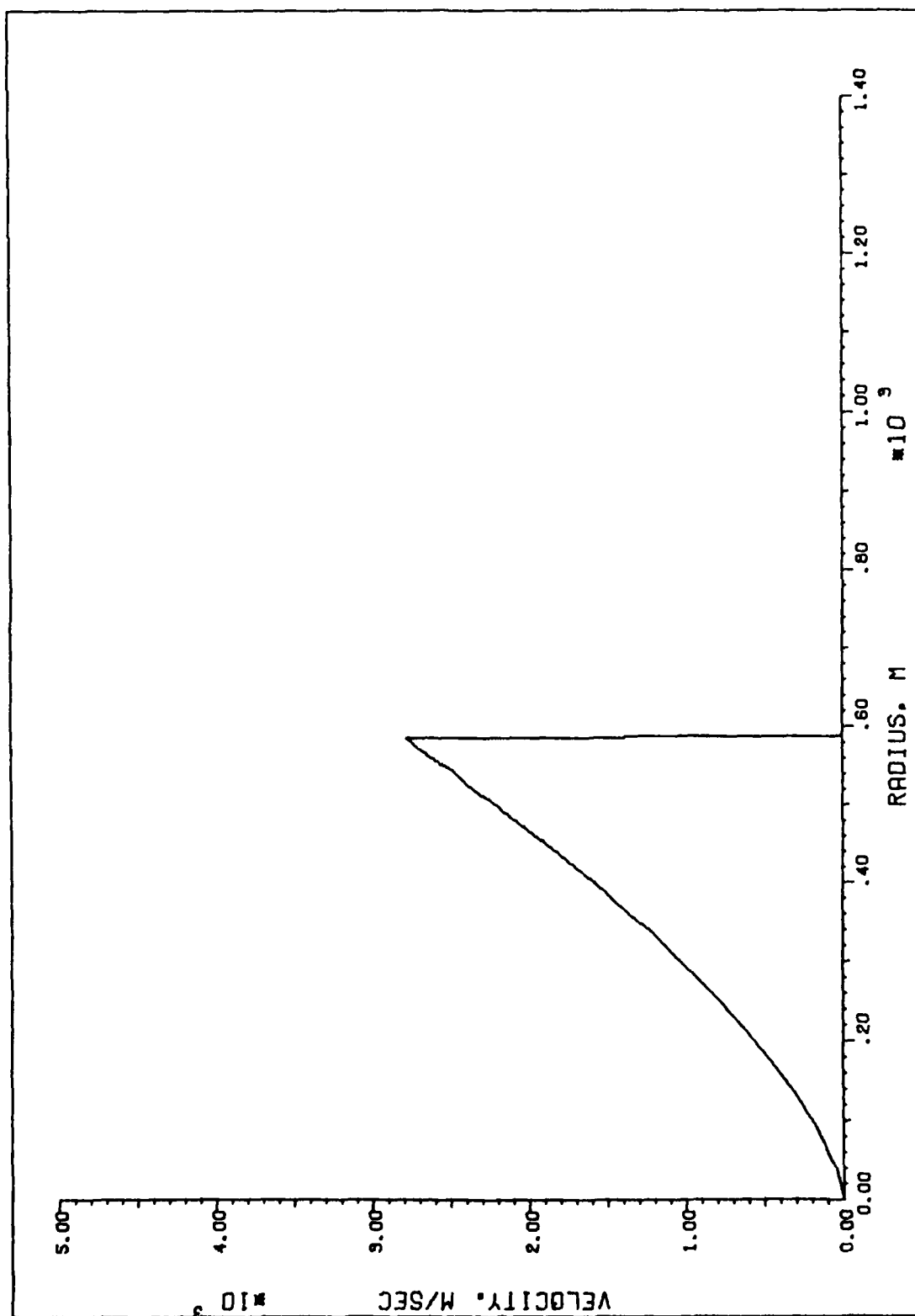
Figure III-8. Initial velocity profile for the 1-D 1 Mt calculation.

thermal power loss is important. The volumetric distribution of this energy loss, as given by the McNamara model, depends on the total fireball power loss and the spatial distribution of internal energy. The total loss rate was taken from a normalized power-time curve given by Figure 7.84 in Glasstone and Dolan (1977). For a total energy loss rate of P from the fireball, the McNamara model predicts a rate of radiation energy loss from each cell of

$$ P \; \frac{m_j \, u_j^3}{M \, U^3} $$

where m_j and u_j are the cell's mass and internal energy, and M and U are the respective mass and total internal energy of the fireball.

Details of the finite difference meshes and calculational procedures are given in table III-1. The calculated pressures, densities and velocities are shown graphically in Appendix C, figures C-1 - C-12 at two times for each of the one-dimensional cases.

Two-Dimensional Calculations

The two-dimensional calculations were performed with a

Table III-1. Programming Comparisons

	1-D		2-D
	1 kt	1 Mt	1 Mt
Number of Zones	100	200	45,000
Initial Zone Size at the Shock (m)	0.1	1.0	1.0
Final Zone Size at the Shock (m) r +z -z	10.07	8.916	8.0623 8.0623 7.2633
Start Time – End Time	0.003-7.67	0.007-10.0	0.07-7.78
Number of Time Steps	5000	7980	8000
Number of Rezonings Required r +z -z	33	12	20 20 19
Mainframe	CDC-CYBER 750		CRAY-1
Speed (CPU user/node pt/time step)	1100		60
Total Field Length	53,000	57,000	381,803

time-step splitting algorithm using a one-dimensional Cartesian SHASTA subroutine for the axial direction and a one-dimensional cylindrical SHASTA subroutine for the radial direction (see Boris and Book and Hain, 1975). Because of large computer storage and time requirements for a two-dimensional calculation, the CRAY-1 mainframe was used. The number of node points was kept small so that the program would run in-core and the total central processor time was minimized.

The two-dimensional solution was made in r-z cylindrical coordinates with the assumption of angular symmetry. Since the motion of the shock wave in the radial direction co-altitude with burst is primarily radial, and since the motion along the z-axis must be axial, the finest mesh point spacing was used in these directions. This causes the aspect ratio (the height of a cell divided by its width) to be very high along the right-hand boundary, and the aspect ratio to be very low along the upper and lower boundaries. Along +45 from the horizontal, the aspect ratio is one. The two-dimensional r-z finite difference mesh is shown in figure III-9. As in the one-dimensional calculations, when the shock front approached the edge of the mesh in the radial, positive axial, or negative axial direction, the region was rezoned and the mesh expanded in that direction (the three directions were tested and adjusted independently).

The initital conditions were identical to the one-dimensional one megaton initial conditions rotated symmetrically about the burst point. The external conditions were varied in
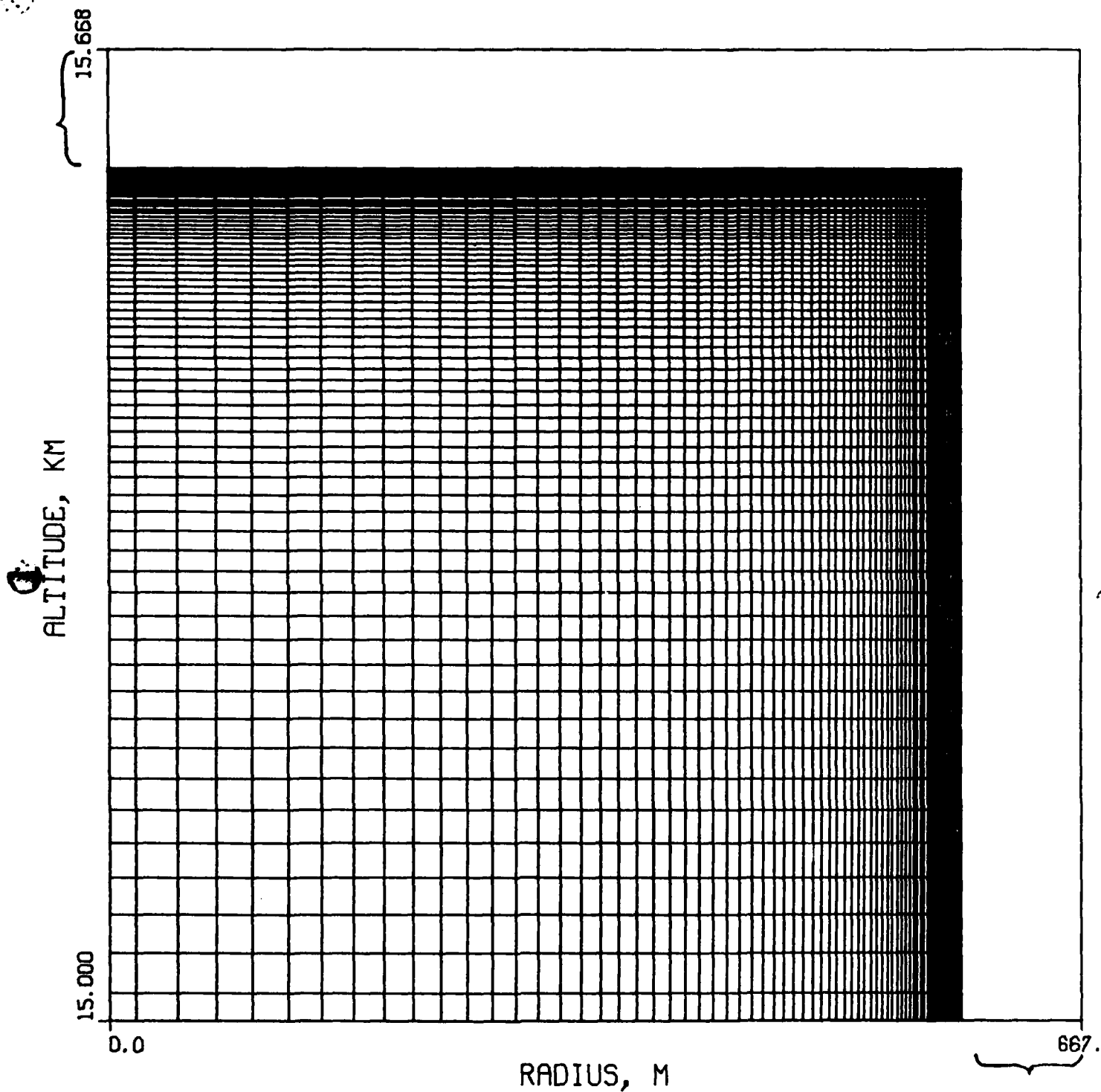
Figure III-9. Two dimensional r-z mesh. Only the upper half of the mesh is shown, the bottom half is symmetric. The burst point is at the lower corner of this figure. The areas indicated by brackets each contain 80 equally spaced mesh intervals, the spacing of which was too small for resolution.

35

the z-direction, since pressure, density and temperature vary with altitude. The atmospheric model used to calculate ambient conditions is explained in Appendix B. The symmetry boundary condition (III-1) was used along the r=0 axis.

The same equation of state and radiation energy loss model used in the one-dimensional calculations were used in two dimensions also. An additional source term was included in the momentum equation for the axial direction time step to account for gravity forces. A varying gravitational acceleration was used to account the the slight variations with altitude to maintain a stable atmosphere (see Appendix B).

The two-dimensional mesh sizes and details of the two-dimensional calculations are shown in table III-1 along with their one-dimensional counterparts. The calculated pressure, density and velocity profiles are shown for two times in Appendix C, figures C-13 - C-18 for the radial co-altitude direction, and in figures C-19 - C-24 for the axial (r=0) direction.

Programming Notes

The one-dimensional calculations were done on the Aeronautical Systems Division's CDC CYBER 750, and the two-dimensional calculations on the Air Force Weapons Laboratory's CRAY-1. The

36

two-dimensional code was vectorized to take full advantage of the CRAY's pipeline processor. In addition, the two-dimensional problem could not have been done on the CYBER in-core since this machine is limited to about 230,000 octal words of storage.

The time step, Δt, was variable and was calculated as the maximum possible to keep max (ε_j)=0.25, where

$$\varepsilon_j = \frac{v_j \, \Delta t}{\Delta r_j} \quad OR \quad \frac{v_j \, \Delta t}{\Delta z_j}$$

and v_j is the sum of material velocity and sonic velocity c_j

$$c_j = \sqrt{\frac{\gamma P_j}{\rho_j}}$$

A significant price was paid for a variable ratio of specific heats. Approximately 43% of the CP time was spent calculating γ.

Chapter IV. Comparisons of Numerical Results to

Scaling Law Predictions

The results of the modified Sachs and Ledsham-Pike scaling of the one-dimensional solution are compared to the two-dimensional finite difference calculations in this chapter. The three most important parameters - shock wave position (or equivalently, time of arrival of the shock wave), dynamic pressure, and overpressure - are used as the basis of the comparison. The errors cited for each of the comparisons were calculated with the two-dimensional finite difference solution used as the standard. For example, the error in the modified Sachs prediction of overpressure would be

$$\frac{\Delta P_{2D} - \Delta P_{MS}}{\Delta P_{2D}}$$

where 2D and MS subscripts represent the finite difference and modified Sachs overpressures.

Range-Time Comparisons

The calculated one-dimensional shock wave positions are shown as functions of scaled time in figure IV-1. These results have been normalized to a common time and radius scale using the

SHOCK ENVELOPES (1-D)
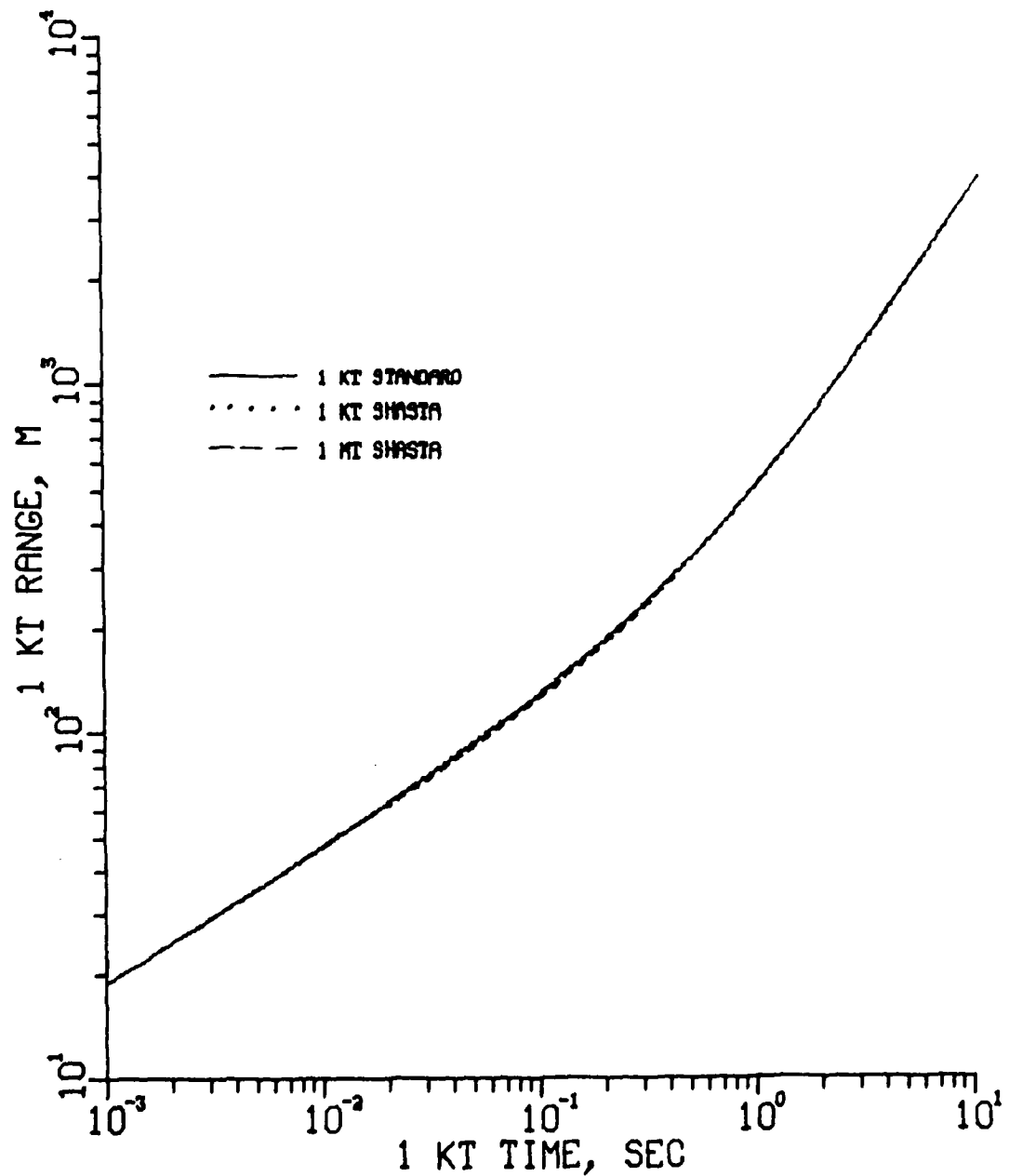
Figure IV-1. One dimensional shock envelopes. The shock front positions as functions of time are compared to the AFWL 1 kt standard.

Sachs scaling procedure described in Chapter II. The common scale is that for a one kiloton burst in a standard atmosphere, which is used so that the results can be compared to the AFWL 1kt standard, also shown in the figure. There is a negligible difference between the three shock envelopes, and the three curves in figure IV-1 are hardly discernible. The one-dimensional range-time data for the one megaton calculation were used for the modified Sachs calculations which follow.

The accuracy of the modified Sachs predictions of shock range vs time is evaluated by comparing their results to the two-dimensional finite difference calculations. The slant range R of the shock wave at time t after burst, according to modified Sachs scaling is obtained by using the Sachs scaling relationships for a uniform atmosphere with ambient conditions at an altitude $R\cos\theta$ above (or below) the burst point, where θ is the angle that the slant range makes with the vertical (see figure IV-2). A slight complication arises from the fact that time must also be scaled to the new altitude. For the one megaton burst at 15 kilometers the following equation was used to calculate the modified Sachs range vs time curve shown in figure IV-3:

$$R = R^* \left(\frac{P_a^*}{P_a} \right)^{\frac{1}{3}} \tag{IV-1}$$

where P_a^* and P_a are the ambient pressures at the burst (15
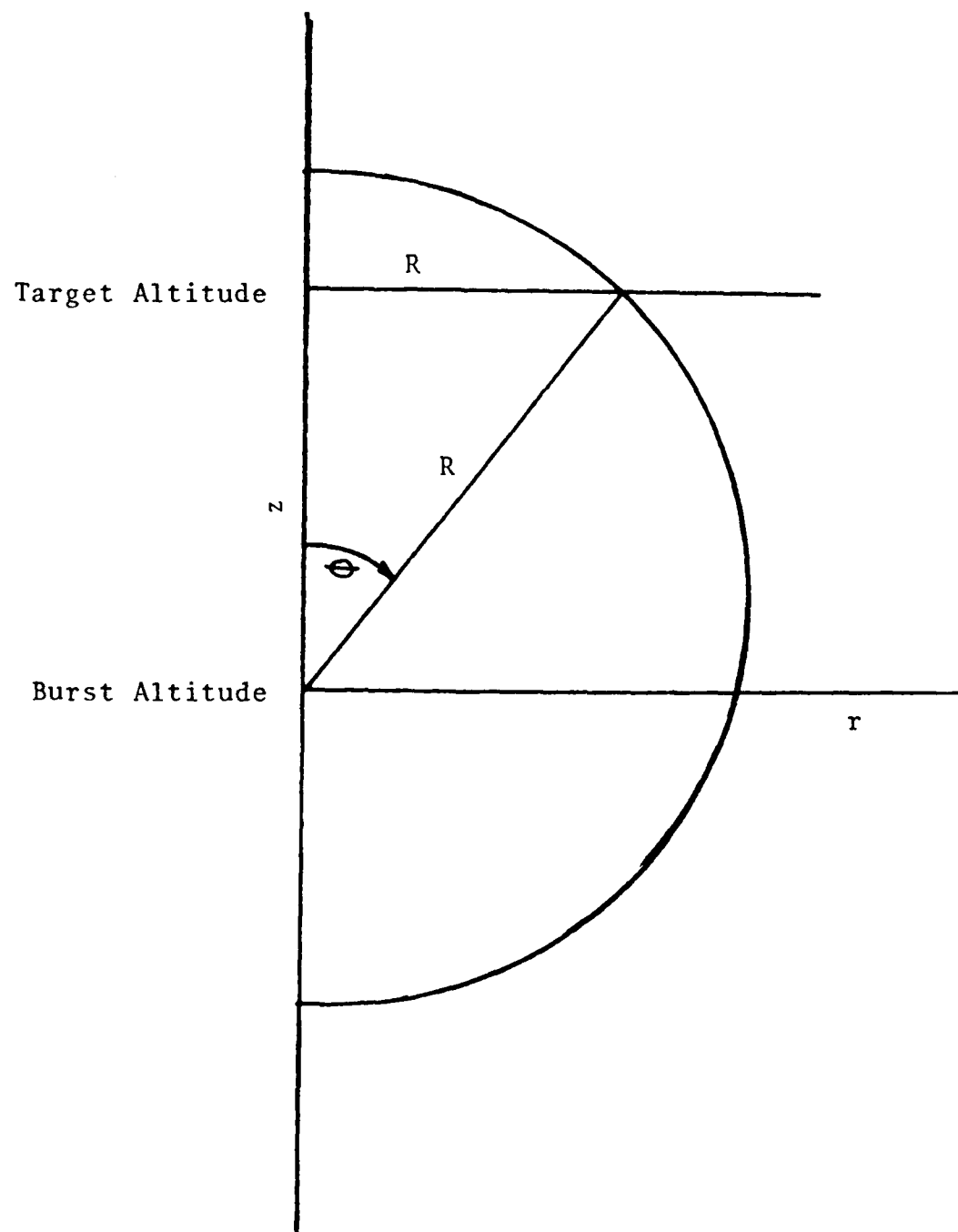
Figure IV-2. Geometry of Modified Sachs Methodology. A hypothetical shock position is shown with the slant range R which makes an angle   with the vertical.

41

kilometers) and at the target altitude (Pc ...... km) and P* is the one-dimensional one megaton shock range calculated at 15 kilometers at time t*. Now the complication arises because this range R occurs at time t which also must be scaled. Since we are interested in comparing ranges at a given time t^* from burst we can take the one dimensional data from those calculated at time

$$t^* = t \left(\frac{T_a}{T_a^*}\right)^{\frac{1}{2}} \left(\frac{P_a}{P_a^*}\right)^{\frac{1}{3}} \tag{IV-2}$$

where T_a^* and T_a are the ambient temperature at 15 km and at (Rcos θ =15 km) respectively, and we have assumed that the quantity $\sqrt{(\quad}$ $-1)C_V$ is the same at both altitudes.

The comparison of shock range as a function of time as calculated by modified Sachs and by the two-dimensional finite difference solution is shown in figure IV-3 for three times after burst. The comparison is better for altitudes beneath the burst point than for above the burst, where the modified Sachs envelopes are consistently higher than those calculated by the two-dimensional code. The errors were averaged for all shock positions between 1.5 and 5.5 kilometers for locations above and below the burst and these average values are shown in figure IV-4. Below the burst, the average error in modified Sachs shock positions stayed between ±5%; while above the burst, the error ranged from -4% to -7%. A difference in the scaling accuracy for altitudes above and below the burst altitude was also observed

42
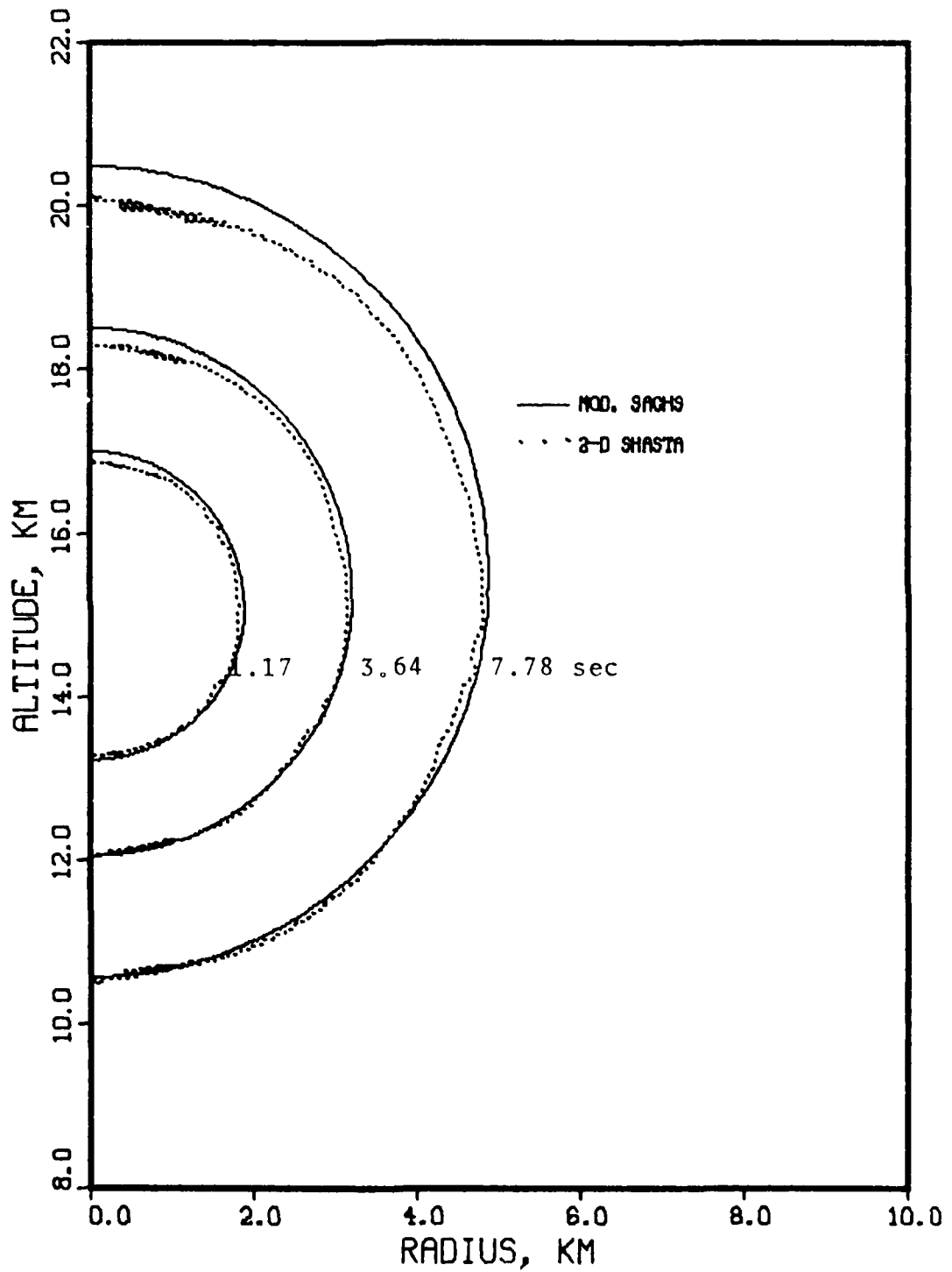
SHOCK ENVELOPES

Figure IV-3. Modified Sachs and 2-D finite difference shock envelopes for three times after burst.

for the dynamic and the static pressures, and the practice of differentiating betweeen the two directions will continue in the accuracy evaluations which follow.

Dynamic Pressure - Range Comparisons

If figure IV-3 were used as the base of a three-dimensional figure with the third dimension being peak dynamic pressure (or overpressure), the peak pressures occurring throughout the region could be observed (regardless of the time of arrival of the shock wave). It is possible to use such a construction to compare the modified Sachs pressures (modified Sachs and Ledsham-Pike for overpressure) to the two-dimensional finite difference calculations. This can be done by passing planes through the three-dimensional figure parallel to the r-z base at selected pressure levels and displaying the resulting intersections of the planes and the figures on a two dimensional graph. These two dimensional plots are called contours.

The one dimensional dynamic pressures are shown as functions of one kiloton range in figure IV-5 with the AFWL 1kt standard. The scaled one megaton dynamic pressures are all lower than the AFWL 1kt standard for each range, and the maximum difference is about 10%. The calculated one-dimensional one megaton results are used in the modified Sachs similarity transformation below.

44
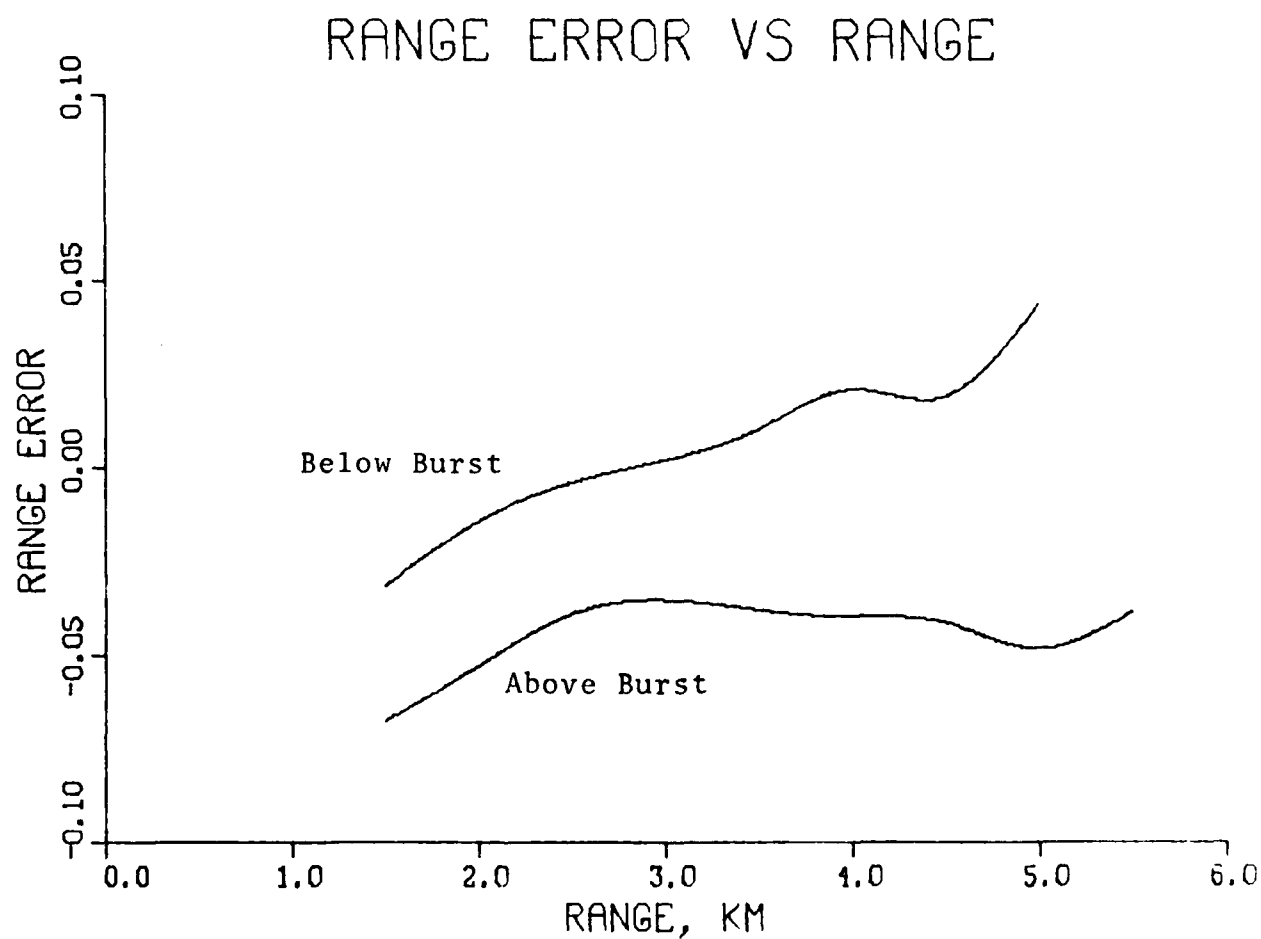
Figure IV-4. Average error of Modified Sachs range as a function of range for ascending and descending directions.

DYNAMIC PRESSURE VS RANGE

Figure IV-5. One dimensional dynamic pressures vs range. The numerically calculated 1 kt and 1 Mt pressures are compared to the AFWL 1 kt standard.

46

The dynamic pressure contours calculated with modified Sachs scaling of the one-dimensional one megaton pressures are compared to the two-dimensional finite difference results in figure IV-6 for dynamic pressure levels of 50, 20, and 5 kpascals. The modified Sachs contours were obtained by transforming the one dimensional ranges and dynamic pressures to the altitude $R \cos \theta$, where R is the slant range and θ the angle between the slant range and the vertical (as shown in figure IV-2). Equation IV-1 was used for the range, and for the dynamic pressure q, the Sachs similarity transformation is the same as for static pressure:

$$q = q^* \frac{P_a}{P_a^*} \qquad (IV-3)$$

where q* is the dynamic pressure at R* in an infinite, homogeneous atmosphere. An iterative procedure was required to produce the modified Sachs contours, since the correct combination of dynamic pressure, range and ambient pressure must be found.

The modified Sachs dynamic pressures are consistently larger than the finite difference pressures at the same range, and the two pressures are closer in magnitude, for all ranges, above the burst altitude than below. The average dynamic pressure errors versus range are shown in figure IV-7. Below the burst, the error was -25% to -35%; while above the burst, the error was -8% to -15%.

47

DYNAMIC PRESSURE CONTOURS
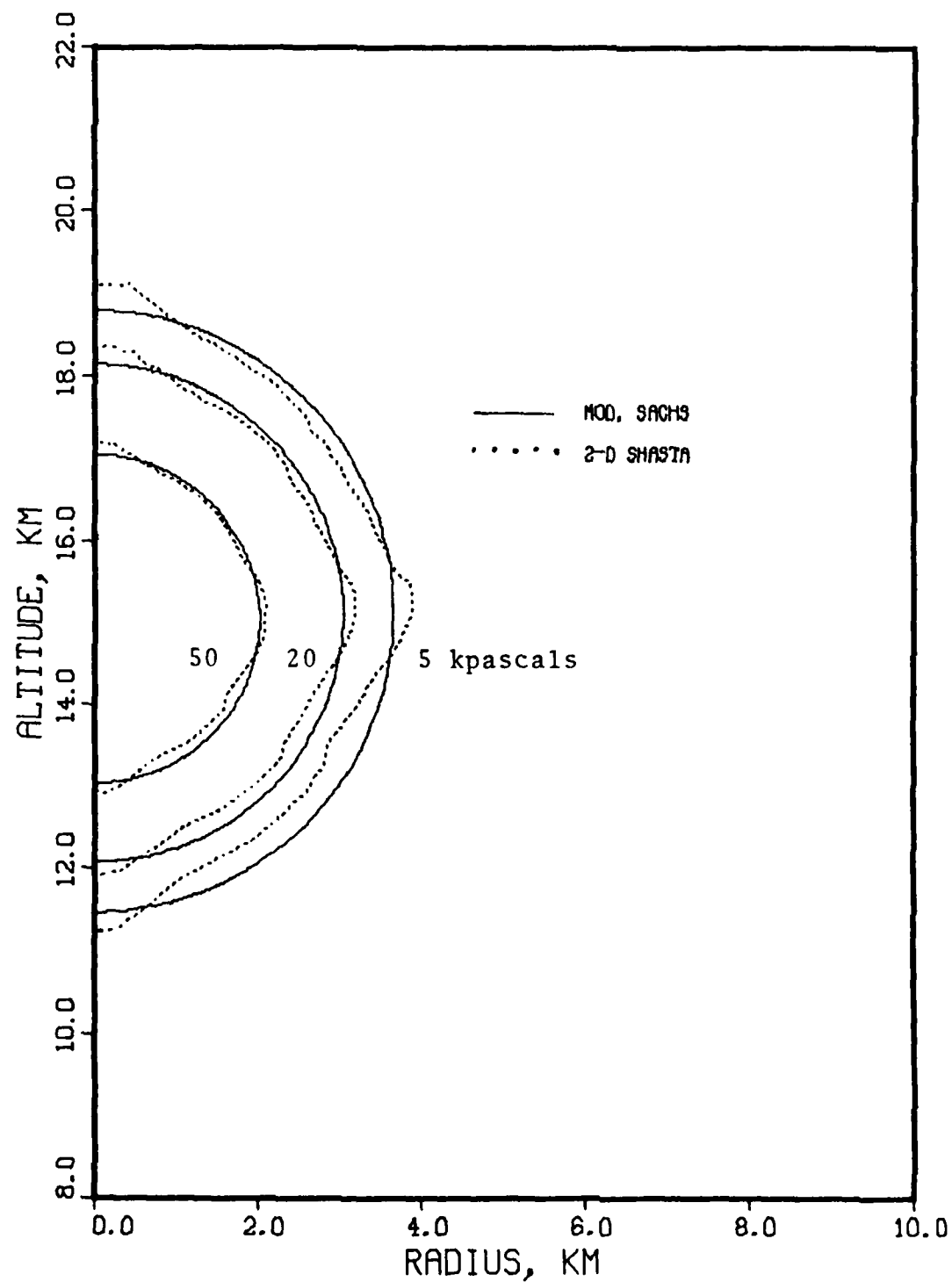
Figure IV-6. Modified Sachs and 2-D finite difference dynamic
pressure contours for three pressure levels.

DYNAMIC PRESSURE ERROR VS RANGE
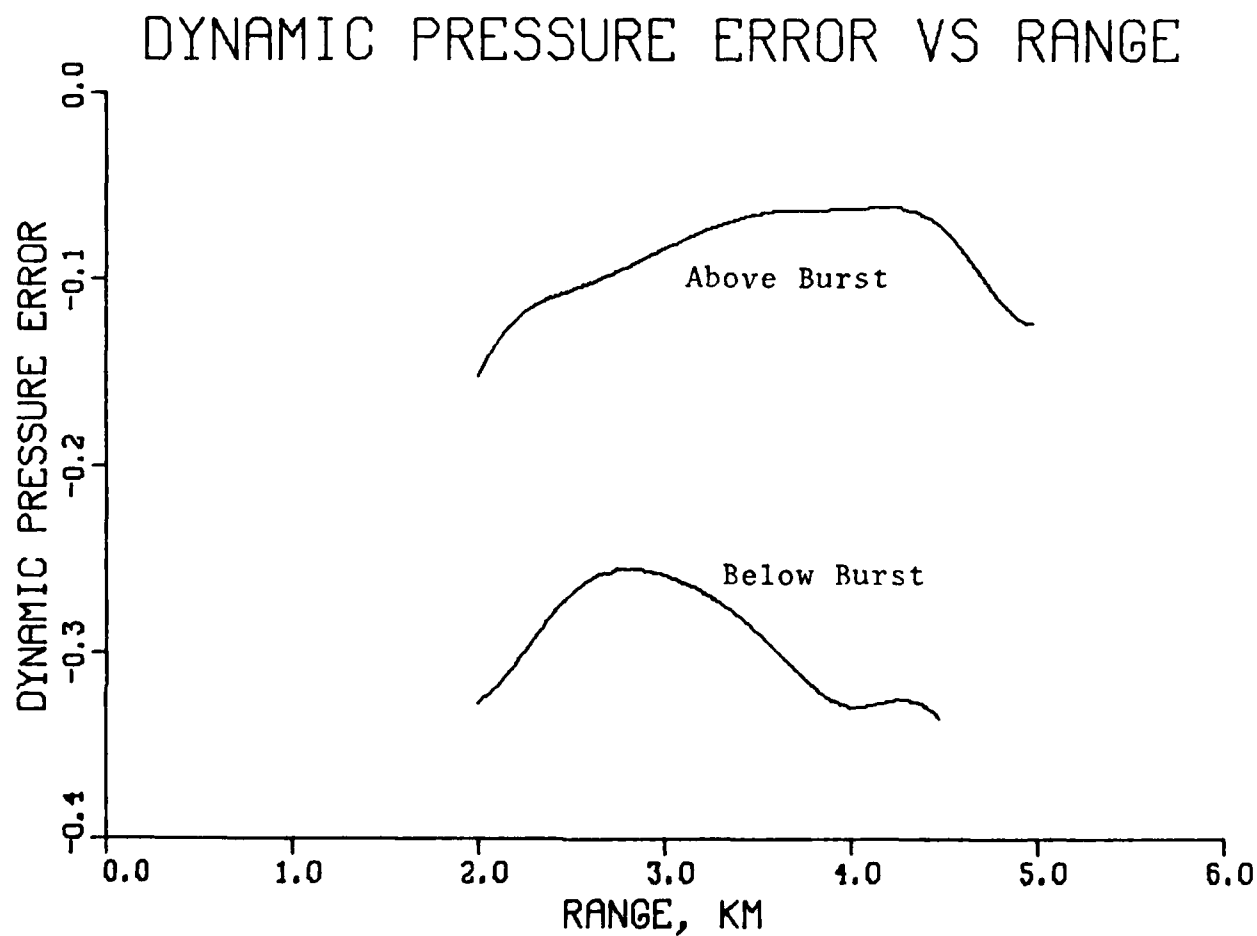
Figure IV-7. Average error of modified Sachs dynamic pressure vs range for ascending and descending directions.

Overpressure-Range Comparisons

The one-dimensional overpressures calculated for the one kiloton and one megaton bursts are plotted in figure IV-8 with the AFWL 1kt standard, where as before the results have been scaled to the 1kt standard.

The maximum difference between the scaled one megaton range and the one kiloton standard was approximately 12% and occurred at a scaled overpressure of about 700 kpascals. In the comparisons that follow, the one-dimensional one megaton overpressures were used for the modified Sachs and Ledsham-Pike scaling.

The overpressure contours calculated using modified Sachs scaling and Ledsham-Pike alpha correction are compared to those calculated with the two-dimensional finite difference code in figure IV-9 for overpressure levels of 60, 30, and 15 kpascals. The slant range R to overpressure Δp is obtained with modified Sachs scaling by using the Sachs scaling relationships for a uniform atmosphere with ambient conditions at $R\cos\theta$ above (or below) the burst point. The range R is scaled as in equation (IV-1), but now R* is the one-dimensional one megaton range to overpressure Δp^*, where
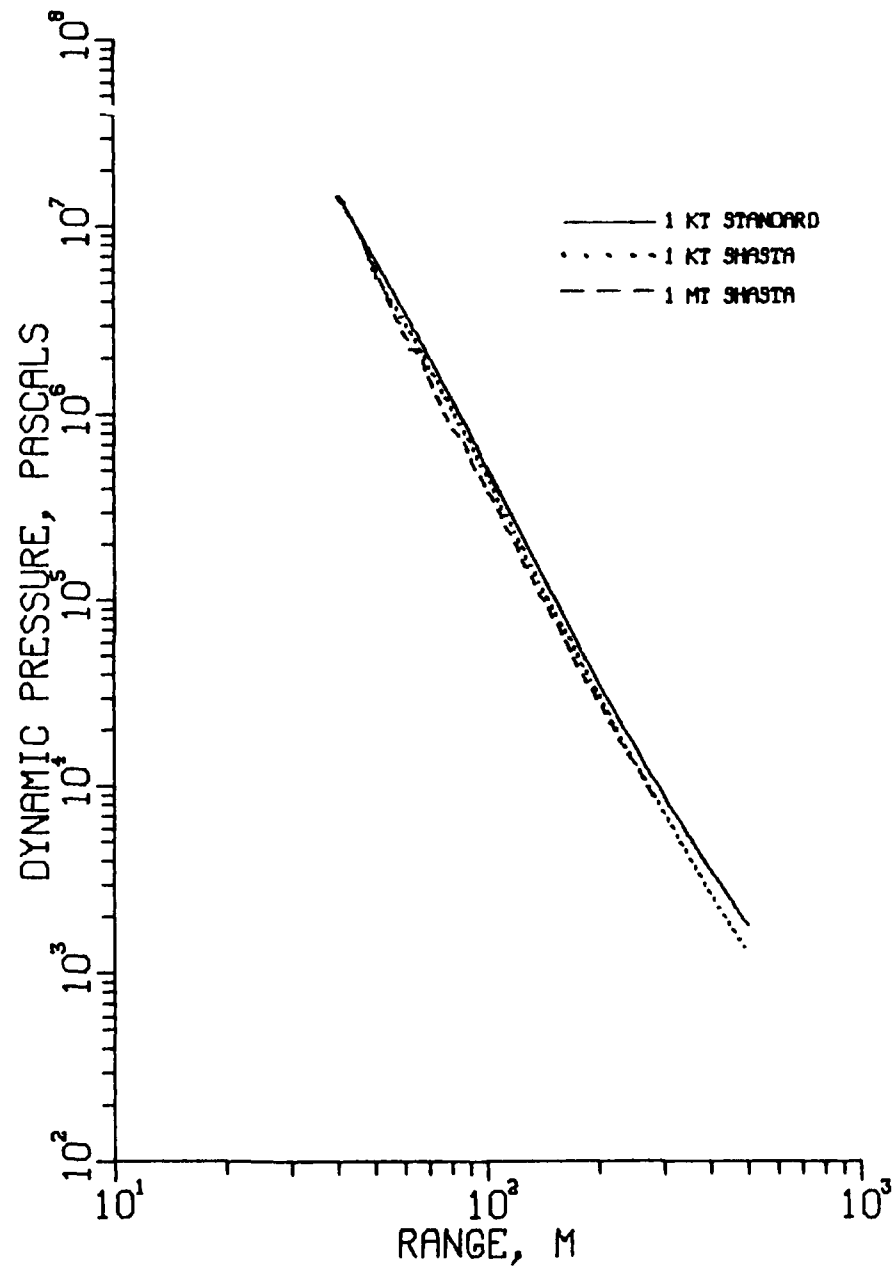
OVERPRESSURES VS. RANGE
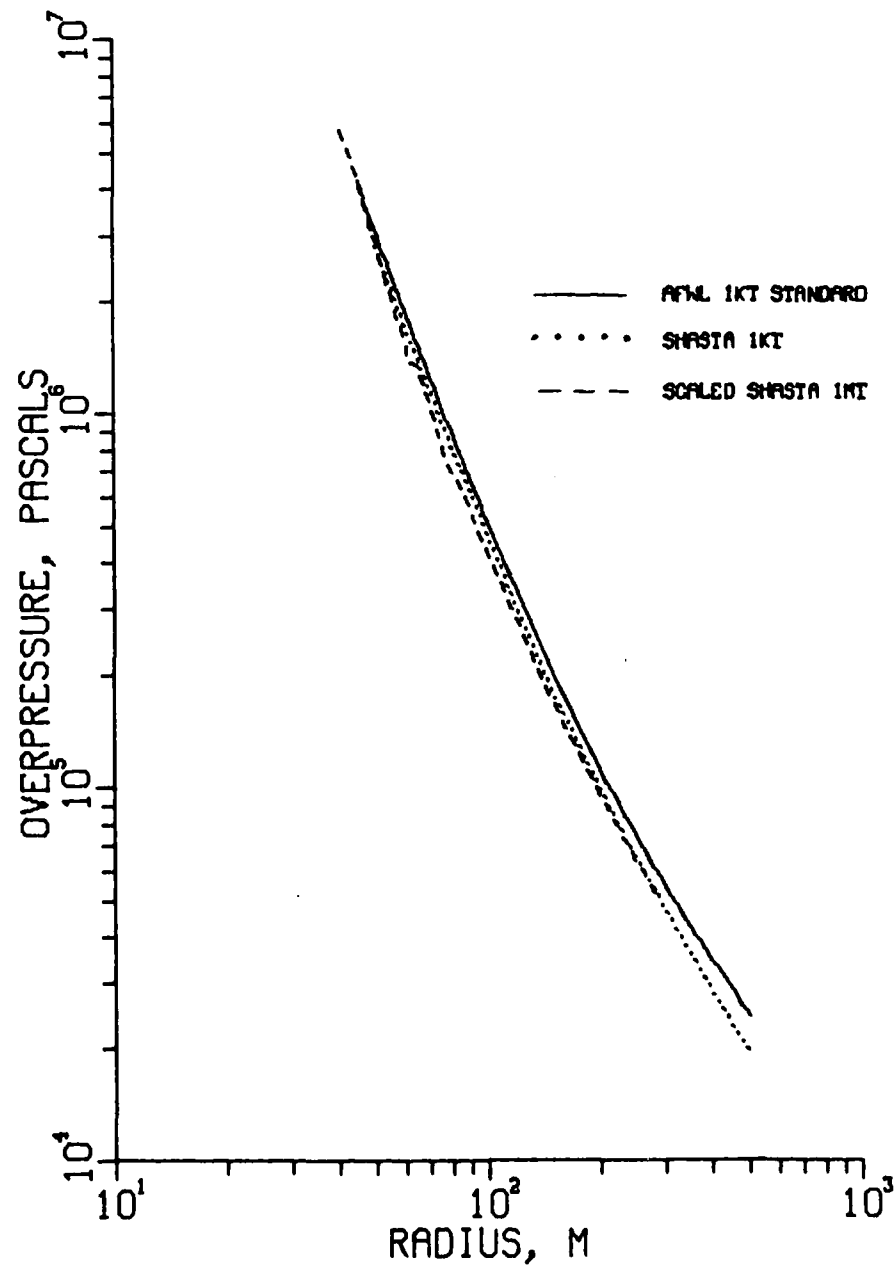
Figure IV-8. One dimensional overpressures vs range. The numerically calculated 1 kt and 1 Mt overpressures are compared to the AFWL 1 kt standard.

$$\Delta P^* = \Delta P \ \frac{P_a^*}{P_a} \qquad\qquad (IV-4)$$

For the Ledsham-Pike method, the overpressure at slant range R is

$$\Delta P = \Delta P^* \left(\frac{P_a}{P_a^*}\right)^\alpha \qquad\qquad (IV-5)$$

where Δp^* is the one-dimensional one megaton overpressure coaltitude with the burst at range R. The α used was the same as that given in figure II-1. An iterative procedure was used to compute the modified Sachs and Ledsham-Pike curves of figure IV-9 to find the correct combinations of overpressures, ranges and ambient pressures.

Two observations are immediately apparent from figure IV-9. The first is that there is practically no difference between the modified Sachs and the Ledsham-Pike overpressure contours. The difference increases slightly with decreasing overpressure levels (longer distances from the burst); however, for the levels shown in figure IV-9, it is reasonable to neglect the difference between overpressures calculated with modified Sachs and Ledsham-Pike. The second observation is that the scaling methods predicted overpressures much closer to the two-dimensional finite difference solution for altitudes above the burst than for altitudes below the burst. The average errors are shown in figure

OVERPRESSURE CONTOURS (SHASTA 1MT)
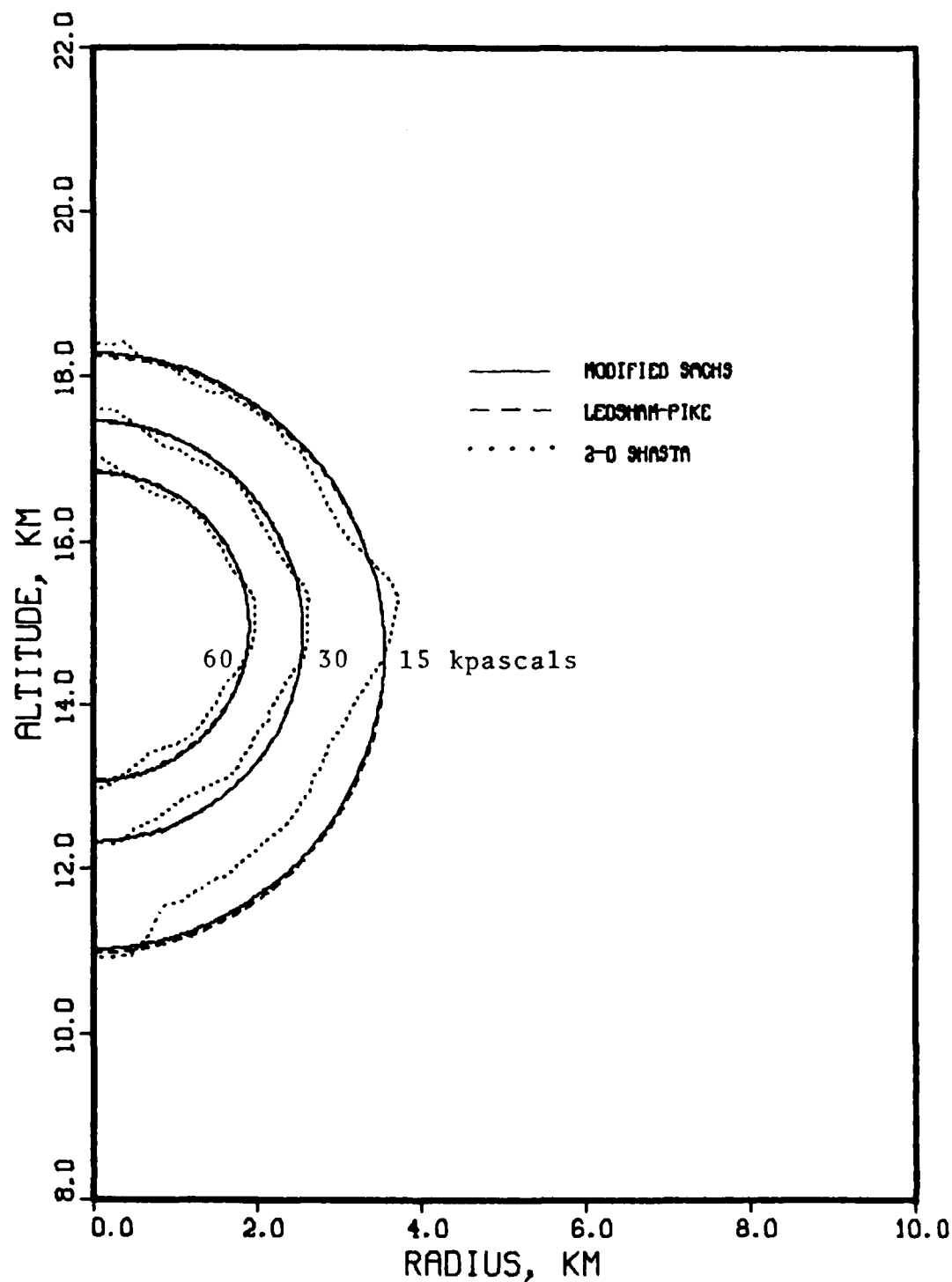
Figure IV-9. Modified Sachs and 2-D finite difference overpressure contours for three overpressure levels.

IV-10, as functions of range. The modified Sachs overpressures were consistently greater than those calculated by the two-dimensional code for a given range. Below the burst altitude, the errors ranged from -20% to -30%, while above the burst the errors were from -6% to -20%. For modified Sachs, this difference cannot be changed; however, with the Ledsham-Pike correction, the situation can be improved.

The difference between the finite difference calculated overpressures and the Ledsham-Pike scaled overpressures can be reduced by adjusting the variable α . Using the calculated values for Δp in equation (II-20), we can compute α as a function of range as

$$\alpha(r) = \frac{\log \Delta P - \log \Delta P^*}{\log P_a - \log P_a^*} \qquad (IV-6)$$

This relationship was used to calculate new values of α for all node points beneath the burst for the last 36 time steps saved on data tapes. Using the method of least squares, these data were then smoothed with a third order polynomial spline, and the resulting $\alpha(r)$ is shown in figure IV-11 with the abscissa scaled one kiloton standard range. Also shown in this figure, is a plot of the original $\alpha(r)$, which when used for the altitudes above the burst point in conjunction with the new values for lower altitudes produced the overpressure contours shown in figure IV-12. The differences between the calculated and scaled results

54

OVERPRESSURE ERROR VS RANGE
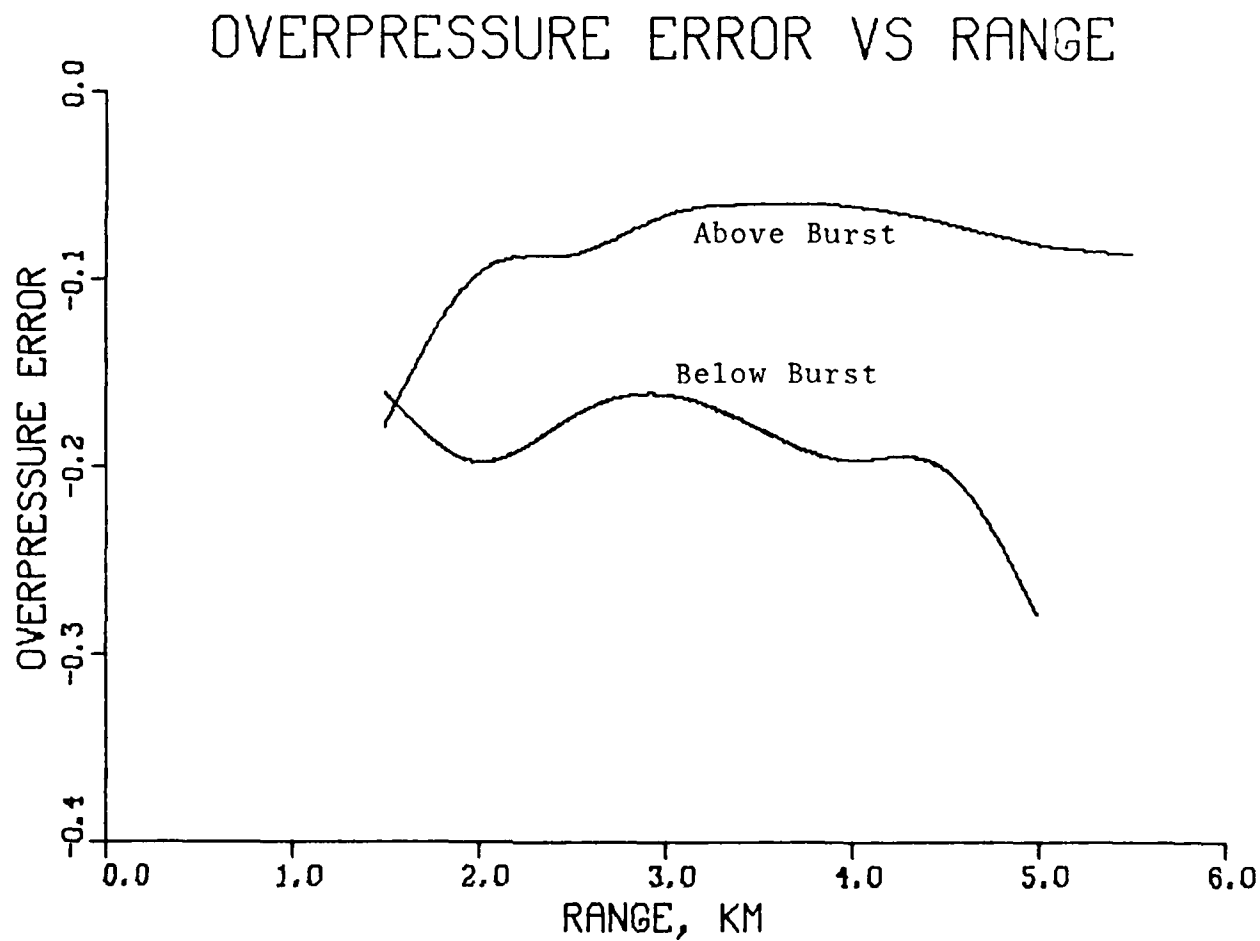
Figure IV-10. Average error of modified Sachs overpressure vs range for ascending and descending directions.
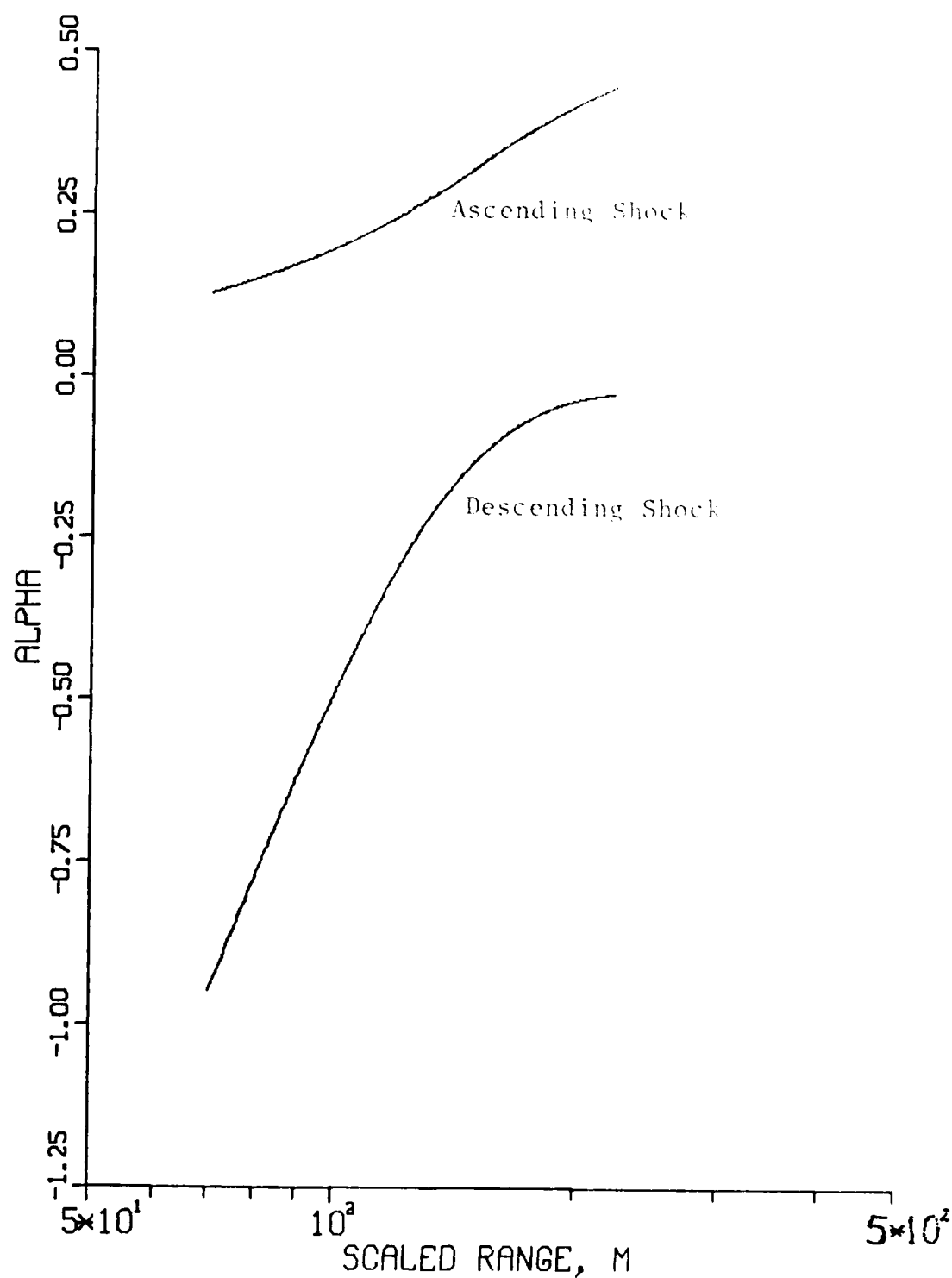
Figure IV-11. New values of Ledsham-Pike alpha correction for descending shock waves. The original values are also shown (for ascending shock waves), and both were used to generate the contours of figure IV-12.

OVERPRESSURE CONTOURS (SHASTA 1MT)
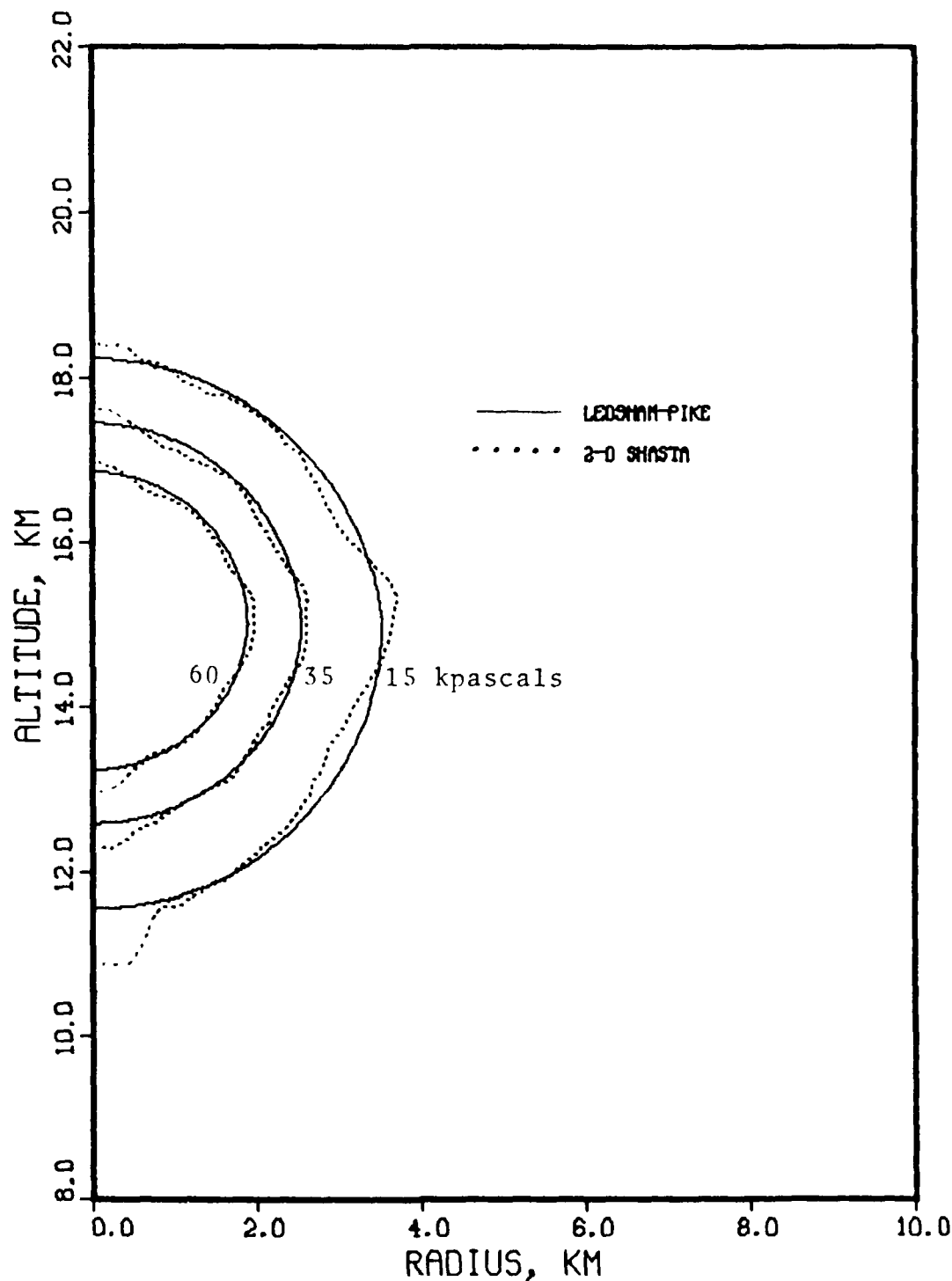
Figure IV-12. Ledsham-Pike and 2-D finite difference overpressure contours for three overpressure levels. The alpha correction factors for the ascending and descending directions are from figure IV-11.

in the descending direction have been reduced to approximately the same values as for the ascending direction.

The validity of this proposed new formulation of the α correction factor depends upon correctly interpreting where the errors occur. In particular, does the true overpressure contour lie near the outside of the "bulge" directly beneath the burst point (which would indicate that modified Sachs and Ledsham-Pike are quite accurate, as shown in figure IV-9), or is the true contour closer to the value indicated by the predominant number of data points further away from the axes and the bulges? The averaging of all data points in the reformulation above implicitly assumes the latter. The answer can be found by running the two-dimensional code a second time with a homogeneous atmosphere. This two-dimensional calculation would in effect simulate a one-dimensional problem, for which we know an exact solution. In a uniform atmosphere, the overpressure contour would be exactly circular at a radius calculated from the one-dimensional results in chapter III with the scaling procedures described in chapter II.

This second calculation was performed, and the resulting 15 kpascal overpressure contour is shown in figure IV-13. The solid line is the "known" solution, and is a semicircle centered about the burst point with radius equal to the range to 15 kpascal overpressure calculated for the one-dimensional one megaton case. Again, the bulges appear along the axes and along the z=15 km line. When figure IV-13 and figure IV-12 are compared, it is
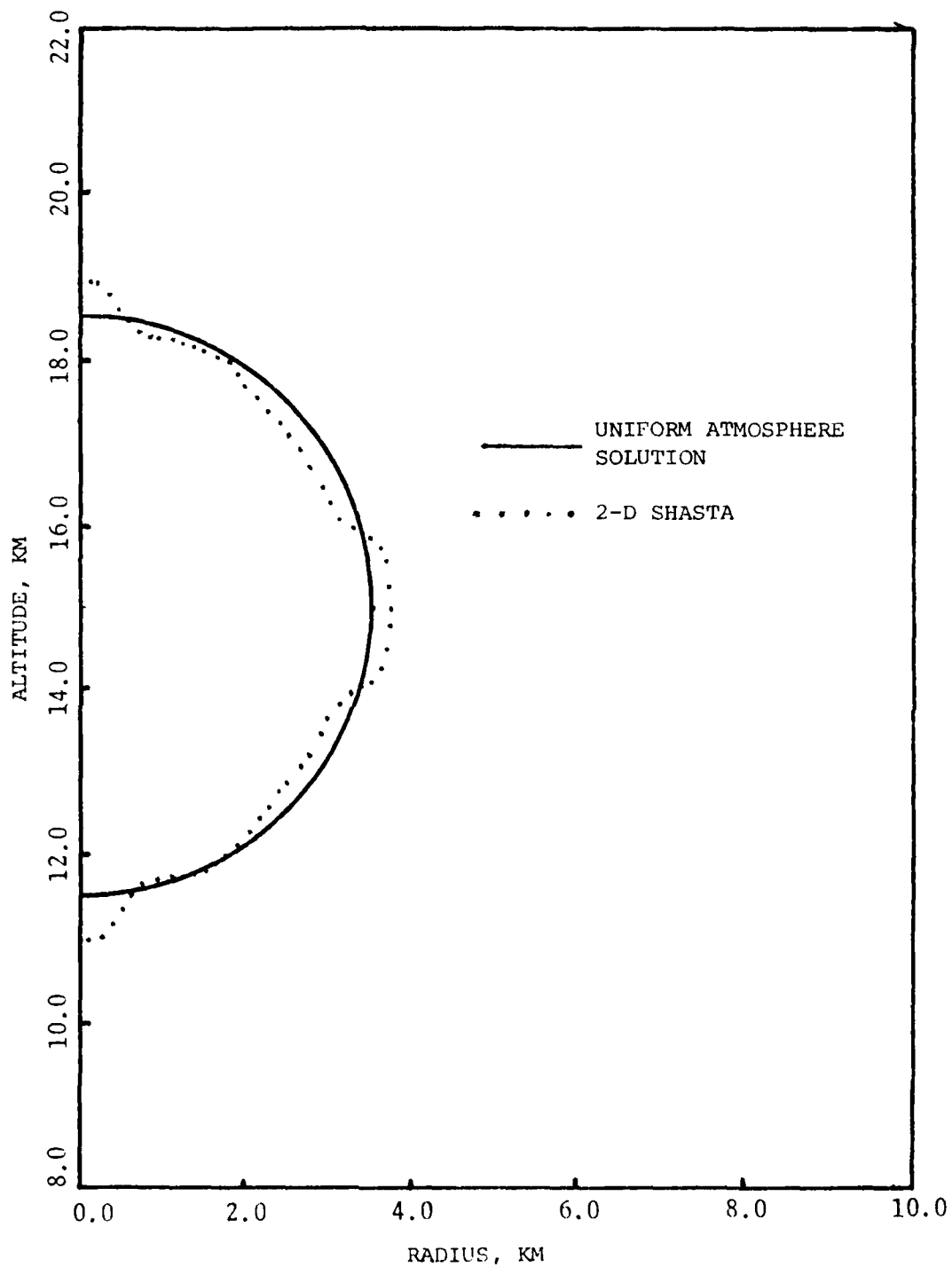
Figure IV-13. Fifteen Kpascal Overpressure Contour for Homogeneous Atmosphere

clear that the two-dimensional solution is nearer the known solution away from these bulges, and therefore the correction factor also is formulated with respect to the two-dimensional solution away from the bulges.

It is reiterated that the uniform atmosphere solution shown in figure IV-13 uses the calculated one-dimensional result from chapter III. The 3.5 km range to 15 kpascal overpressure is slightly lower than the AFWL 1 kt standard scaled to 1 Mt at 15 km height of burst, which is approximately 3.7 km. In fact, if the 3.7 km range was used, it would appear that the outsides of the bulges are the correct result. This is believed to be coincidental. To eliminate the common errors between the one-dimensional and two-dimensional results (especially the "clipping" phenomenon inherent in SHASTA, which affects peak values, see Boris and Book, 1973), the correct one-dimensional reference must be the same calculation. It is also noted that the currently accepted ranges for the 1 kt standard to overpressures less than 30 kpascals are being revised in the direction of the results presented here.*

* Private communication with Lt Tom Lutton, Air Force Weapons Laboratory, January 1983.

Chapter V. Conclusions

The accuracy of the modified Sachs scaling method of transforming one-dimensional blast wave results to account for atmospheric variations with altitude has been evaluated. The shock wave position, peak dynamic pressure, and peak overpressure as functions of position and time as calculated by the modified Sachs method were compared to the results of a two- dimensional finite difference calculation for a one megaton burst at an altitude of 15 kilometers. It was found that the shock wave position predicted by modified Sachs was quite close to that calculated by the two-dimensional code - the magnitude of the average error was less than 8%. The dynamic and the static pressures predicted by modified Sachs were both closer to the two-dimensional calculation for altitudes above the burst point than for altitudes below the burst. The modified Sachs dynamic pressure and overpressure average errors were both about 12% above the burst, while below the burst they averaged about 30% and 25% respectively. Thus, modified Sachs pressures for the descending shock front (which moves into regions of increasing density and pressure) contained twice the error of those for the ascending shock front. These overpressure errors are only slightly higher than those calculated by Lutzky and Lehto for downward propagating shocks.

The Ledsham-Pike correction of scaled overpressures was found to be practically identical to modified Sachs. New values

of the correction factor for the descending shock front were cal-
culated from the two-dimensional finite difference overpressures.
These new values are the best fit to the data calculated by one
method for one set of burst conditions, and to test their accura-
cy and reliability they should be used in further comparisons
with other yields at different altitudes.

The SHASTA flux-corrected transport method was used for the
one- dimensional calculations in spherical coordinates, and for
the two-dimensional calculations with a time step splitting al-
gorithm which alternated between Cartesian and cylindrical coor-
dinates. In all cases, the method kept the shock sharp, with a
thickness three or four mesh intervals wide, and produced no
observable oscillations in the solutions.

Appendix A: The SHASTA Finite Difference Scheme

All flux-corrected transport schemes consist of two steps: the transport, or convective stage and the anti-diffusive, or corrective stage. In the transport stage the flow quantities (density, momentum, and energy) are convected one time step using some conservative difference scheme which includes a large diffusive component. This erroneous diffusion is removed in the antidiffusive stage where special conditions are applied near shocks to retain sharp gradients.

The SHASTA finite difference scheme used here is the original flux-corrected transport method of Boris and Book (1973). Diffusion is included inherently, and there is no need to add pseudo-viscosity as in Lax-Wendroff, leapfrog, donor cell, or other "conventional" schemes. To illustrate the transport stage of SHASTA, consider the one-dimensional mass transfer example shown in figure A-1. The density profile is shown as a solid line at the time t^n at the node points j-1, j, and j+1. The density is assumed to be constant over the mesh interval $(j-\frac{1}{2}, j+\frac{1}{2})$. The arrows at the node points indicate displacements over the time interval $\Delta t = t^{n+1} - t^n$. The transported density values ρ_{j-1}^-, ρ_{j-1}^-, ρ_j^-, and ρ_{j+1}^+ are determined by conserving mass during the time step in a Lagrangian sense. For example, conservation of mass for the cell $(j, j+\frac{1}{2})$ requires

$$\left(\rho_j^n + S_j^+ \Delta t\right)\left(\frac{r_{j+1} - r_j}{2}\right) = \rho_j^+ \left[\frac{(r_{j+1} + v_{j+1}\Delta t) - (r_j - v_j \Delta t)}{2}\right] \tag{A-1}$$

63
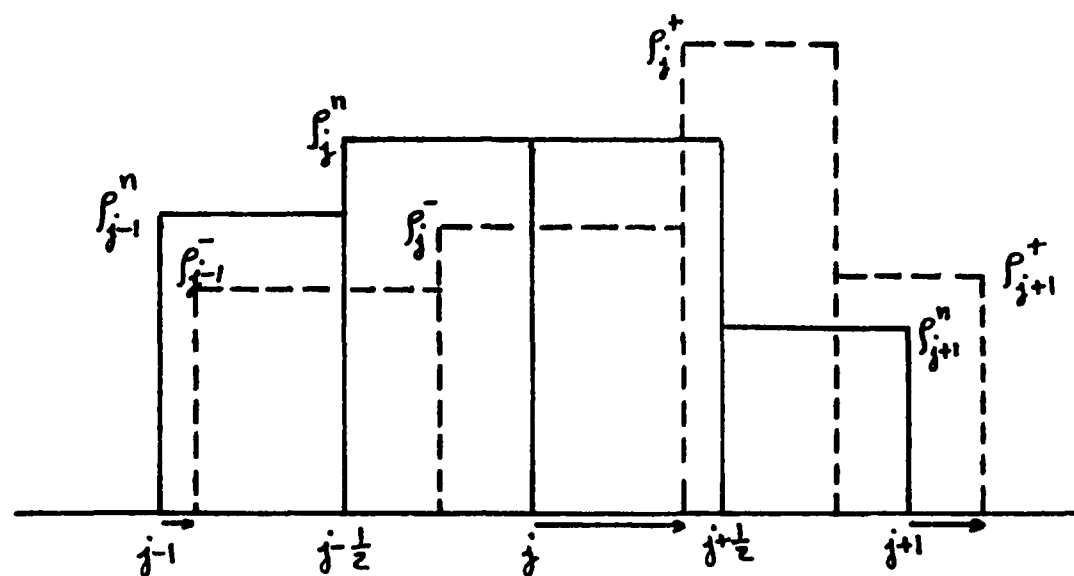
Figure A-1. One dimensional mass advection. The density profile is advected one time step with variable velocities.

or,

$$\rho_j^+ = \frac{\rho_j^n + S_j^+ \Delta t}{1 + \frac{\Delta t}{(r_{j+1} - r_j)}(v_{j+1} - v_j)} \quad \text{(A-2)}$$

where S* is the source term. (Note that in the equations of hydrodynamics, there is no mass source term, but there are sources of momentum and energy.) The other cells are treated similarly, resulting in

$$\rho_{j-1}^- = \frac{\rho_{j-1}^n + S_j^- \Delta t}{1 + \frac{\Delta t}{(r_j - r_{j-1})}(v_j - v_{j-1})} \quad \text{(A-3)}$$

$$\rho_j^- = \frac{\rho_j^n + S_j^- \Delta t}{1 + \frac{\Delta t}{(r_j - r_{j-1})}(v_j - v_{j-1})} \quad \text{(A-4)}$$

$$\rho_{j+1}^+ = \frac{\rho_{j+1}^n + S_j^+ \Delta t}{1 + \frac{\Delta t}{(r_{j+1} - r_j)}(v_{j+1} - v_j)} \quad \text{(A-5)}$$

To ensure that no grid point convects past a cell boundary, we require

65

$$\left| \mathcal{v}_i \; \frac{\Delta t}{\Delta r_i} \right| \; < \; \frac{1}{2} \qquad\qquad (A-6)$$

This transport process exactly conserves mass in each mesh interval, and if the new density values at time t^{n+1} were computed by summing the contributions of each convected cell, there would be no diffusion. To introduce a diffusive component, Boris and Book linearly interpolate between adjacent node points for the density values. These fluid element trapezoids are shown in figure A-2. Clearly, the area under each trapezoid equals the area under the corresponding pair of rectangles in A-1, and hence mass is fully conserved; however, some mass that was convected into cell $(j-\frac{1}{2}, \; j+\frac{1}{2})$ is transfered to adjacent cells by the linear interpolation. This is the origin of mass diffusion. The diffused mass is represented in figure A-3 by the shaded areas.

Figure A-3 shows the details of the transport and diffusion of mass for cell $(j-\frac{1}{2}, \; j+\frac{1}{2})$. The density for this cell at time t^{n+1} is $\rho_j^{n+1} = \rho_j^{TD}$, where superscript TD stands for transported and diffused. ρ_j^{TD} is computed by summing the contributions to the cell from each adjacent trapezoid:

$$\rho_j^{TD} \left[\frac{r_{j+1} - r_j}{2} + \frac{r_j - r_{j-1}}{2} \right] \; =$$

$$\frac{1}{2}\left[\rho_j^+ + \frac{\rho_j^+ \left(r_{j+1} + v_{j+1}\Delta t - \frac{r_j + r_{j+1}}{2}\right) + \rho_{j+1}^- \left(\frac{r_j + r_{j+1}}{2} - r_j - v_j \Delta t\right)}{(r_{j+1} - r_j) + \Delta t (v_{j+1} - v_j)} \right] \left(\frac{r_{j+1} + r_j}{2} - r_j - v_j \Delta t \right)$$

$$+ \frac{1}{2}\left[\rho_j^- + \frac{\rho_{j-1}^- \left(r_j + v_j \Delta t - \frac{r_j + r_{j-1}}{2}\right) + \rho_j^- \left(\frac{r_j + r_{j-1}}{2} - r_{j-1} - v_{j-1}\Delta t\right)}{(r_j - r_{j-1}) + \Delta t (v_j - v_{j-1})} \right] \left(r_j - \frac{r_j + r_{j-1}}{2} + v_j \Delta t \right)$$

$$(A-7)$$

Figure A-2. Fluid element trapezoids. The area under each trapezoid equals the area under each corresponding rectangle of figure A-1, but there is a net loss of mass in the cell (j-   ,j+).
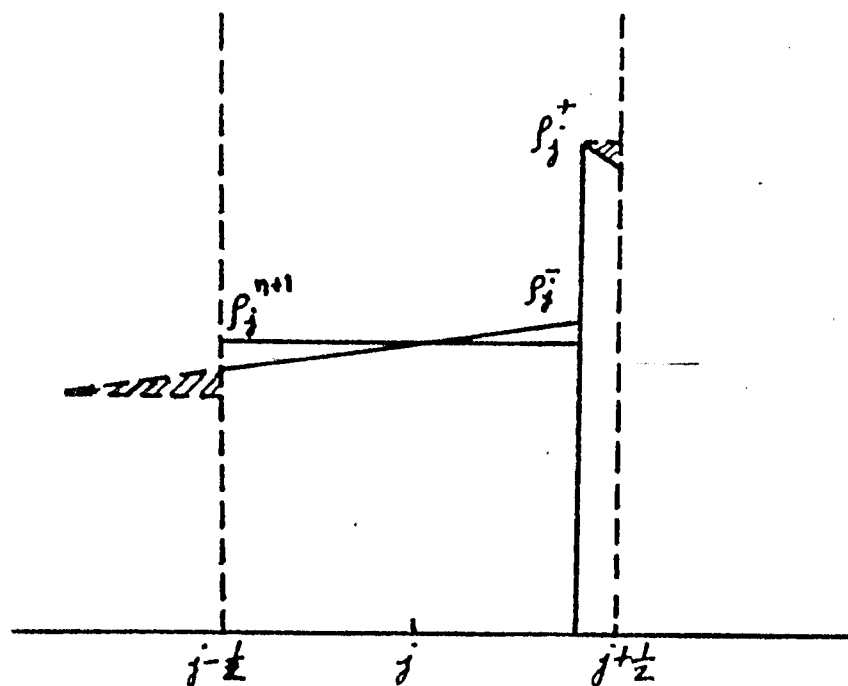
Figure A-3. Transported and diffused density. The density at time t   is the sum of the contributions from the two surrounding trapezoids. The diffused mass is represented by the shaded area.

Now introduce two very convenient parameters

$$Q_j^+ = \frac{\frac{1}{2} - v_j^{\cdot} \frac{\Delta t}{(r_{j+1} - r_j)}}{1 + \frac{\Delta t}{(r_{j+1} - r_j)}(v_{j+1} - v_j)} \tag{A-8}$$

$$Q_j^- = \frac{\frac{1}{2} + v_j^{\cdot} \frac{\Delta t}{(r_j - r_{j-1})}}{1 + \frac{\Delta t}{(r_j - r_{j-1})}(v_j - v_{j-1})} \tag{A-9}$$

and substitute (A-2)-(A-5) into (A-7):

$$\rho_j^{TD} = \left(\frac{r_j - r_{j-1}}{r_{j+1} - r_{j-1}}\right)(Q_j^-)^2 (\rho_{j-1}^n - \rho_j^n) + \left(\frac{r_{j+1} - r_j}{r_{j+1} - r_{j-1}}\right)(Q_j^+)^2 (\rho_{j+1}^n - \rho_j^n)$$

$$+ 2\left(\frac{r_{j+1} - r_j}{r_{j+1} - r_{j-1}}\right) Q_j^+ (\rho_j^n - S_j^+) + 2\left(\frac{r_j - r_{j-1}}{r_{j+1} - r_{j-1}}\right) Q_j^- (\rho_j^n - S_j^-) \tag{A-10}$$

Equation (A-10) is a generalization of the SHASTA difference equation given by Boris and Book (1973). The scheme consists of an essentially second order differencing of the convection term plus a strong diffusion. For a uniformly vanishing velocity field, this strong diffusion amounts to operating on the initial density profile in the following way:

68

$$f_i^{n+1} = f_i^n + \frac{2}{(r_{j+1} - r_{j-1})} \, \eta \left[(r_{j+1} - r_j) f_{j+1}^n - (r_{j+1} - r_{j-1}) f_j^n + (r_j - r_{j-1}) f_{j-1}^n \right] \tag{A-11}$$

For uniform zero velocities, $\eta = \frac{1}{8}$; but for non-zero velocities, η is $\frac{1}{8}$ plus small velocity- and wave number-dependent terms. The effect of these small corrections to η are shown by Boris and Book (1973) and Boris, Book and Hain (1975) to be small, and they are neglected in this study. Thus, $\eta = \frac{1}{8}$.

We wish to write (A-10) in "flux" form,

$$f_j^{TD} = f_j^n + 2 \left(\frac{r_j - r_{j-1}}{r_{j+1} - r_{j-1}} \right) \left(\tilde{f}_{j-1}^D + \tilde{f}_{j-1}^T \right) - 2 \left(\frac{r_{j+1} - r_j}{r_{j+1} - r_{j-1}} \right) \left(\tilde{f}_{j+1}^D + \tilde{f}_{j+1}^T \right) \tag{A-12}$$

where $\tilde{f}^D$ and $\tilde{f}^T$ are the diffusive and transportive fluxes, and where we have temporarily neglected the source terms. We know that

$$\tilde{f}_{j \pm 1}^D = \pm \, \eta \left(f_j^n - f_{j \pm 1}^n \right) \tag{A-13}$$

because the diffused solution

$$f_j^D = f_j^n + \eta \left(f_{j+1}^n - 2 f_j^n + f_{j-1}^n \right) \tag{A-14}$$

implies

$$\rho_j^D = \rho_j^n + \tilde{f}_{j-\frac{1}{2}}^D - \tilde{f}_{j+\frac{1}{2}}^D \tag{A-15}$$

Now (A-10) and (A-12) can be equated, and after some algebra we find

$$\tilde{f}_{j+\frac{1}{2}}^T = \left[\frac{1}{2}(Q_j^+)^2 - Q_j^+ - \eta + \frac{1}{2}\right]\rho_j^n - \left[\frac{1}{2}(Q_j^+)^2 - \eta\right]\rho_{j+1}^n \tag{A-16}$$

$$\tilde{f}_{j-\frac{1}{2}}^T = \left[\frac{1}{2}(Q_j^-)^2 - \eta\right]\rho_j^n - \left[\frac{1}{2}(Q_j^-)^2 - Q_j^- - \eta + \frac{1}{2}\right]\rho_j^n \tag{A-17}$$

Written in flux form, equation (A-12) explicitly states that the transported and diffused density at time t^{n+1} equals the old value at t^n plus the influx due to transport and diffusion minus the outflux. Appropriate scale factors are included to account for a non-uniform grid.

Another set of scale factors must be added to allow use of (A-12) for a curvilinear coordinate system. The generalized one-dimensional radial continuity equation can be written (again neglecting source terms)

$$\frac{\partial \rho}{\partial t} + \frac{1}{r^\nu}\frac{\partial}{\partial r}(r^\nu \rho v) = 0 \tag{A-18}$$

where $\nu = 0$, 1, or 2 for a one-dimensional Cartesian, cylindrical, or spherical coordinate system respectively. Using $\tilde{f}_{j\pm\frac{1}{2}}$ as the in- and out-fluxes, the finite difference approximation of (A-18) is

$$\rho_j^{n+1} = \rho_j^n + \left(\frac{r_{j-\frac{1}{2}}}{r_j}\right)^\nu \tilde{f}_{j-\frac{1}{2}} - \left(\frac{r_{j+\frac{1}{2}}}{r_j}\right)^\nu \tilde{f}_{j+\frac{1}{2}} \qquad \text{(A-19)}$$

The one-dimensional difference equation (A-12) written for variable mesh spacing, generalized coordinates, and with source terms is thus

$$\rho_j^{TD} = \rho_j^n + \left(\frac{r_{j-\frac{1}{2}}}{r_j}\right)^\nu \left(\frac{r_j - r_{j-1}}{r_{j+1} - r_{j-1}}\right)\left(\tilde{f}_{j-\frac{1}{2}}^D + \tilde{f}_{j-\frac{1}{2}}^T\right) - \left(\frac{r_{j+\frac{1}{2}}}{r_j}\right)^\nu\left(\frac{r_{j+1} - r_j}{r_{j+1} - r_{j-1}}\right)\left(\tilde{f}_{j+\frac{1}{2}}^D + \tilde{f}_{j+\frac{1}{2}}^T\right)$$
$$- 2\left(\frac{r_{j+1} - r_j}{r_{j+1} - r_{j-1}}\right) Q_j^+ S_j^+ \quad - \quad 2\left(\frac{r_j - r_{j-1}}{r_{j+1} - r_{j-1}}\right) Q_j^- S_j^-$$
$$\text{(A-20)}$$

This difference equation advances the mass, momentum, and energy densities one time step by conservative transportive convection, but it includes a large diffusive component.

The second stage of flux-corrected transport is the antidiffusive stage. Antidiffusive fluxes are added to the solution to remove the erroneous diffusion from the transport stage in a conservative, but nonlinear manner. The diffusive fluxes $\tilde{f}_{j\pm\frac{1}{2}}^D$ would

71

be exactly cancelled if these values were subtracted from the values everywhere they were added to the solution; however, as shown below, the antidiffusive fluxes are limited in magnitude so as to eliminate dispersively generated ripples in the solution. Although the magnitude of this corrective diffusion depends only on the local values of ρ from point to point, the antidiffusion operation is conservative.

Since ρ^{TD} is the result of diffusive transport, the antidiffusive stage of flux-corrected transport results in the final values ρ^{n+1} :

$$\rho_i^{n+1} = \rho_j^{TD} - \tilde{f}_{j+\frac{1}{2}}^A + \tilde{f}_{i-\frac{1}{2}}^A \tag{A-21}$$

where $\tilde{f}^A$ is the antidiffusive flux, and the scale factors are temporarily omitted. For exact cancellation of diffusion

$$\tilde{f}_{i\pm\frac{1}{2}}^A = \pm\eta\left(\rho_{j\pm 1}^{TD} - \rho_i^{TD}\right) \tag{A-22}$$

Such a prescription is obviously conservative, since every diffusive flux is added once to the solution and then subtracted once somewhere else. In addition to this definition of antidiffusion, Boris and Book prescribe the following qualitative limitation to inhibit generating nonphysical oscillations in the

72

solution:

"The antidiffusive stage should generate no new maxima or minima in the solution, nor should it accentuate already existing extrema." (Boris and Book, 1976)

The values $\tilde{f}^A$ are limited term-by-term so that no antidiffusive flux transfer of mass can push the density value at any grid point beyond the density value at neighboring points. The corrected fluxes $\tilde{f}^c$ are given by

$$\tilde{f}^c_{j+\frac{1}{2}} = S \cdot \max\left\{ 0, \min\left[S \cdot \Delta_{j-\frac{1}{2}} \, , \, \gamma \cdot \Delta_{j+\frac{1}{2}} \, , \, S \cdot \Delta_{j+\frac{3}{2}} \right] \right\} \qquad (A-23)$$

where

$$\Delta_{j+\frac{1}{2}} = \rho^{TD}_{j+1} - \rho^{TD}_{j}$$

$$S = \text{sign} \; \Delta_{j+\frac{1}{2}}$$

It can be shown that (A-23) is the correct formula to quantify the perscribed qualitative limitation on the fluxes by considering all possible permutations of the signs of $\tilde{f}^A_{j+\frac{1}{2}}$, $\Delta_{j-\frac{1}{2}}$, and $\Delta_{j+\frac{3}{2}}$ (See Boris, Book and Hain, Section IV.) In particular, a local extrema is indicated for the value ρ^{TD}_j if either $\Delta_{j-\frac{1}{2}}$ or $\Delta_{j+\frac{1}{2}}$ are opposite in sign to $\tilde{f}^A_{j+\frac{1}{2}}$. In this case the flux limiter sets $\tilde{f}^c_{j+\frac{1}{2}}$ =0. On the other hand, when $\tilde{f}^A_{j+\frac{1}{2}}$, $\Delta_{j-\frac{1}{2}}$, and $\Delta_{j+\frac{3}{2}}$ are all the same sign, the flux limiter leaves $\tilde{f}^c_{j+\frac{1}{2}} = \tilde{f}^A_{j+\frac{1}{2}}$ unless the jth point would be pushed below the $(j-1)^{st}$, or if the $(j+1)^{st}$ point would

73

be pushed above or below the $(j+2)^{nd}$. In this case, $\tilde{f}^A_{i+\frac{1}{2}}$ is corrected to avoid creating a new extrema.

Using the corrected antidiffusive fluxes, the new values ρ^{n+1}_j are computed as

$$\rho^{n+1}_j = \rho^{TD}_j - \left(\frac{r_{j+\frac{1}{2}}}{r_j}\right)^\nu \tilde{f}^C_{i+\frac{1}{2}} + \left(\frac{r_{j-\frac{1}{2}}}{r_j}\right)^\nu \tilde{f}^C_{i-\frac{1}{2}} \qquad (A-24)$$

Time-Step Splitting

The two-dimensional solution procedure was a time-step splitting technique, using a separate Cartesian and cylindrical subroutine for the z- and r-directions. For a centered time integration, provisional values are calculated for one-half time steps, and these provisional values are used to advance the values one full time step.

If we represent the operator $F[U,v,S,\Delta r,\Delta t]$ as that which advances $\{U\}$ a time-step Δt on a grid Δr (or Δz) using velocities v and source terms S, then the complete cycle is as follows:

74

first the r half cycle

$$v_r = \rho v_r / \rho$$

$$v_z = \rho v_z / \rho$$

$$P = (\gamma - 1)\left[E - \tfrac{1}{2}\rho(v_r)^2 - \tfrac{1}{2}\rho(v_z)^2\right]$$

$$\rho = F\left[\rho,\ v_r,\ 0,\ \Delta r,\ \Delta t/2\right]$$

$$\rho v_r = F\left[\rho v_r,\ v_r,\ \partial P/\partial r,\ \Delta r,\ \Delta t/2\right]$$

$$\rho v_z = F\left[\rho v_z,\ v_r,\ 0,\ \Delta r,\ \Delta t/2\right]$$

$$E = F\left[E,\ v_r,\ \partial(P v_r)/\partial r,\ \Delta r,\ \Delta t/2\right]$$

then the r whole cycle

$$v_r = \rho v_r / \rho$$

$$v_z = \rho v / \rho$$

$$P = (\gamma - 1)\left[E - \tfrac{1}{2}\rho(v_r)^2 - \tfrac{1}{2}\rho(v_z)^2\right]$$

$$\rho = F\left[\rho,\ v_r,\ 0,\ \Delta r,\ \Delta t\right]$$

$$\rho v_r = F\left[\rho v_r,\ v_r,\ \partial P/\partial r,\ \Delta r,\ \Delta t\right]$$

$$\rho v_z = F\left[\rho v_z,\ v_r,\ 0,\ \Delta r,\ \Delta t\right]$$

$$E = F\left[E,\ v_r,\ \partial(P v_r)/\partial r,\ \Delta r,\ \Delta t\right]$$

next the z half cycle

$$v_z = \rho v_z / \rho$$

$$v_r = \rho v_r / \rho$$

$$P = (\gamma - 1)\left[E - \tfrac{1}{2}\rho(v_r)^2 - \tfrac{1}{2}\rho(v_z)^2\right]$$

$$\rho = F\left[\rho,\ v_z,\ 0,\ \Delta z,\ \Delta t/2\right]$$

$$\rho v_r = F\left[\rho v_r,\ v_z,\ 0,\ \Delta z,\ \Delta t/2\right]$$

$$\rho v_z = F\left[\rho v_z,\ v_z,\ \partial P\ /\partial z,\ \Delta z,\ \Delta t/2\right]$$

$$E = F\left[E,\ v_z,\ \partial(P v_z)/\partial z,\ \Delta z,\ \Delta t/2\right]$$

and finally the z whole cycle

$$v_z = \rho v_z / \rho$$

$$v_r = \rho v_r / \rho$$

$$P = (\gamma - 1)\left[E - \tfrac{1}{2}\rho(v_r)^2 - \tfrac{1}{2}\rho(v_z)^2\right]$$

$$\rho = F\left[\rho,\ v_z,\ 0,\ \Delta z,\ \Delta t\right]$$

$$\rho v_r = F\left[\rho v_r,\ v_z,\ 0,\ \Delta z,\ \Delta t\right]$$

$$\rho v_z = F\left[\rho v_z,\ v_z,\ \partial P/\partial z,\ \Delta z,\ \Delta t\right]$$

$$E = F\left[E,\ v_z,\ \partial(P v_z)/\partial z,\ \Delta z,\ \Delta t\right]$$

Appendix B: Stable Atmospheric Model

The earth's atmospheric temperature profile was modeled as consisting of six linear segments. Hydrostatic equlibrium was assumed, and the air was treated as a homogeneous mixture of its constituent gases.

The exact values of temperature were taken from the U.S. Standard Atmosphere (1976) for the base of each of the six linear segments, and the corresponding pressure is calculated to satisfy hydrostatic equilibrium

$$\frac{dP}{dz} = -g(z)\, \rho(z) \qquad \text{(B-1)}$$

where $g(z)$ is the altitude-dependent gravitational acceleration. The pressure, temperature and density of the air are related by the ideal gas law

$$P(z) = \frac{\rho(z)\, R\, T(z)}{M} \qquad \text{(B-2)}$$

where R is the universal gas constant and M is the molecular weight. Dividing (B-1) by p yields

$$\frac{dP}{P} = d(\ln P) = \frac{-g(z)M}{RT}dz \qquad \text{(B-3)}$$

The inverse square law of gravitation is used to find g(z)

$$g(z) = g_0 \left(\frac{r}{r_0 + z}\right)^2 \qquad \text{(B-4)}$$

where g_0 is the sea level acceleration of gravity (9.80665 m/sec) and r_0 is the effective radius of the earth (6356.766 km).

Within each of the linear segments the temperature is

$$T(z) = T_b + L_b(z - z_b) \qquad \text{(B-5)}$$

where T_b is the temperature of the base of the segment (i.e. at $z = z_b$) and the temperature gradient is L_b. Substituting (B-4) and (B-5) into (B-3) gives

$$d(\ln P) = -g_0 \left(\frac{r_0}{r_0 + z}\right) \frac{M}{R[T_b + L_b(z - z_b)]} \qquad \text{(B-6)}$$

Integrating over the length of the segment,

$$\ln \frac{P_t}{P_b} = -\frac{g_0 r_0^2 M}{R} \int_{z_b}^{z_t} \frac{1}{(r_0 + z)^2 [T_b + L_b(z - z_b)]} dz \qquad \text{(B-7)}$$

where z_b and z_t are the altitudes at the base and top of the segment, and P_b and P_t are the respective pressures. Carrying out the integration gives

$$P_z = P_b \exp\left\{ \frac{g_0 r_0^2 M}{R L_b \left(r_0 + z_b - T_b/L_b\right)} \left[\frac{z_b - z_z}{\left(r_0 + z_z\right)\left(r_0 + z_b\right)} \right.\right.$$

$$\left.\left. - \frac{1}{r_0 + z_b - T_b/L_b} \; \ln \frac{\left(r_0 + z_z\right) T_b}{\left(r_0 + z_b\right)\left[T_b + L_b\left(z_z - z_b\right)\right]} \right] \right\} \qquad \text{(B-8)}$$

Using equation (B-8), the pressure at any altitude below 86 km can be calculated. For example, at the bases of each of the six linear temperature segments the pressures are as shown in table B-1. To calculate the pressure at any general altitude, the temperature is found from (B-5) and then (B-8) is used with (p)z instead of p and z=z . With the pressure and temperature known, the equation of state is used to calculate density.

Table B-1. Base Values of Pressure, Temperature, and Temperature Gradient

Altitude, km	Pressure, Pascals	Temperature, K	Gradient, K/km
0	101325.0	288.150	-6.488727
11	22702.70	216.774	-0.00956044
20.1	5446.865	216.687	0.9974380
32.2	863.9094	228.756	2.756184
47.4	110.2434	270.650	-0.05878049
51.5	66.21404	270.409	-2.738829
72.0	3.841296	214.263	-1.956643
86.0	0.3737405	186.870	0.1087500

Appendix C: Shock Profiles
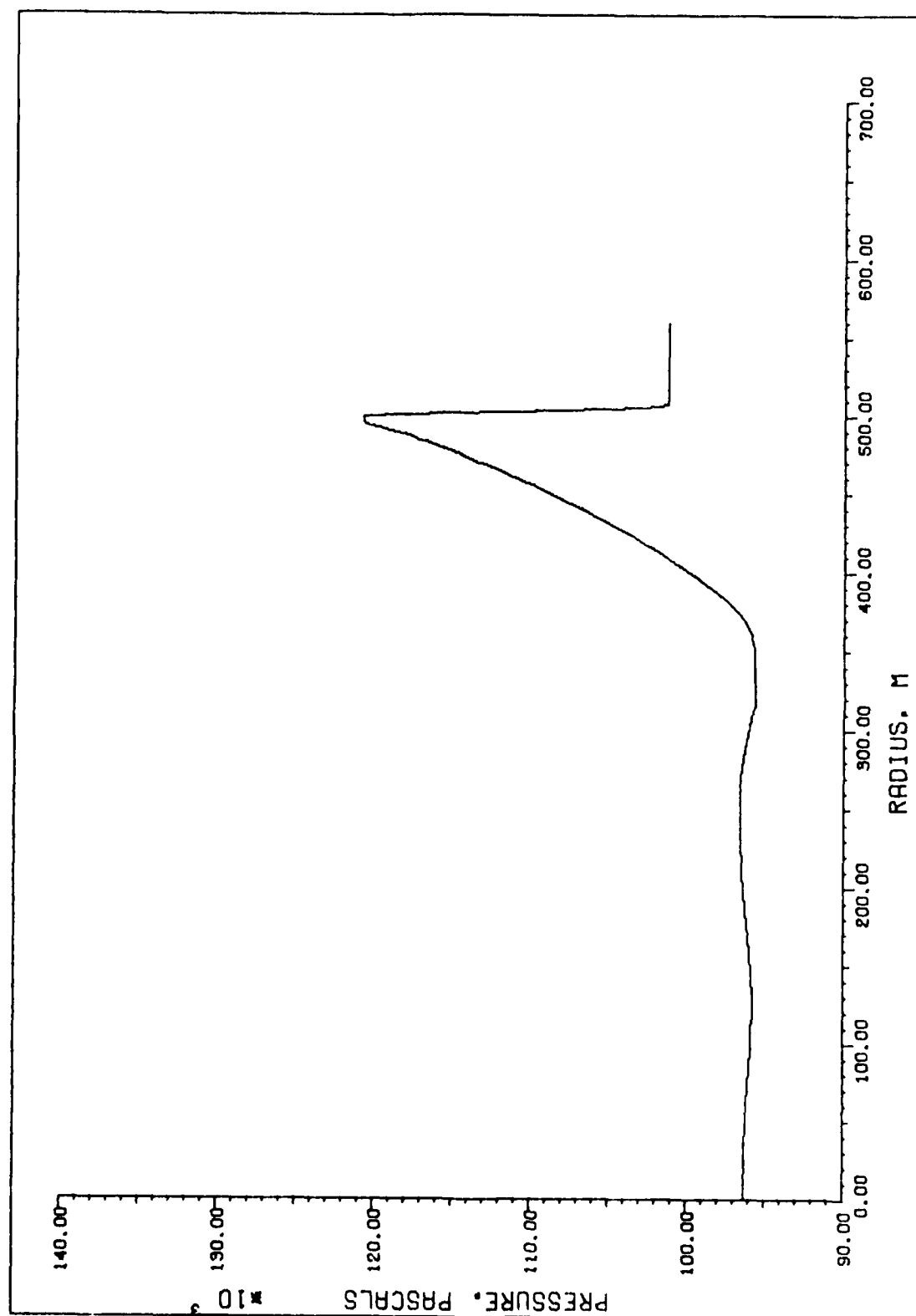
Figure C-1. Pressure profile of 1-D 1 kt burst at 1 sec after burst.

81
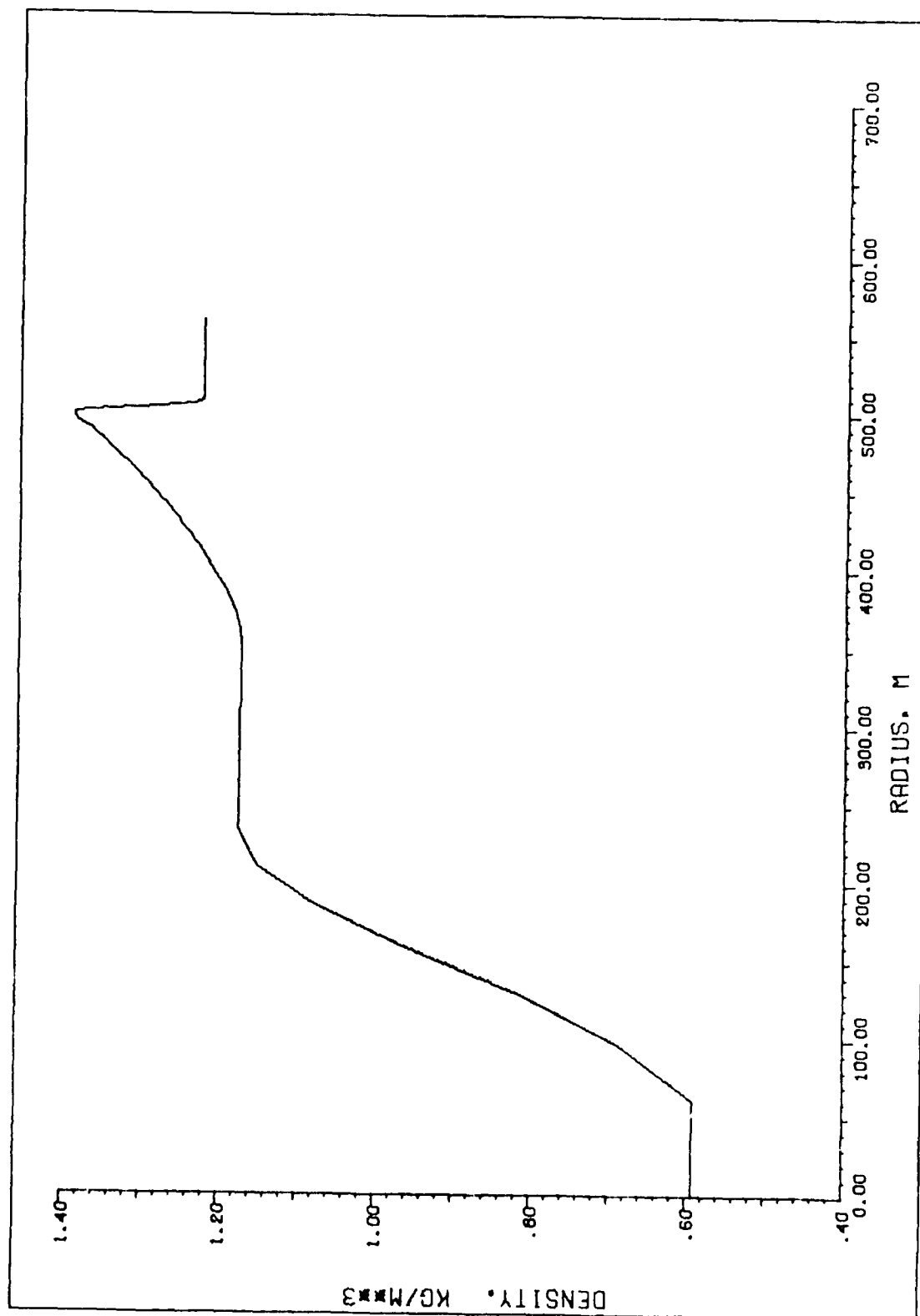
Figure C-2. Density profile of 1-D 1 kt burst at 1 sec after burst.
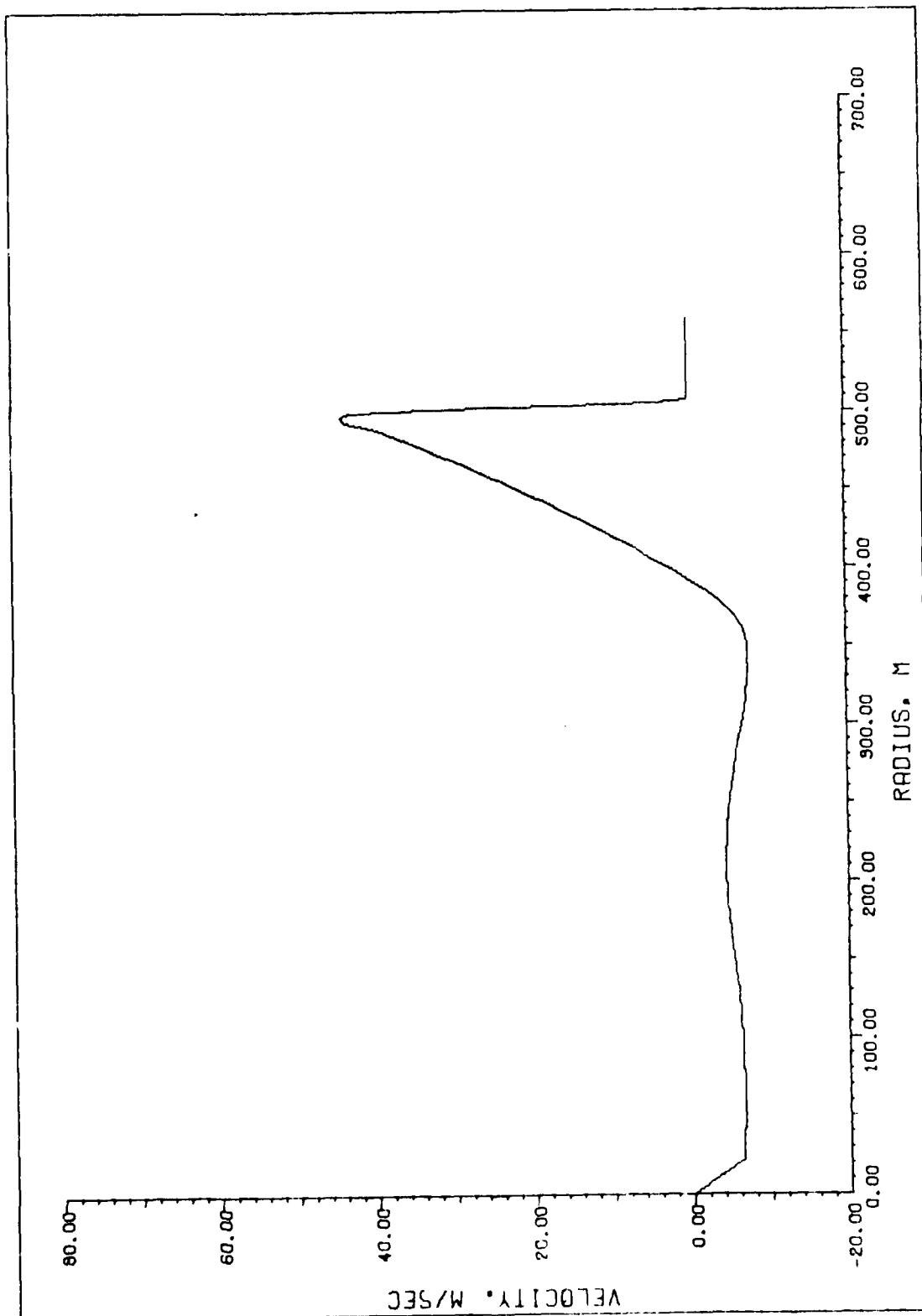
Figure C-3. Velocity profile fo 1-D 1 kt burst at 1 sec after burst.

83
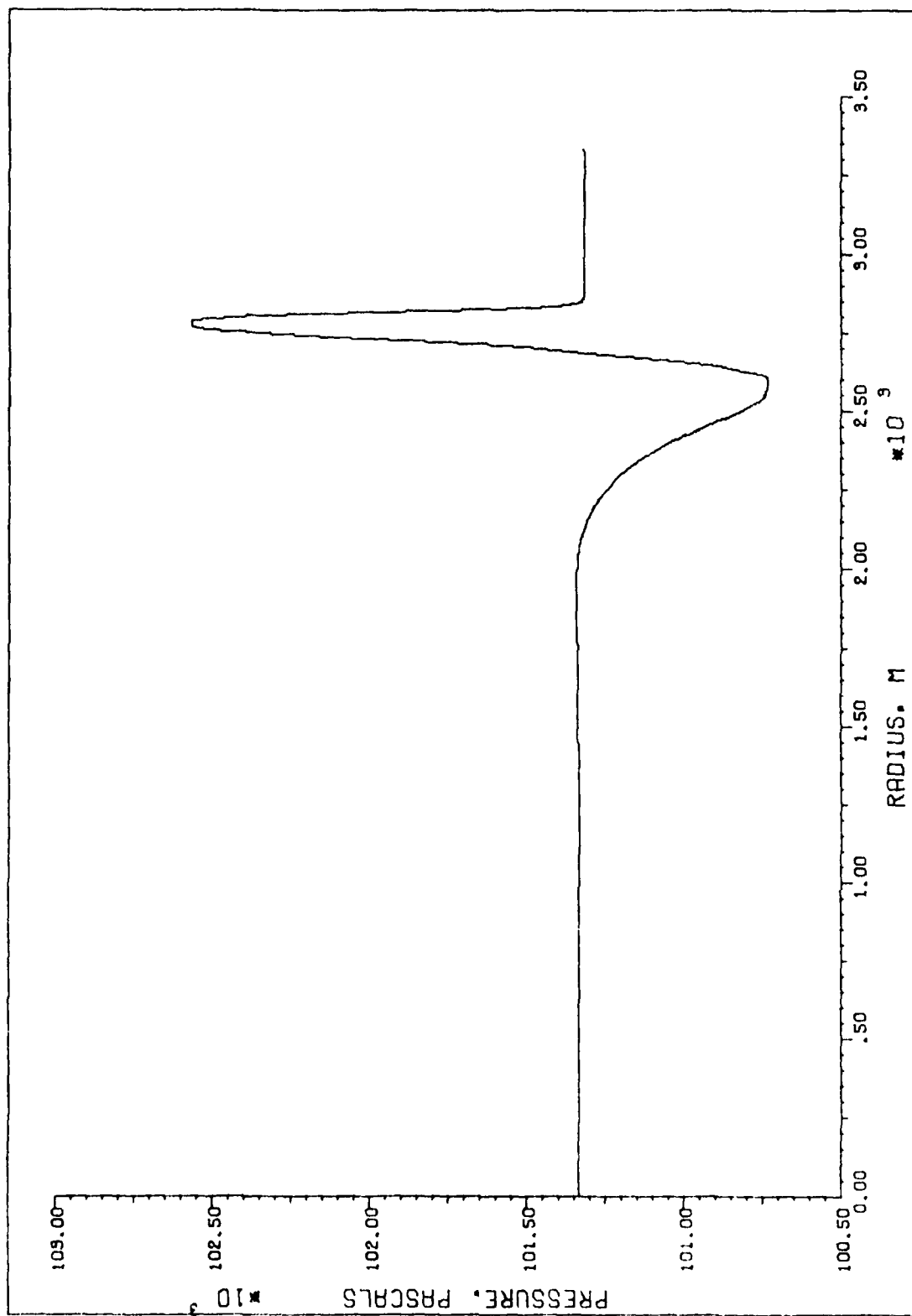
Figure C-4. Pressure profile of 1-D 1 kt burst at 7.67 sec after burst.
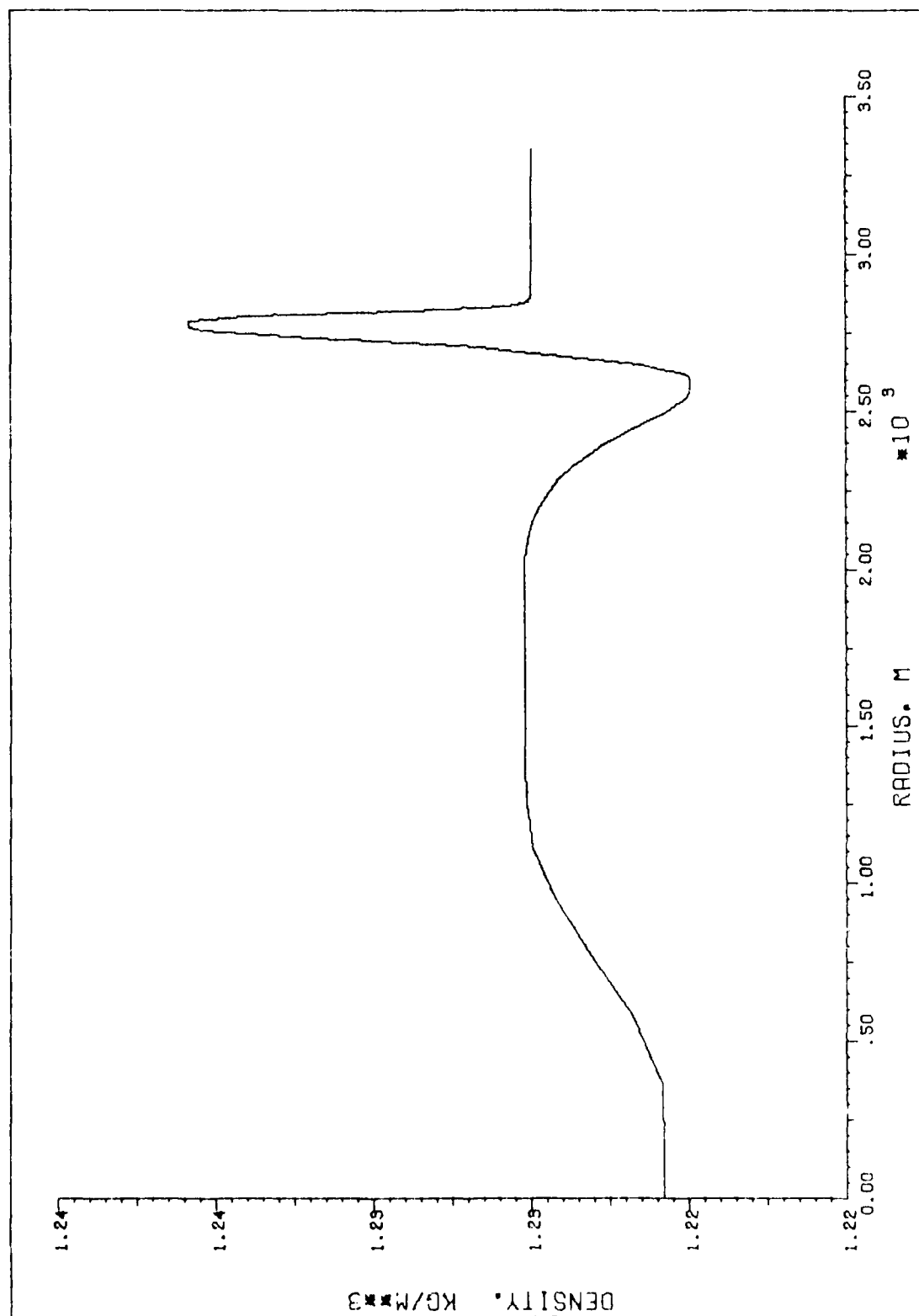
Figure C-5. Density profile of 1-D 1 kt burst at 7.67 sec after burst.
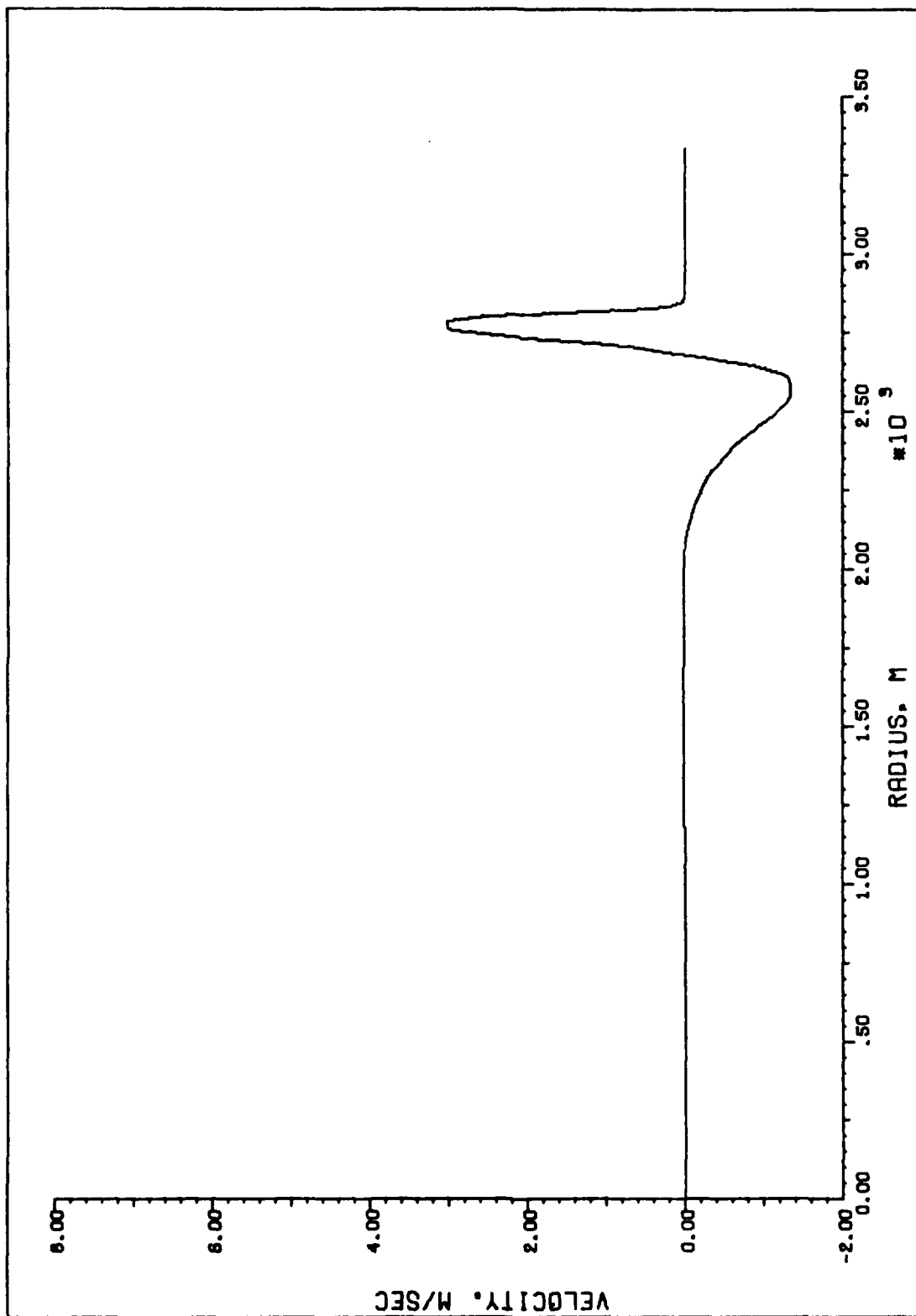
Figure C-6. Velocity profile of 1-D 1 kt burst at 7.67 sec after burst.
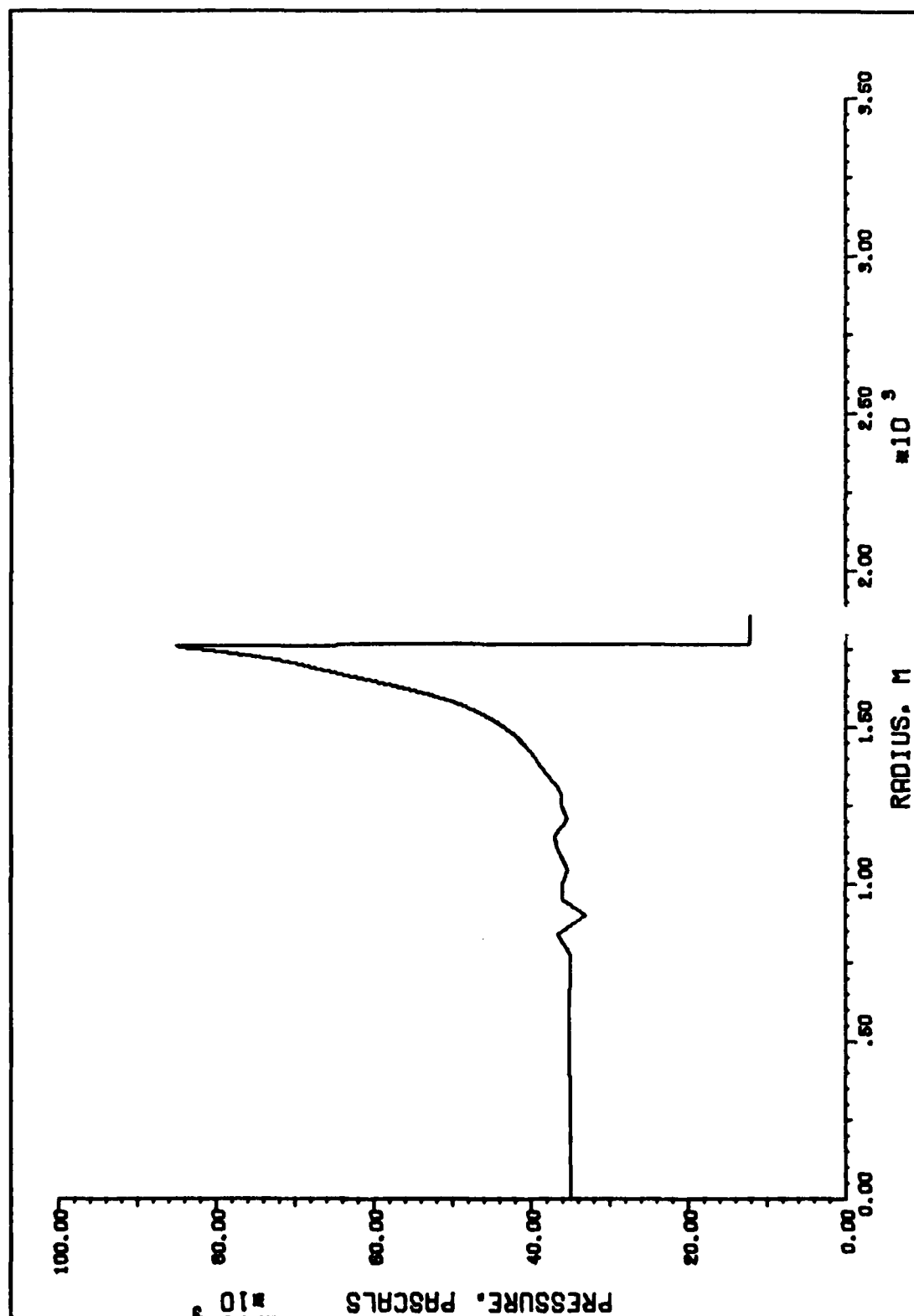
Figure C-7. Pressure profile of 1-D 1 Mt burst at 1 sec after burst.
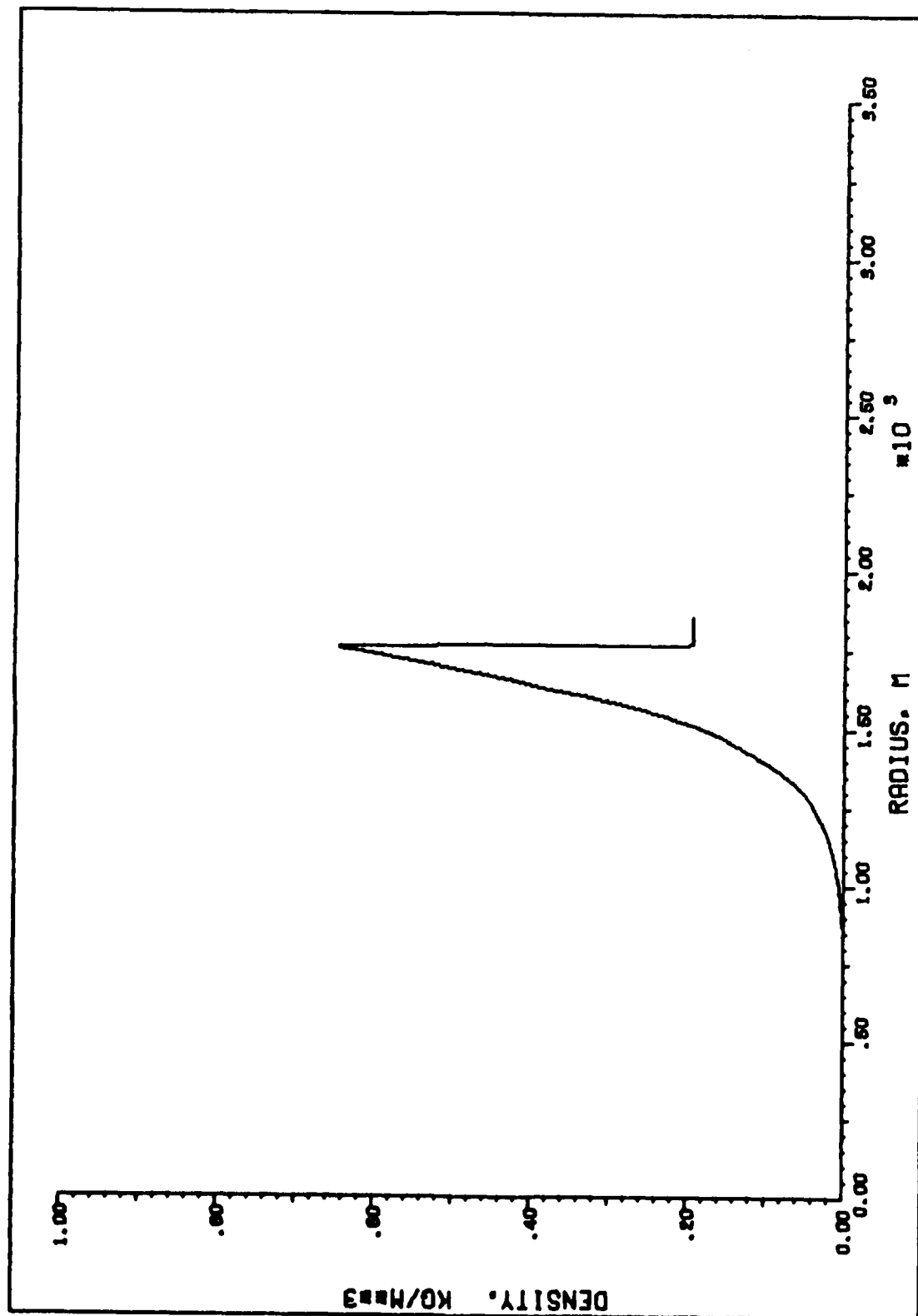
Figure C-8. Density profile of 1-D 1 Mt burst at 1 sec after burst.
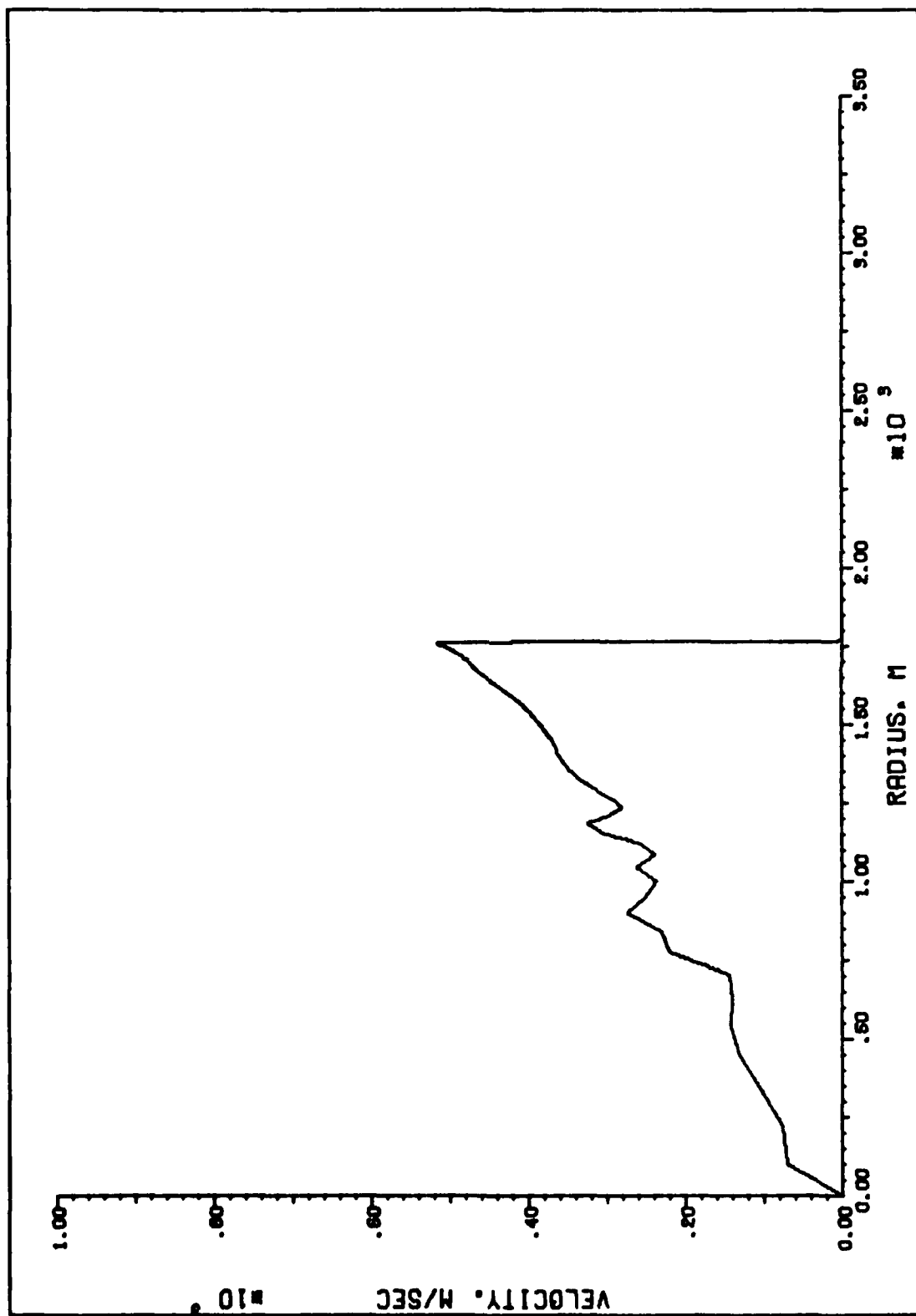
Figure C-9. Velocity profile of 1-D 1 Mt burst at 1 sec after burst.
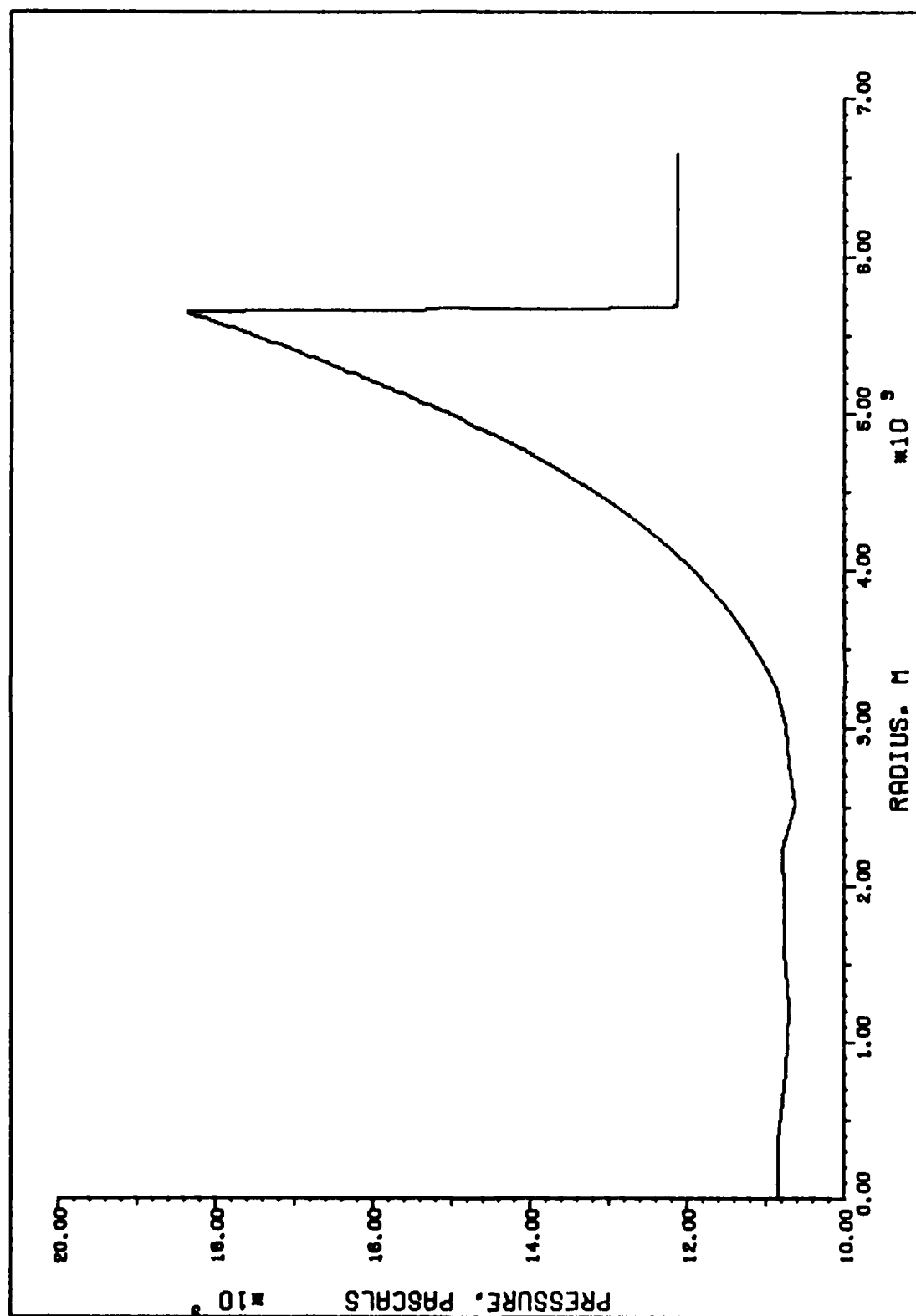
Figure C-10. Pressure profile of 1-D 1 Mt burst at 10 sec after burst.
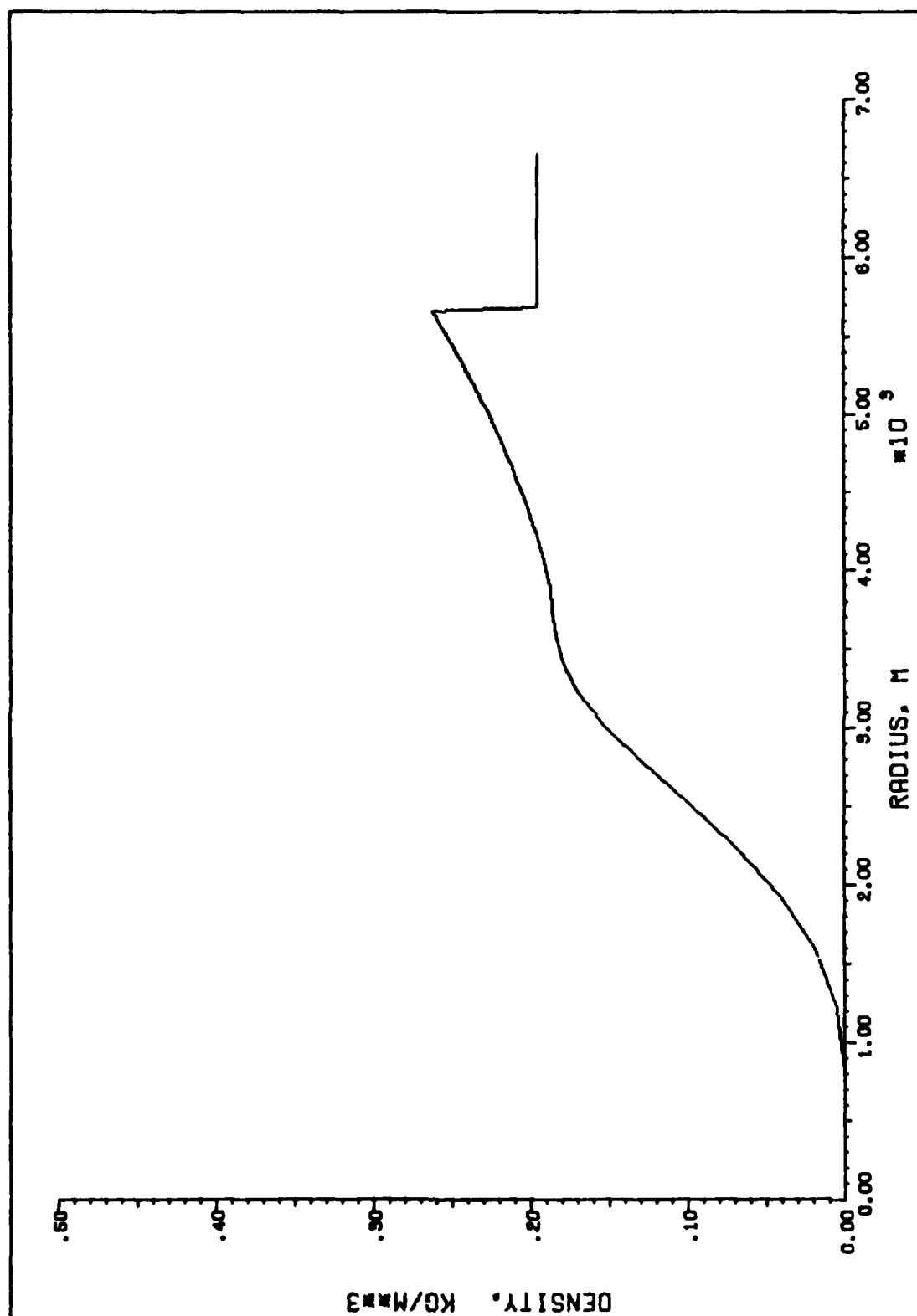
Figure C-11. Density profile of 1-D 1 Mt burst at 10 sec after burst.
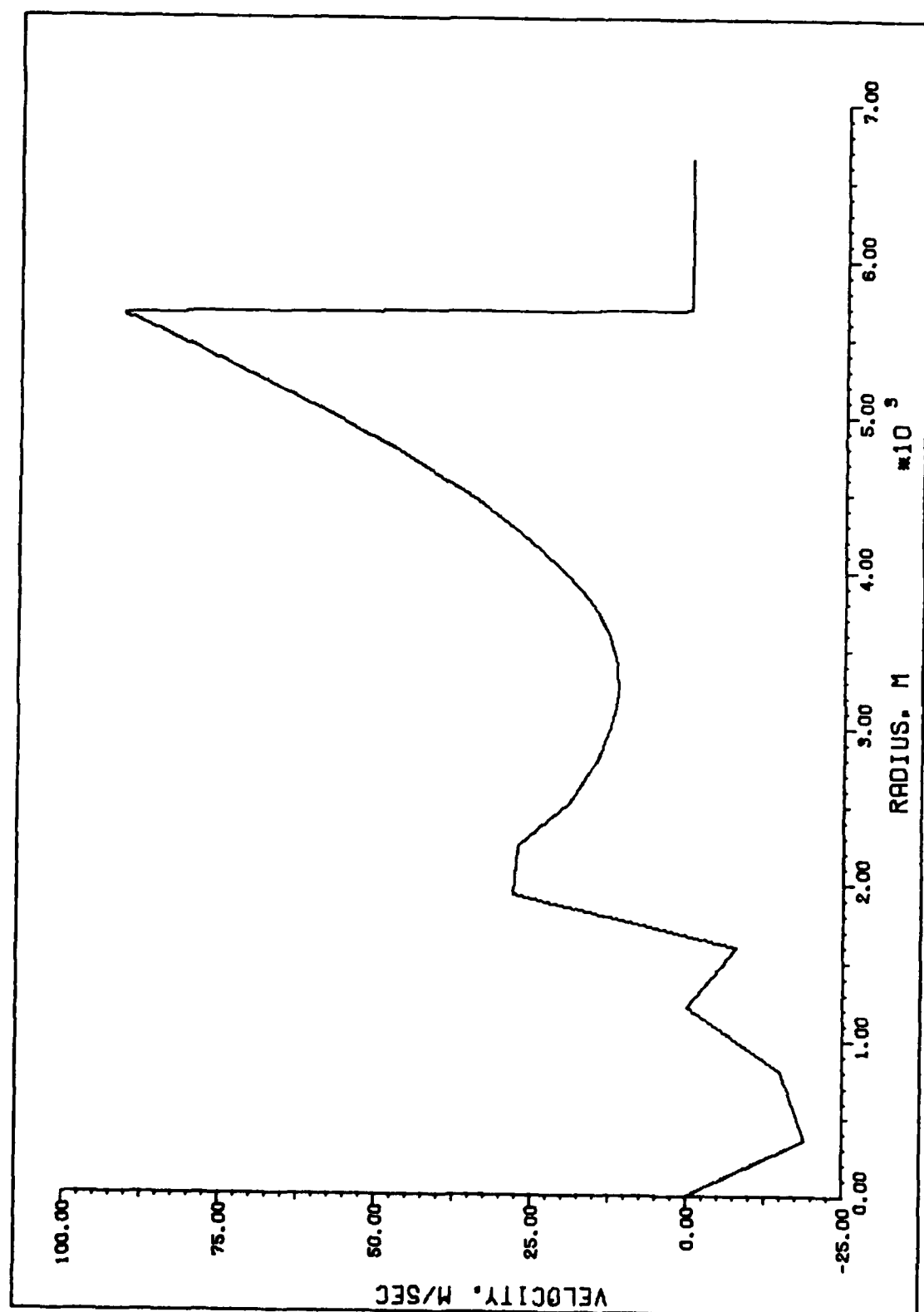
Figure C-12. Velocity profile of 1-D 1 Mt burst at 10 sec after burst.
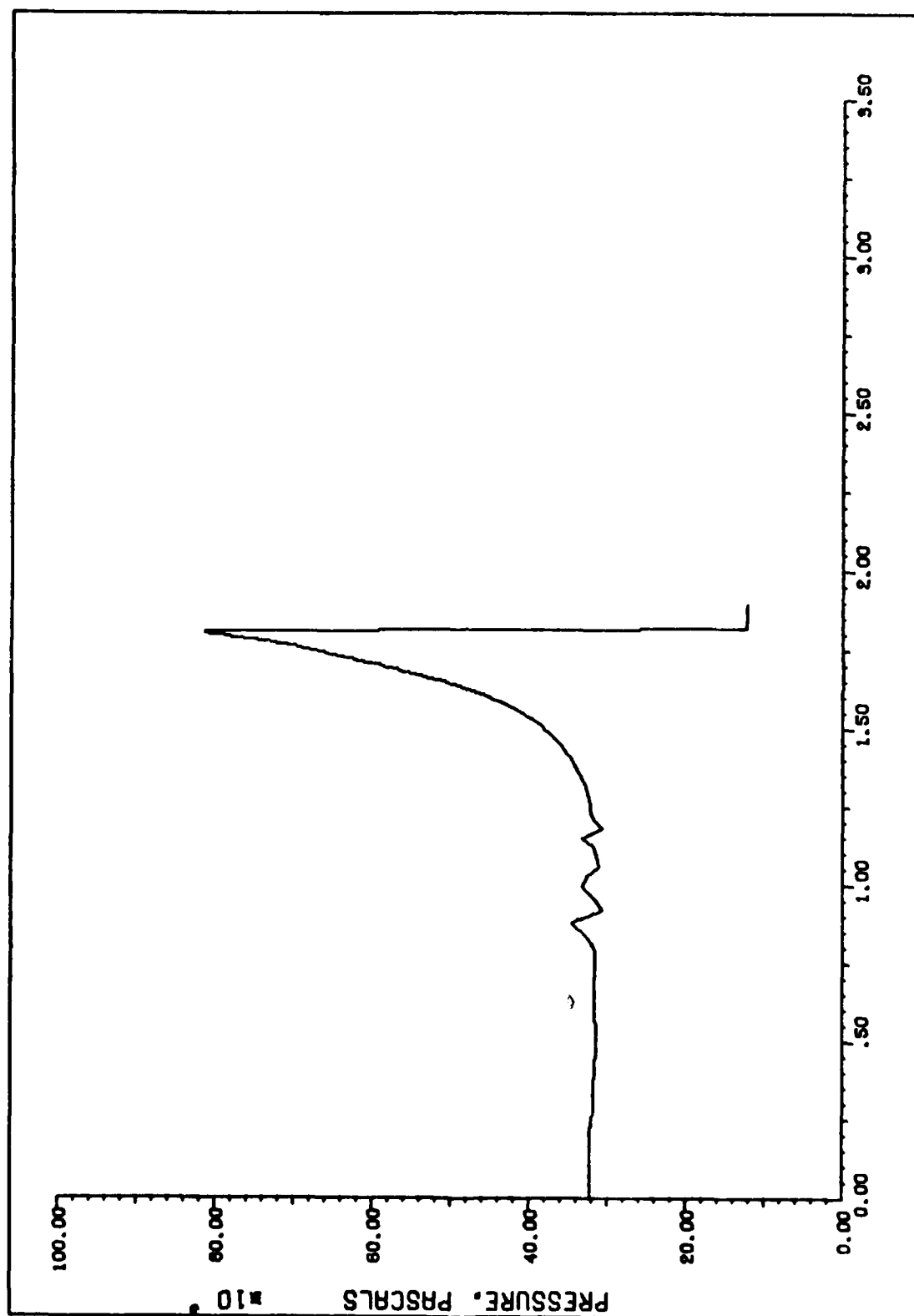
Figure C-13. Radial coaltitude pressure profile of 2-D 1 Mt burst at 1.168 sec after burst.
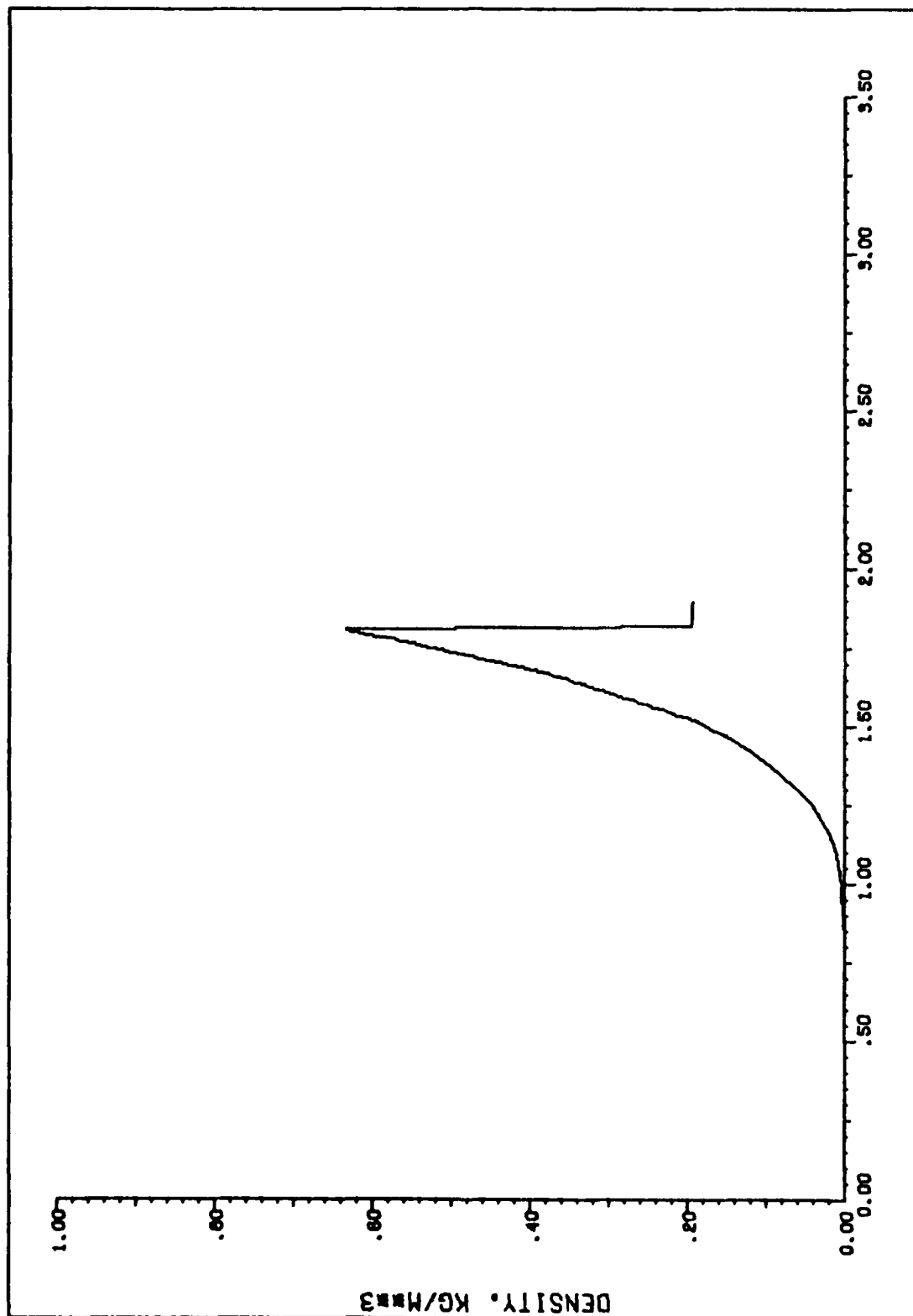
Figure C-14. Radial coaltitude density profile of 2-D 1 Mt burst at 1.168 sec after burst.
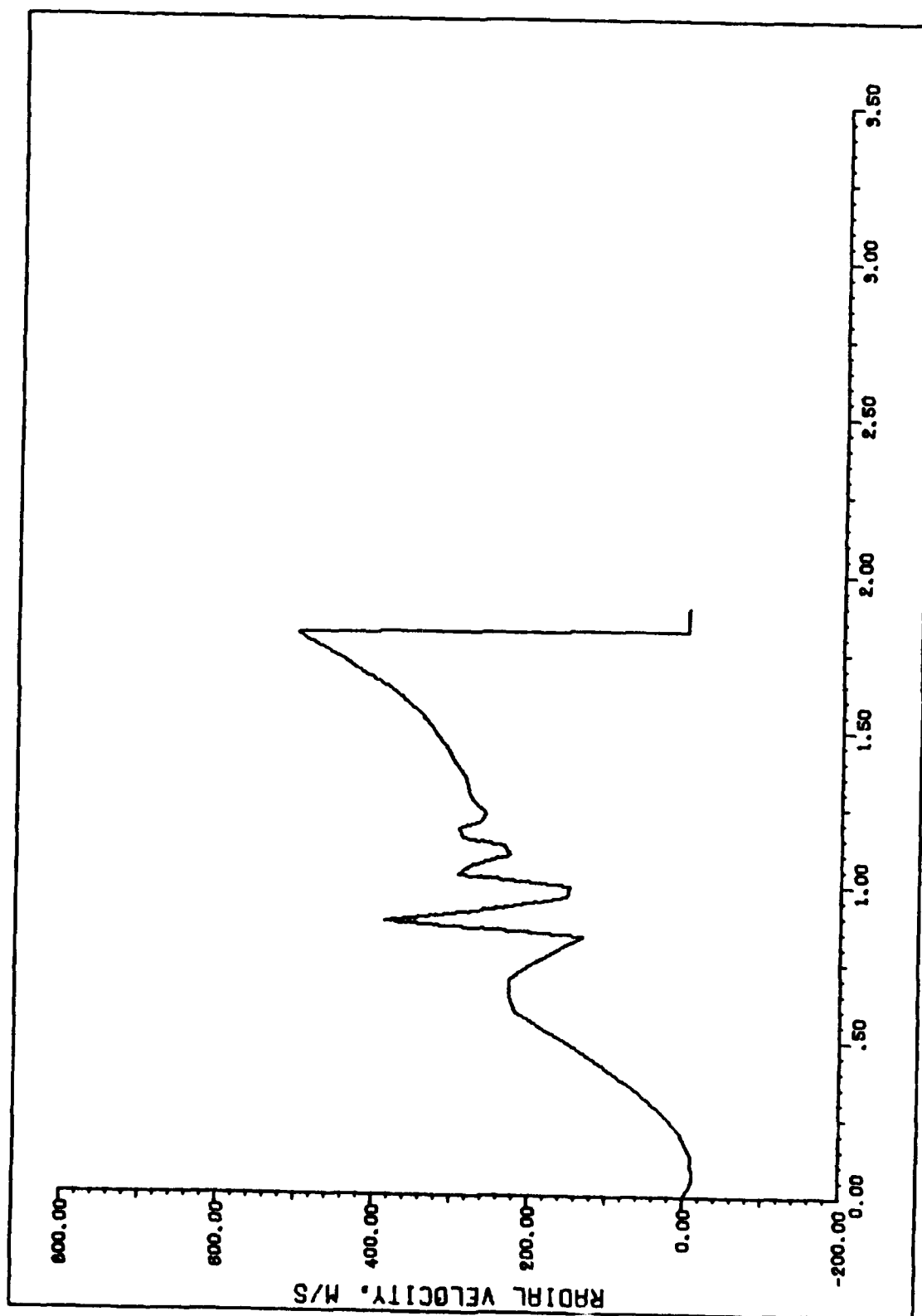
Figure C-15. Radial coaltitude velocity profile of 2-D 1 Mt burst at 1.168 sec after burst.

95
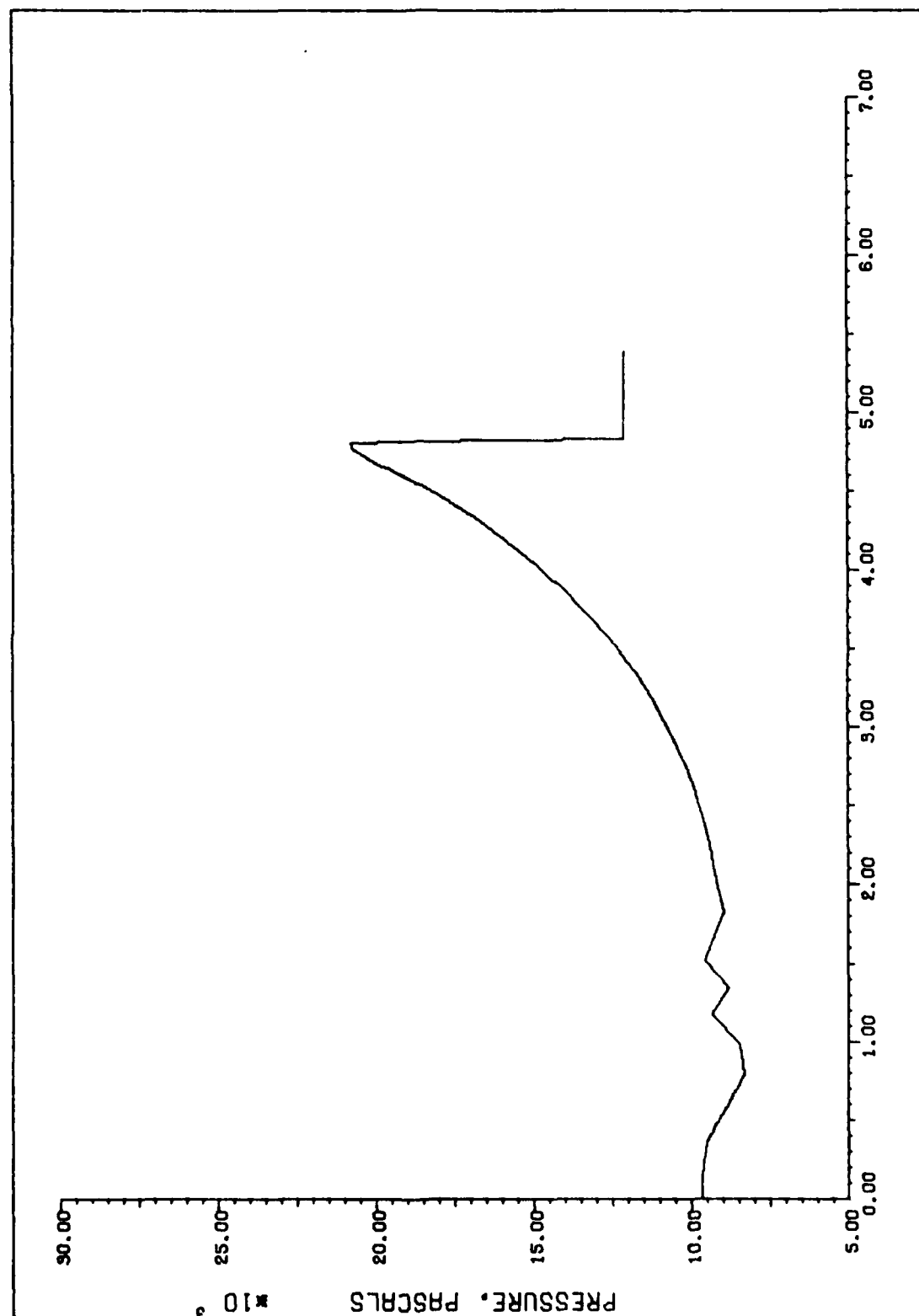
Figure C-16. Radial coaltitude pressure profile of 2-D 1 Mt burst at 7.781 sec after burst.
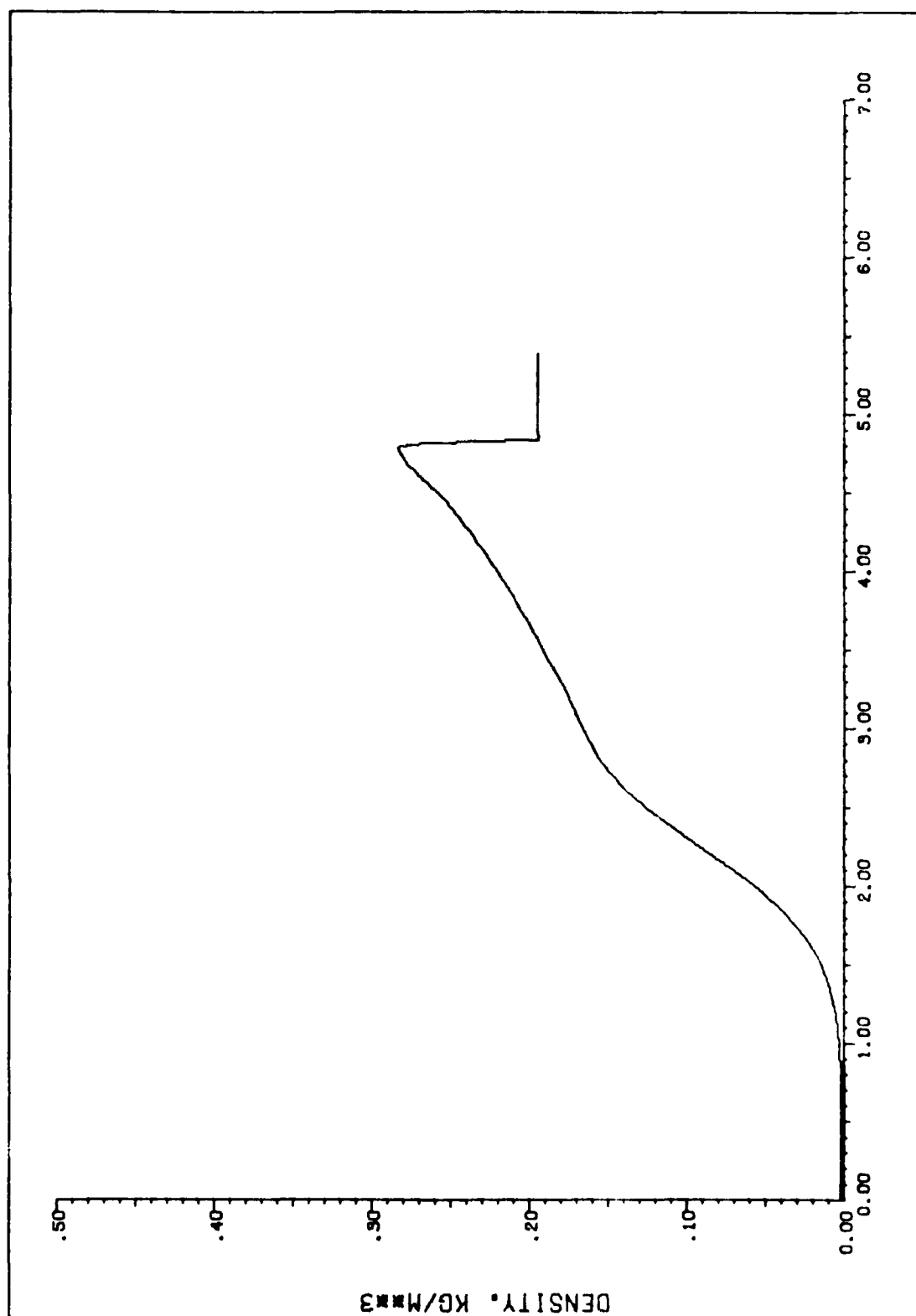
Figure C-17. Radial coaltitude density profile of 2-D 1 Mt burst
at 7.781 sec after burst.
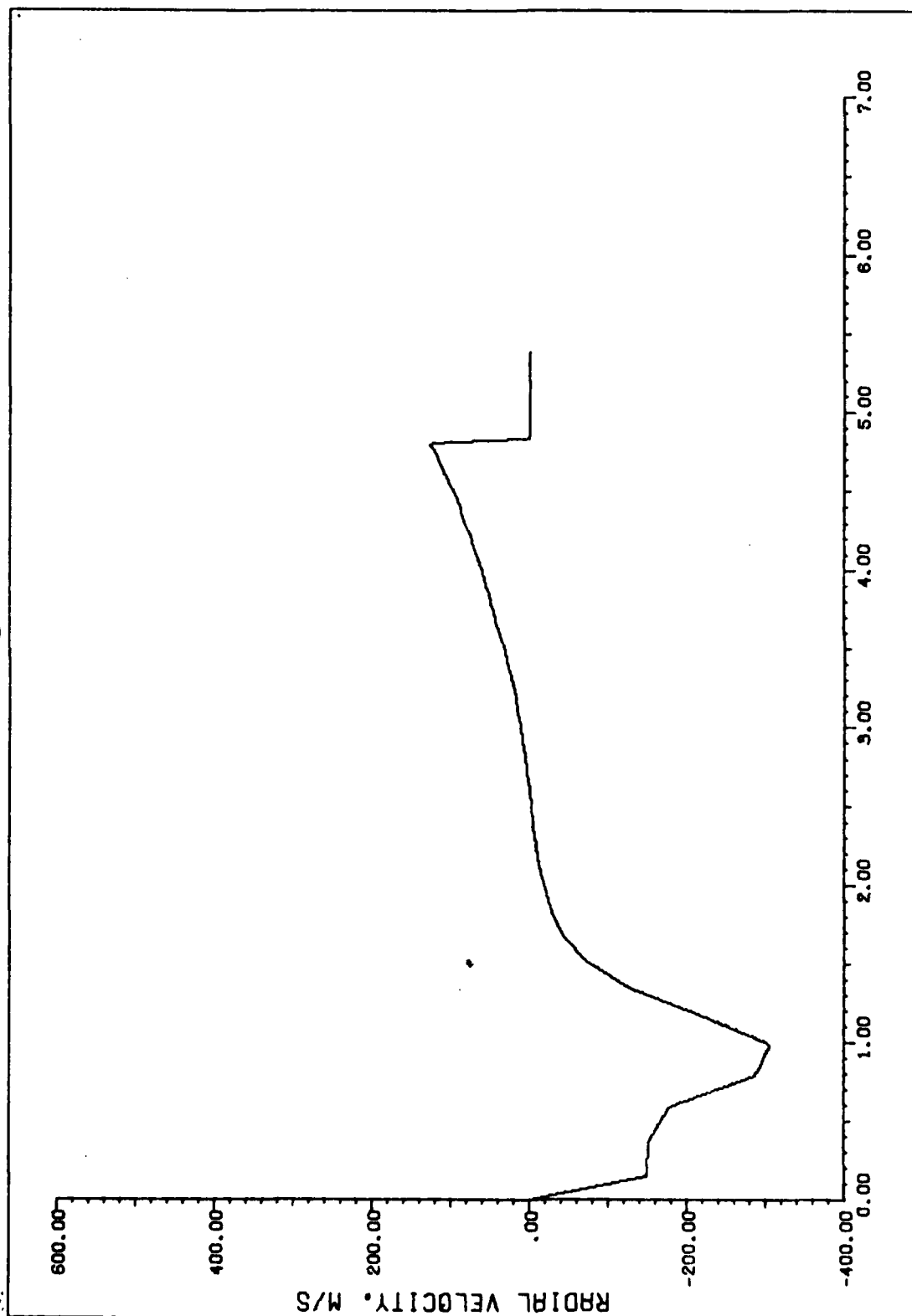
Figure C-18. Radial coaltitude velocity profile of 2-D 1 Mt burst at 7.781 sec after burst.
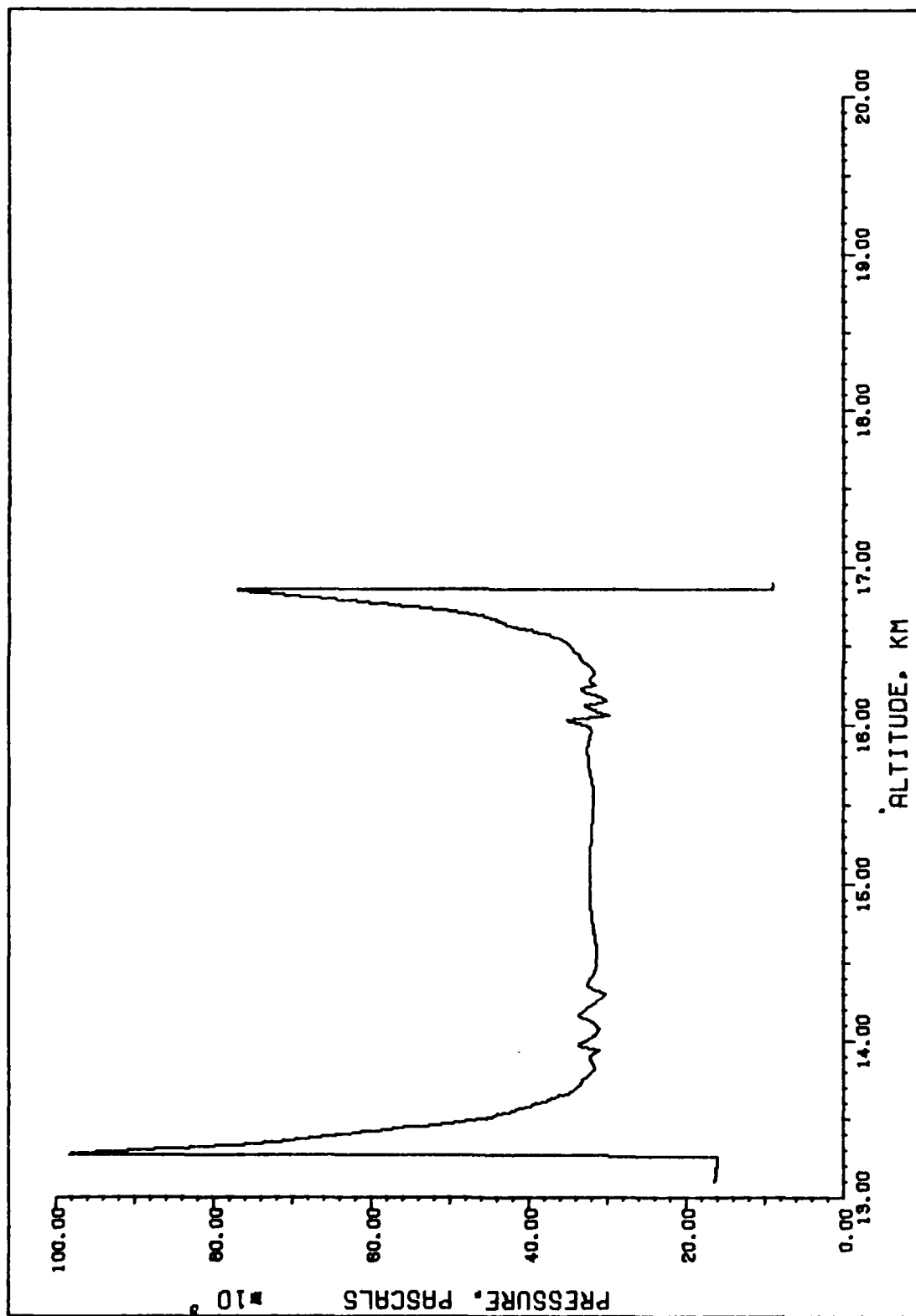
Figure C-19. Axial (r=0) pressure profile of 2-D 1 Mt burst at 1.168 sec after burst.
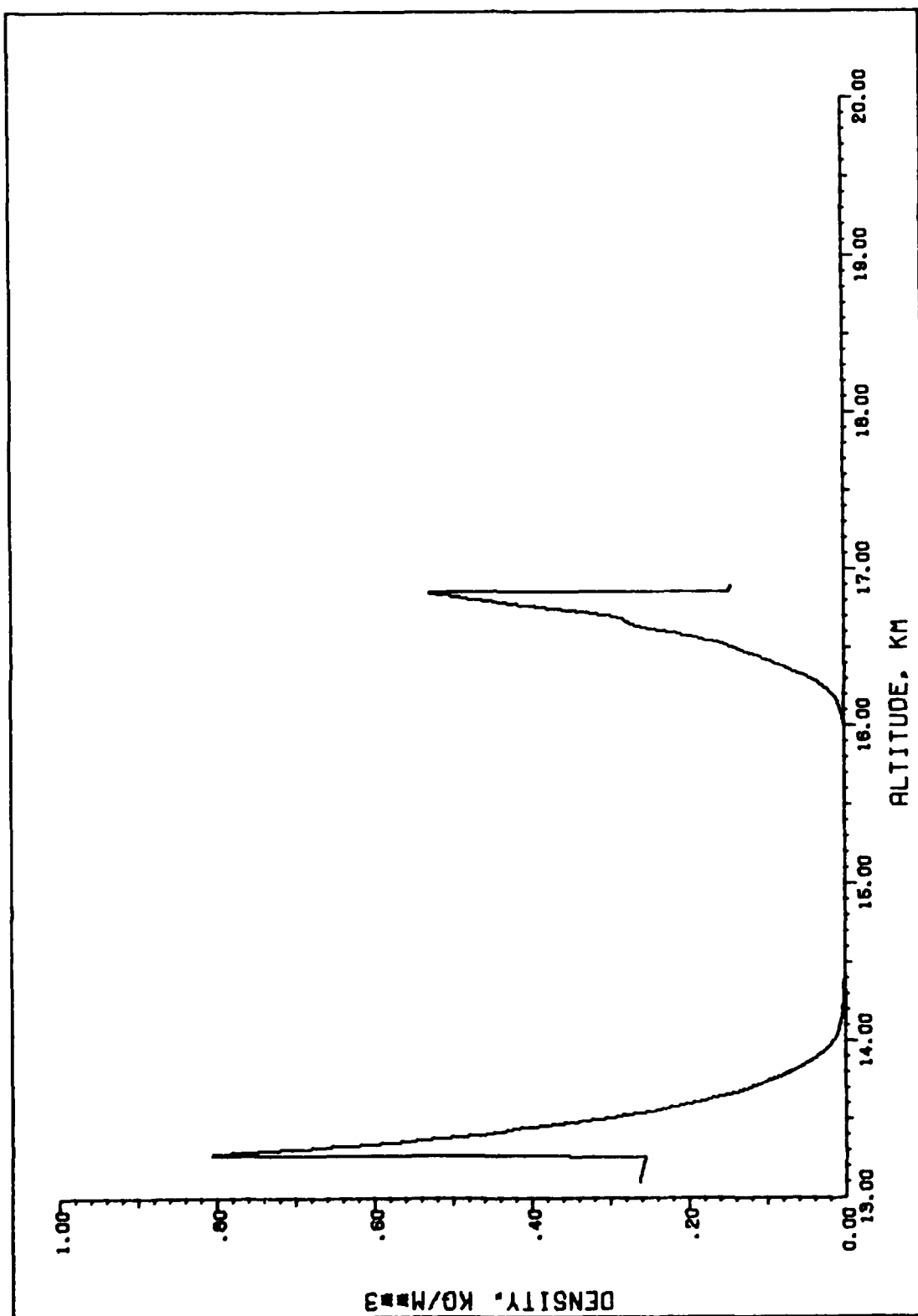
Figure C-20. Axial (r=0) density profile of 2-D 1 Mt burst at 1.168 sec after burst.
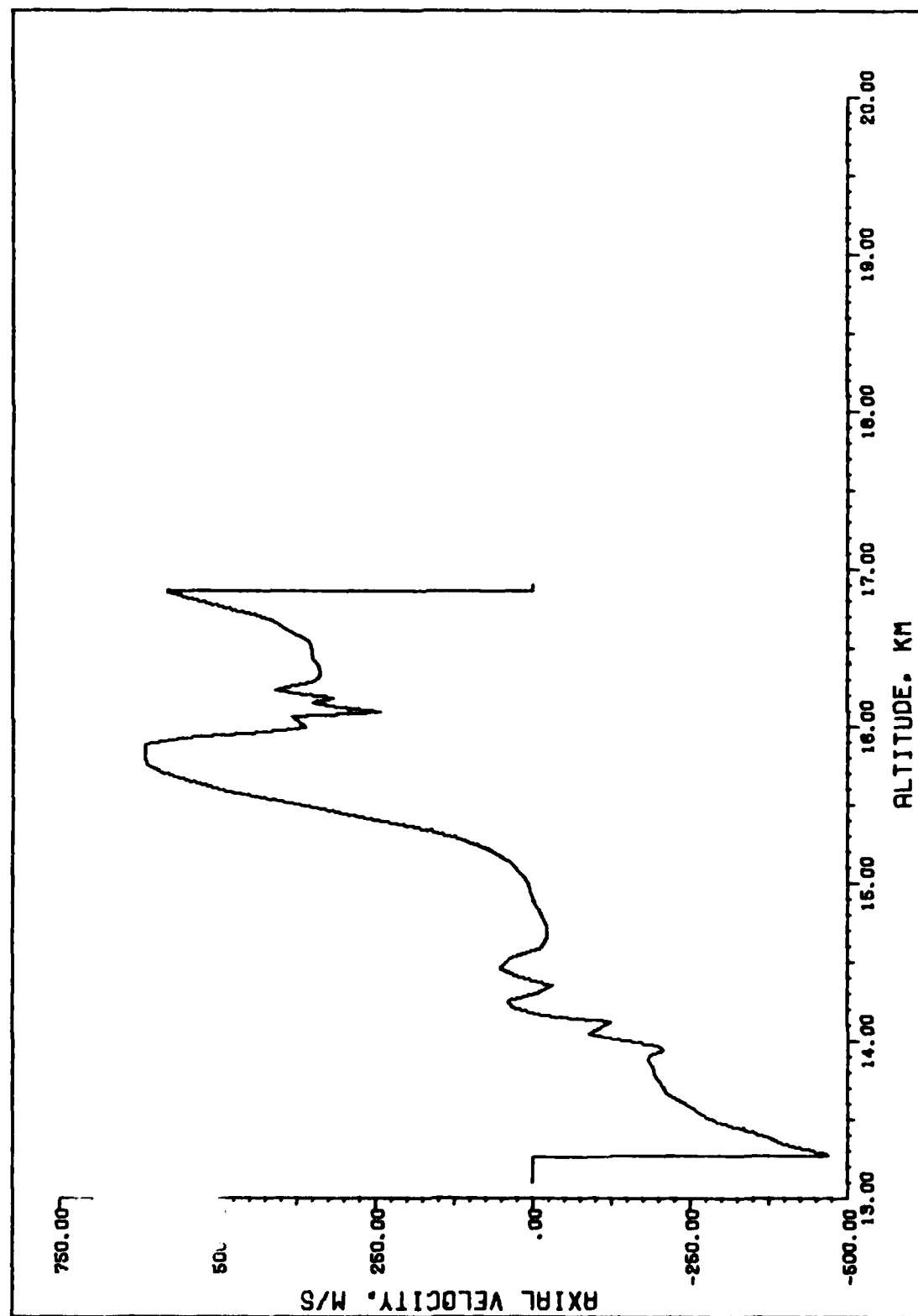
Figure C-21. Axial (r=0) velocity profile of 2-D 1 Mt burst at 1.168 sec after burst.
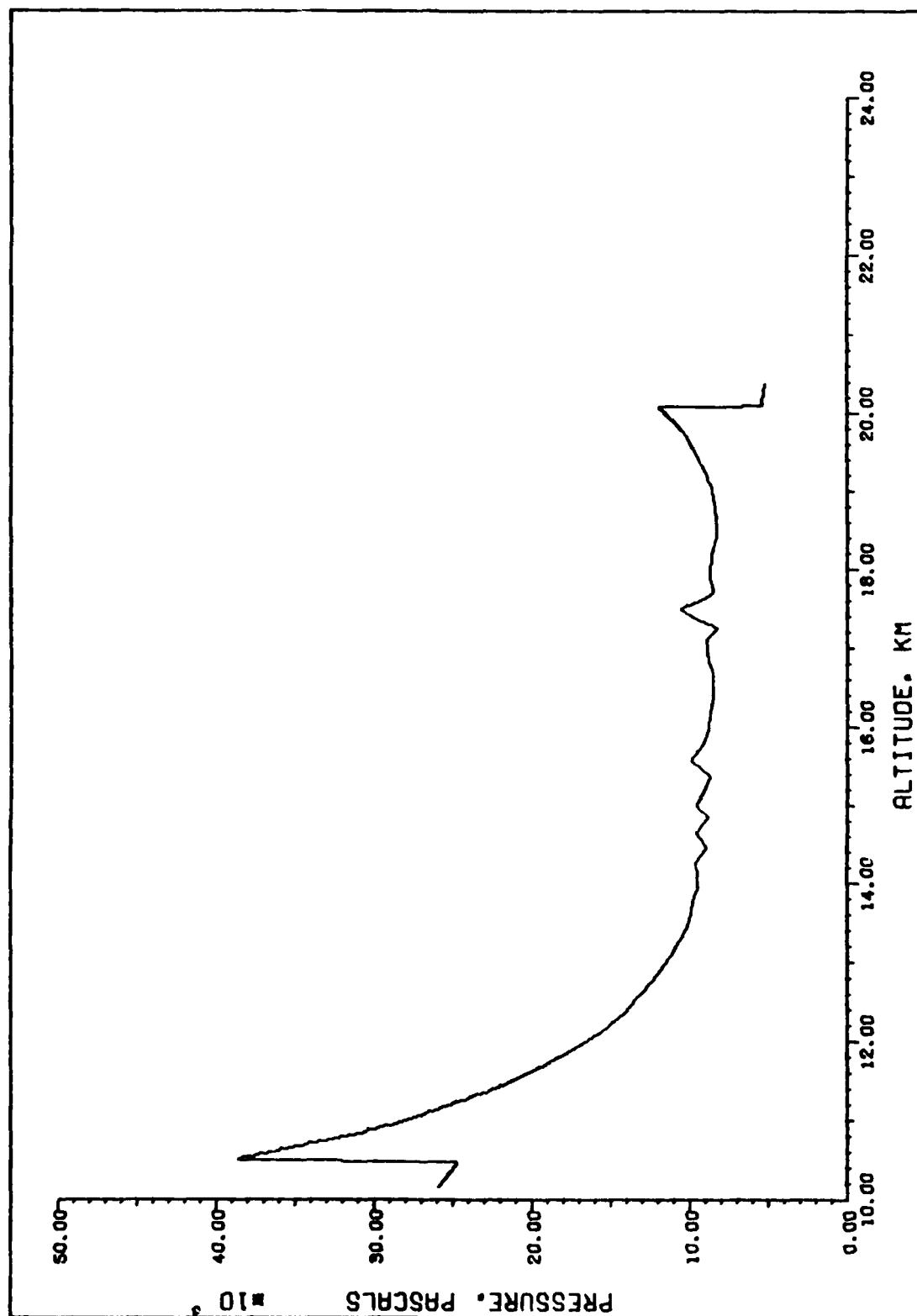
Figure C-22. Axial (r=0) pressure profile of 2-D 1 Mt burst at 7.781 sec after burst.
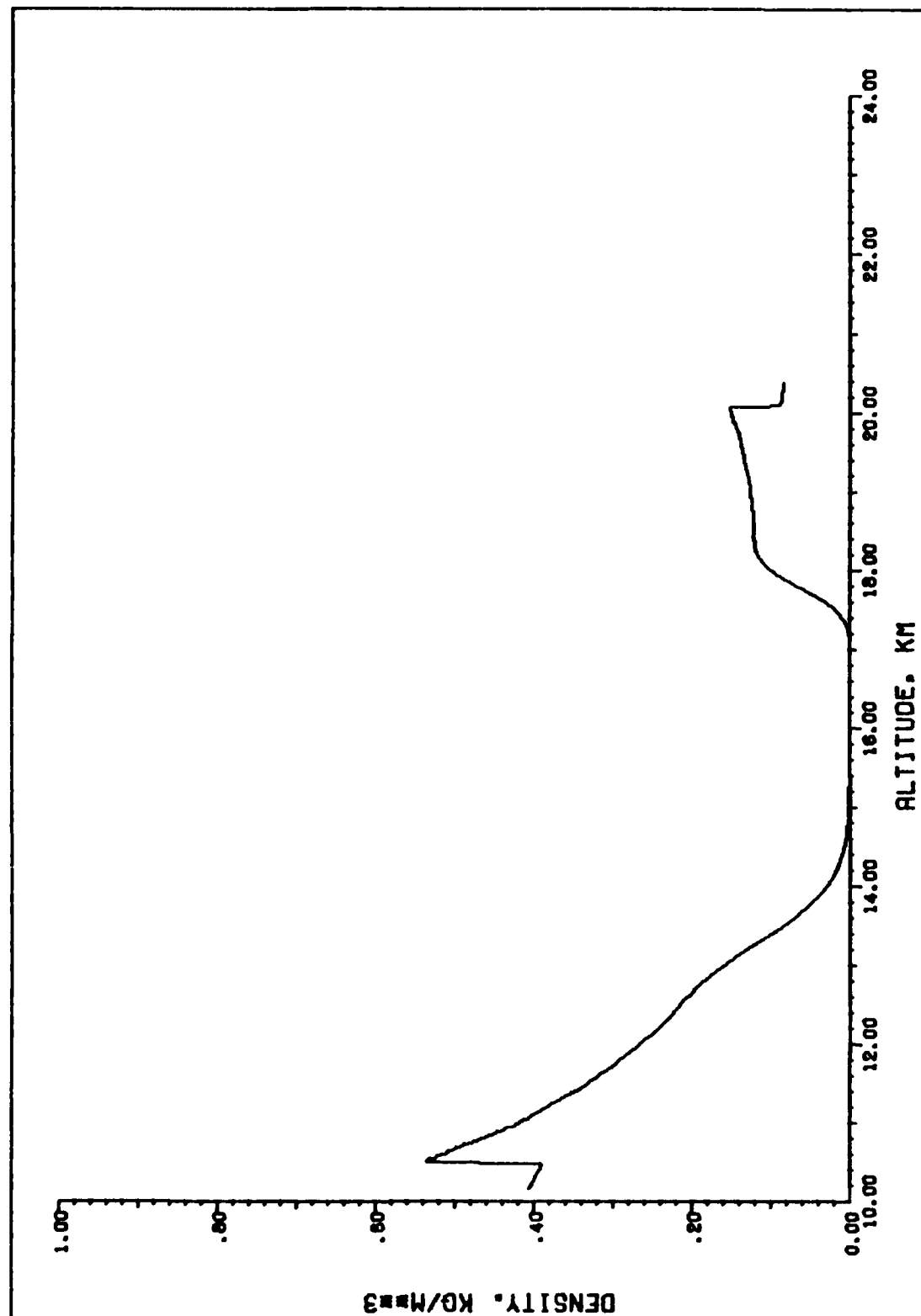
Figure C-23. Axial (r=0) density profile of 2-D 1 Mt burst at 7.781 sec after burst.
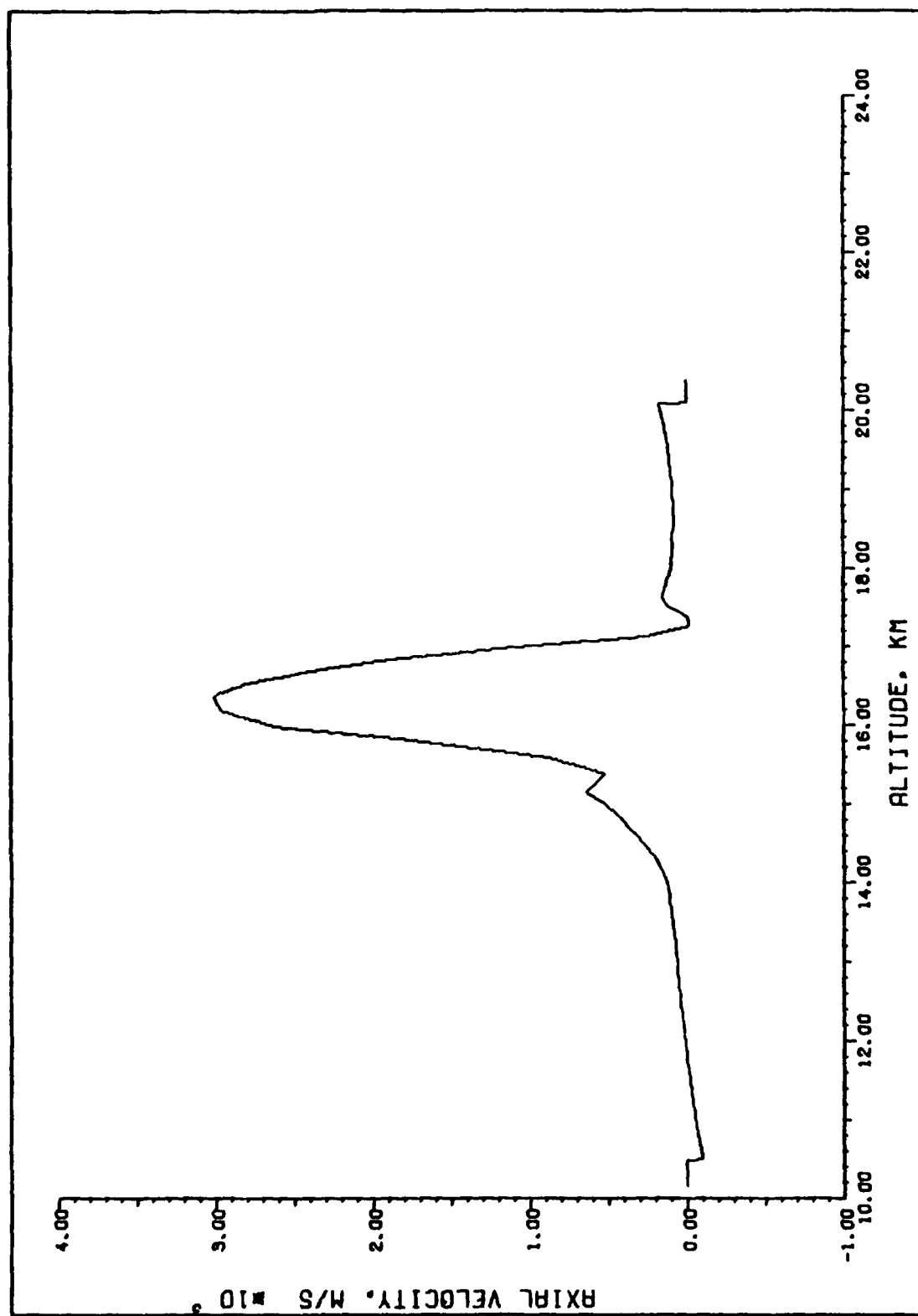
Figure C-24. Axial (r=0) velocity profile of 2-D 1 Mt burst at 7.781 sec after burst.

Appendix D: Computer Program Listing

```
         PROGRAM MAIN
         DIMENSION A(0:318156),V(0:300,4),QPLUS(0:300),SPLUS(0:300),
      C    CENVEL(0:300),R(0:300),Z(0:300),RN(0:300),ZN(0:300)
         DIMENSION IOUT(3),JOUT(3)
         DIMENSION FD(0:300),FT(0:300),VTD(0:300),DVTD(0:300),FC(0:300),
      C    P1(0:300),P2(0:300),P3(0:300),P4(0:300)
         DIMENSION RHO(0:300),E(0:300),GMONE(0:300),E1(0:300),E11(0:300),
      C    WD(0:300),FC(0:300),FDN(0:300),BETA(0:300),FN(0:300),FE(0:300)
      C    ,S>(0:300)
         N=151
         M=2*N-1
         NM=N*M
         DO 1 J=0,7*NM-1
       1 A(J)=0.
         DO 2 J=0,M-1
         QPLUS(J)=0.
         SPLUS(J)=0.
         DO 2 I=1,4
       2 V(J,I)=0.
         NOUT=1
C
C     SET UP AND INITIALIZE THE MESH
C
         CALL INDATA(A,N,M,NM,IOUT,JOUT,NROWS,NCOLS,V,TSTOP,NSTOP,NRITE,
      C    DT,TIME,NSTEP,R,Z)
         NOUTO=NSTEP
C
C     CHECK THE INITIAL CONDITIONS
C
         CALL OUTDATA(A,N,M,NM,IOUT,JOUT,NROWS,NCOLS,DT,TIME,NSTEP,R,Z,0)
C
C
C
      10 HT = DT / 2.
C
C
C*********************************************************************************
C
C
C     ADVANCE THE PROPERTIES IN THE RADIAL DIRECTION.
C
         DO 20 J=0,M-1
C
C     FIRST THE R-HALF STEP.
C
C     ADVANCE DENSITY, R- AND Z-MOMENTUM, AND ENERGY ONE-HALF STEP.
C
         CALL VELCENR(A,N,NM,J,CENVEL,HT,R)
         CALL QSETUP(N,HT,QPLUS,CENVEL,R)
         CALL SSETO(N,SPLUS)
         CALL RHASTAR(NM,V(0,1),0,A,N,J,QPLUS,SPLUS,R,FD,FT,VTD,DVTD,
      C    FC,P1,P2,P3,P4)
         CALL RHASTAR(NM,V(0,3),2,A,N,J,QPLUS,SPLUS,R,FD,FT,VTD,DVTD,
      C    FC,P1,P2,P3,P4)
         CALL SSETMR(A,N,NM,J,HT,SPLUS,R)
         CALL RHASTAR(NM,V(0,2),1,A,N,J,QPLUS,SPLUS,R,FD,FT,VTD,DVTD,
      C             FC,P1,P2,P3,P4)
         CALL QSETER(A,N,NM,J,HT,SPLUS,R)
         CALL RHASTAR(NM,V(0,4),3,A,N,J,QPLUS,SPLUS,R,FD,FT,VTD,DVTD,
```

106

```
      C    FC,R1,R2,R3,R4)
      C
      C    COMPUTE TIME CENTERED VELOCITIES AND PRESSURES.
      C
 31.         CALL VELPRR(A,N,NM,J,V,M,RHO,E,GMONE,E1,E11,WS,FO,FON,BETA,
      C    FN,FE,EX)
      C
      C    NOW THE R-FULL STEP.
      C
 32.         CALL VELCENR(A,N,NM,J,CENVEL,DT,R)
 33.         CALL QSETUP(N,DT,QPLUS,CENVEL,R)
 34.         CALL SSETC(N,SPLUS)
 35.         CALL SHASTAR(NM,V(0,1),0,A,N,J,QPLUS,SPLUS,R,FO,FT,VTO,DVTO,
      C    FC,R1,R2,R3,R4)
 36.         CALL SHASTAR(NM,V(0,3),2,A,N,J,QPLUS,SPLUS,R,FO,FT,VTO,DVTO,
      C    FC,R1,R2,R3,R4)
 37.         CALL SSETMR(A,N,NM,J,DT,SPLUS,R)
 38.         CALL SHASTAR(NM,V(0,2),1,A,N,J,QPLUS,SPLUS,R,FO,FT,VTO,DVTO,
      C    FC,R1,R2,R3,R4)
 39.         CALL SSETER(A,N,NM,J,DT,SPLUS,R)
 40.         CALL SHASTAR(NM,V(0,4),3,A,N,J,QPLUS,SPLUS,R,FO,FT,VTO,DVTO,
      C    FC,R1,R2,R3,R4)
      C
      C    COMPUTE VELOCITIES AND PRESSURES.
      C
 41.         CALL VELPRR(A,N,NM,J,V,M,RHO,E,GMONE,E1,E11,WS,FO,FON,BETA,
      C    FN,FE,EX)
      C
      C    SUBSTITUTE NEW VALUES FROM THE V-SCRATCH ARRAY INTO A.
      C
 42.         CALL SUBR(A,V,N,NM,J,M)
      C
 43.      20 CONTINUE
 C****************************************************************************
      C
      C    ADVANCE THE PROPERTIES IN THE AXIAL DIRECTION.
      C
 44.         DO 30 I=0,N-1
      C
      C    FIRST THE Z-HALF STEP.
      C
 45.         CALL VELCENZ(A,N,M,NM,I,CENVEL,HT,Z)
 46.         CALL QSETUP(M,HT,QPLUS,CENVEL,Z)
 47.         CALL SSETC(M,SPLUS)
 48.         CALL SHASTAZ(NM,V(0,1),0,A,N,M,I,QPLUS,SPLUS,Z,FO,FT,VTO,
      C    DVTO,FC,F1,F2)
 49.         CALL SHASTAZ(NM,V(0,2),1,A,N,M,I,QPLUS,SPLUS,Z,FO,FT,VTO,
      C    DVTO,FC,F1,F2)
 50.         CALL SSETMZ(A,N,M,NM,I,HT,SPLUS,Z)
 51.         CALL SHASTAZ(NM,V(0,3),2,A,N,M,I,QPLUS,SPLUS,Z,FO,FT,VTO,
      C    DVTO,FC,F1,F2)
 52.         CALL SSETEZ(A,N,M,NM,I,HT,SPLUS,Z)
 53.         CALL SHASTAZ(NM,V(0,4),3,A,N,M,I,QPLUS,SPLUS,Z,FO,FT,VTO,
      C    DVTO,FC,F1,F2)
      C
      C    COMPUTE TIME CENTERED VELOCITIES AND PRESSURES.
      C
 54.         CALL VELPRZ(A,N,M,NM,I,V,RHO,E,GMONE,E1,E11,WS,FO,FON,BETA,
```

107

```fortran
      C    FN,FE,EX)
      C
      C    FINALLY, THE Z-FILL STEP.
      C
55.        CALL VELCENZ(A,N,M,NM,I,CENVEL,DT,Z)
56.        CALL QCETUP(M,DT,QPLUS,CENVEL,Z)
57.        CALL SSETO(M,SPLUS)
58.        CALL SHASTAZ(NM,V(0,1),0,A,N,M,I,QPLUS,SPLUS,Z,FD,FT,VTD,
      C    DVTD,FC,R1,R2)
59.        CALL SHASTAZ(NM,V(0,2),1,A,N,M,I,QPLUS,SPLUS,Z,FD,FT,VTD,
      C    DVTD,FC,R1,R2)
60.        CALL SSETMZ(A,N,M,NM,I,DT,SPLUS,Z)
61.        CALL SHASTAZ(NM,V(0,3),2,A,N,M,I,QPLUS,SPLUS,Z,FD,FT,VTD,
      C    DVTD,FC,R1,R2)
62.        CALL SSETEZ(A,N,M,NM,I,DT,SPLUS,Z)
63.        CALL SHASTAZ(NM,V(0,4),3,A,N,M,I,QPLUS,SPLUS,Z,FD,FT,VTD,
      C    DVTD,FC,R1,R2)
      C    COMPUTE FINAL VELOCITIES AND PRESSURES.
      C
64.        CALL VELPRZ(A,N,M,NM,I,V,RHO,E,GMONE,E1,E11,WS,FO,FON,BETA,
      C    FN,FE,EX)
      C
      C    SUBSTITUTE NEW VALUES INTO A.
      C
65.        CALL SUBZ(A,V,N,M,NM,I)
      C
66.   30 CONTINUE
      C
      C    REMOVE ENERGY FROM THE FIREBALL LOST VIA RADIATION.
      C
67.        CALL RADIAT(A,N,M,NM,E,Z,TIME,DT)
      C
      C    ADVANCE TIME AND CHECK FOR OUTPUT STEP AND STOP.
      C
68.        TIME = TIME + DT
69.        NSTEP = NSTEP + 1
70.        IF (NSTEP.GE.NSTOP.OR.TIME.GE.TSTOP) THEN
71.        CALL OUTDATA(A,N,M,NM,IOUT,JOUT,NROWS,NCOLS,DT,TIME,NSTEP,R,Z,1)
72.        STOP
73.        ELSE
74.        IF(NSTEP.EG.NOUT*NRITE+NOUTO) THEN
75.        CALL OUTDATA(A,N,M,NM,IOUT,JOUT,NROWS,NCOLS,DT,TIME,NSTEP,R,Z,0)
76.        NOUT = NOUT + 1
77.        END IF
78.        ENDIF
      C
      C    FIND MAXIMUM TIME STEP AND REPEAT THE CALCULATIONS.
      C
79.        CALL MAXT(A,N,M,NM,DT,E,Z,NMAXR,NMAXZL,NMAXZH)
80.        IF(NMAXR.GE.N-10)  CALL REZONE(0,A,N,M,NM,R,Z,RN,ZN,V)
81.        IF(NMAXZL.LE.10)   CALL REZONE(1,A,N,M,NM,R,Z,RN,ZN,V)
82.        IF(NMAXZH.GE.M-10) CALL REZONE(-1,A,N,M,NM,R,Z,RN,ZN,V)
      C
      C
83.        GO TO 10
84.        END
```

108

```
1.          SUBROUTINE QSETUP(N,DT,QPLUS,CENVEL,R)
2.          DIMENSION QPLUS(0:N-1),CENVEL(0:N-1),R(0:N-1)
      C
      C  SET UP THE Q ARRAYS.
      C
3.          DO 10 IC=0,N-2
4.          DR = R(IC+1)-R(IC)
5.          QPLUS(IC) = (0.5-CENVEL(IC)*DT/DR)/(1.+DT/DR*(CENVEL(IC+1)-
      C    CENVEL(IC)))
6.       10 CONTINUE
7.          RETURN
8.          END
```
VECTOR BLOCK BEGINS AT SEQ. NO.   1. P=   173

```
1.          SUBROUTINE VELCENR(A,N,NM,J,CENVEL,DT,R)
2.          DIMENSION A(0:7*NM-1),CENVEL(0:N-1),R(0:N-1)
3.          I1=5*NM+J*N
      C
      C
      C CALCULATE RADIALLY CENTERED VELOCITIES FOR ROW J
      C
4.          DO 10 IC=1,N-2
5.          DR=R(IC+1)-R(IC)
6.          EPS=ABS(A(IC+I1)*DT/DR)
7.          I2=CVMGP(1,-1,A(IC+I1))
8.          CENVEL(IC) = (1.-EPS/2.)*A(IC+I1)+EPS/2.*A(IC+I1+I2)
9.       10 CONTINUE
10.         CENVEL(0)=0.
11.         CENVEL(N-1) =0.0
12.         RETURN
13.         END
```

```
1.          SUBROUTINE VELCENZ(A,N,M,NM,I,CENVEL,DT,Z)
2.          DIMENSION A(0:7*NM-1),CENVEL(0:M-1),Z(0:M-1)
3.          I1=6*NM+I
      C
      C  CALCULATE AXIALLY CENTERED VELOCITIES FOR COLUMN I.
      C
4.          DO 10 JC=1,M-2
5.          DR=Z(JC+1)-Z(JC)
6.          EPS=ABS(A(N*JC+I1)*DT/DR)
7.          I2=CVMGP(N,-N,A(N*JC+I1))
8.          CENVEL(JC) = (1.-EPS/2.)*A(N*JC+I1)+EPS/2.*A(N*JC+I1+I2)
9.       10 CONTINUE
10.         CENVEL(0)=0.
11.         CENVEL(M-1) = 0.0
12.         RETURN
13.         END
```

109

```fortran
1.          SUBROUTINE SSETD(N,SPLUS)
2.          DIMENSION SPLUS(0:N-1)
C
C   DENSITY SOURCE ARRAY.
C
3.          DO 10 IC=0,N-2
4.          SPLUS(IC) = 0.0
5.       10 CONTINUE
6.          RETURN
7.          END
```

```fortran
1.          SUBROUTINE SSETMR(A,N,NM,J,DT,SPLUS,R)
2.          DIMENSION A(0:7*NM-1),SPLUS(0:N-1),R(0:N-1)
3.          I1=4*NM+J*N+1
4.          I2=4*NM+J*N
C
C   RADIAL MOMENTUM SOURCE ARRAYS FOR ROW J.
C
5.          DO 10 IC=0,N-2
6.          DR = R(IC+1)-R(IC)
7.          SPLUS(IC) = (A(IC+I1)-A(IC+I2))*DT/DR
8.       10 CONTINUE
9.          RETURN
10.         END
```

```fortran
1.          SUBROUTINE SSETER(A,N,NM,J,DT,SPLUS,R)
2.          DIMENSION A(0:7*NM-1),SPLUS(0:N-1),R(0:N-1)
3.          I1=4*NM+J*N+1
4.          I2=4*NM+J*N
5.          I3=5*NM+J*N+1
6.          I4=5*NM+J*N
C
C   RADIAL ENERGY SOURCE ARRAYS FOR ROW J.
C
7.          DO 10 IC=0,N-2
8.          DR = R(IC+1)-R(IC)
9.          R2=(R(IC+1)+R(IC))/2.
10.         SPLUS(IC) = (R(IC+1)*A(IC+I1)*A(IC+I3)-R(IC)*A(IC+I2)*A(IC+I4))/
C      R2/DR*DT
11.      10 CONTINUE
12.         RETURN
13.         END
```

```fortran
1.          SUBROUTINE SSETMZ(A,N,M,NM,I,DT,SPLUS,Z)
2.          DIMENSION A(0:7*NM-1),SPLUS(0:M-1),Z(0:M-1)
3.          I1=4*NM+I+N
4.          I2=4*NM+I
C
C     AXIAL MOMENTUM SOURCE ARRAYS FOR COLUMN I.
C
5.          DO 10 JC=0,M-2
6.          DR = Z(JC+1)-Z(JC)
7.          ZP = 6356766.+Z(JC)
8.          SPLUS(JC) = ((A(N*JC+I1)-A(N*JC+I2))/DR+A(N*JC+I)*
     C      3.9627176145E14/ZP/ZP)*DT
9.       10 CONTINUE
10.         RETURN
11.         END
```

```fortran
1.          SUBROUTINE SSETEZ(A,N,M,NM,I,DT,SPLUS,Z)
2.          DIMENSION A(0:7*NM-1),SPLUS(0:M-1),Z(0:M-1)
3.          I1=4*NM+I+N
4.          I2=4*NM+I
5.          I3=6*NM+I+N
6.          I4=6*NM+I
C
C     AXIAL ENERGY SORCES ARRAYS FOR COLUMN I.
C
7.          DO 10 JC=0,M-2
8.          DR = Z(JC+1)-Z(JC)
9.          ZP = 6356766.+Z(JC)
10.         SPLUS(JC) = ((A(N*JC+I1)*A(N*JC+I3)-A(N*JC+I2)*A(N*JC+I4))/DR
     C      +A(N*JC+I)*A(N*JC+I4)*3.9627176145E14/ZP/ZP)*DT
11.      10 CONTINUE
12.         RETURN
13.         END
```

```fortran
1.          SUBROUTINE SUBR(A,V,N,NM,J,M)
2.          DIMENSION A(0:7*NM-1),V(0:M-1,4)
C
C     SUBSTITUTE DENSITY, RADIAL AND AXIAL MOMENTA, AND ENERGY FROM THE
C     V SCRATCH ARRAY INTO A, FOR ROW J.
C
3.          DO 10 IC=0,N-2
4.          NODE = IC + J*N
5.          A(NODE) = V(IC,1)
6.          A(NM+NODE) = V(IC,2)
7.          A(2*NM+NODE) = V(IC,3)
8.          A(3*NM+NODE) = V(IC,4)
9.       10 CONTINUE
10.         RETURN
11.         END
```

111

```fortran
      1.         SUBROUTINE SUBZ(A,V,N,M,NM,I)
      2.         DIMENSION A(0:7*NM-1),V(0:M-1,4)
      C
      C    SUBSTITUTE DENSITY,AXIAL AND RADIAL MOMENTA, AND ENERGY FROM THE V
      C    SCRATCH ARRAY INTO A, FOR COLUMN I.
      C
      3.         DO 10 JC=0,M-2
      4.         NODE = I + JC*N
      5.         A(NODE) = V(JC,1)
      6.         A(NM+NODE) = V(JC,2)
      7.         A(2*NM+NODE) = V(JC,3)
      8.         A(3*NM+NODE) = V(JC,4)
      9.      10 CONTINUE
     10.         RETURN
     11.         END




      1.         SUBROUTINE VELPER(A,N,NM,J,V,M,RHO,E,GMONE,E1,E11,WS,FO,FON,
      C     BETA,FN,FE,EX)
      2.         DIMENSION A(0:7*NM-1),V(0:M-1,4)
      3.         DIMENSION RHO(0:N-1),E(0:N-1),GMONE(0:N-1),E1(0:N-1),E11(0:N-1),
      C     WS(0:N-1),FO(0:N-1),FON(0:N-1),BETA(0:N-1),FN(0:N-1),FE(0:N-1)
      C     ,EX(0:N-1)
      C
      C    LOAD RADIAL VELOCITIES AND PRESSURES INTO A FROM SCRATCH ARRAY V FOR
      C    ROW J.
      C
      4.         JN=J*N
      5.         I1=5*NM+JN
      6.         I2=6*NM+JN
      7.         I3=4*NM+JN
      8.         DO 10 I=0,N-1
      9.      10 A(I+I1) = V(I,2)/V(I,1)
     10.         DO 15 I=0,N-1
     11.      15 A(I+I2)=V(I,3)/V(I,1)
     12.         DO 20 I=0,N-1
     13.      20 A(I+I1)=CVMGT(0.,A(I+I1),ABS(A(I+I1)).LT.1.E-1)
     14.         DO 25 I=0,N-1
     15.         A(I+I2)=CVMGT(0.,A(I+I2),ABS(A(I+I2)).LT.1.E-1)
     16.         V(I,2)=CVMGT(0.,V(I,2),ABS(V(I,2)).LT.1.E-3)
     17.      25 V(I,3)=CVMGT(0.,V(I,3),ABS(V(I,3)).LT.1.E-3)
     18.         DO 30 I=0,N-1
     19.         E(I)=ABS((V(I,4)-V(I,2)*A(I+I1)/2.-V(I,3)*A(I+I2)/2.)/V(I,1))
     20.      30 RHO(I) = V(I,1)
     21.         CALL AIR(RHO,E,1.293,GMONE,1.E6,N,E1,E11,WS,FO,FON,BETA,FN,FE,EX)
     22.         DO 40 I=0,N-1
     23.      40 A(I+I3) = GMONE(I)*E(I)*RHO(I)
     24.         RETURN
     25.         END
```

112

```fortran
1.         SUBROUTINE VELPRZ(A,N,M,NM,I,V,RHO,E,GMONE,E1,E11,WS,FO,FON,
      C     BETA,FN,FE,EX)
2.         DIMENSION A(0:7*NM-1),V(0:M-1,4)
3.         DIMENSION RHO(0:M-1),E(0:M-1),GMONE(0:M-1),E1(0:M-1),E11(0:M-1),
      C     WS(0:M-1),FO(0:M-1),FON(0:M-1),BETA(0:M-1),FN(0:M-1),FE(0:M-1)
      C     ,EX(0:M-1)
      C
      C  LOAD AXIAL VELOCITIES AND PRESSURES INTO A FROM SCRATCH ARRAY V FOR
      C  COLUMN I.
      C
4.         I1=5*NM+I
5.         I2=6*NM+I
6.         I3=4*NM+I
7.         DO 10 J=0,M-1
8.      10 A(N*J+I1)=V(J,2)/V(J,1)
9.         DO 15 J=0,M-1
10.     15 A(N*J+I2)=V(J,3)/V(J,1)
11.        DO 20 J=0,M-1
12.     20 A(N*J+I1)=CVMGT(0.,A(N*J+I1),ABS(A(N*J+I1)).LT.1.E-1)
13.        DO 25 J=0,M-1
14.        A(N*J+I2)=CVMGT(0.,A(N*J+I2),ABS(A(N*J+I2)).LT.1.E-1)
15.        V(J,2)=CVMGT(0.,V(J,2),ABS(V(J,2)).LT.1.E-3)
16.     25 V(J,3)=CVMGT(0.,V(J,3),ABS(V(J,3)).LT.1.E-3)
17.        DO 30 J=0,M-1
18.        RHO(J)=V(J,1)
19.     30 E(J)=ABS((V(J,4)-V(J,2)*A(N*J+I1)/2.-V(J,3)*A(N*J+I2)/2.)/V(J,1))
20.        CALL AIR(RHO,E,1.293,GMONE,1.E6,M,E1,E11,WS,FO,FON,BETA,FN,FE,EX)
21.        DO 40 J=0,M-1
22.     40 A(J*N+I3)=GMONE(J)*E(J)*RHO(J)
23.        RETURN
24.        END
```

113

```
1.          SUBROUTINE MAXT(A,N,M,NM,DT,R,Z,NMAXR,NMAXZL,NMAXZH)
2.          DIMENSION A(0:7*NM-1) ,R(0:N-1),Z(0:M-1)
    C
    C    FIND MAXIMUM VELOCITY AND CALCULATE TIME STEP.
    C
3.          DT=1.E10
4.          NUM2=(M-1)/2*N
5.          NUM1=5*NM+NUM2
6.          NUM=4*NM+NUM2
7.          PMAX=A(NUM)
8.          DO 10 I=1,N-2
9.          DT1=0.25*(R(I+1)-R(I))/(ABS(A(NUM1+I))+SQRT(1.4*A(NUM+I)/
    C              A(NUM2+I)))
10.         IF(DT1.LT.DT)DT=DT1
11.         IF(A(NUM+I).LT.PMAX)GO TO 10
12.         PMAX=A(NUM+I)
13.         NMAXR=I
14.     10 CONTINUE
15.         PMAX=A(NUM)
16.         NUM1=6*NM
17.         NUM=4*NM
18.         DO 20 J=(M-1)/2+1,M-2
19.         DT1=0.25*(Z(J+1)-Z(J))/(ABS(A(NUM1+J*N))+SQRT(1.4*A(NUM+J*N)/A
    C        (J*N)))
20.         IF(DT1.LT.DT)DT=DT1
21.         IF(A(NUM+J*N).LT.PMAX)GO TO 20
22.         PMAX=A(NUM+J*N)
23.         NMAXZH=J
24.     20 CONTINUE
25.         PMAX=A(NUM)
26.         DO 30 J=1,(M-1)/2
27.         DT1=0.25*(Z(J)-Z(J-1))/(ABS(A(NUM1+J*N))
    C        +SQRT(1.4*A(NUM+J*N)/A(J*N)))
28.         IF(DT1.LT.DT)DT=DT1
29.         IF(A(NUM+J*N).LT.PMAX)GO TO 30
30.         PMAX=A(NUM+J*N)
31.         NMAXZL=J
32.     30 CONTINUE
33.         RETURN
34.         END
```

114

```
1.         SUBROUTINE REZONE(IDIF,A,N,M,NM,R,Z,RN,ZN,V)
2.         DIMENSION A(0:7*NM-1),R(0:N-1),Z(0:M-1),RN(0:N-1),ZN(0:M-1),
    C    V(0:M-1,4)
3.         M12=(M-1)/2
4.         RN(0)=0.0
5.         ZN(M12)=15000.
    C
6.         IF(IDIF) 25,50,75
    C
    C   REZONE THE UPPER HALF OF THE MESH.
    C
7.      25 CONTINUE
8.         DO 26 J=M12+1,M-1
9.      26 ZN(J)=(Z(J)-Z(M12))*1.11+Z(M12)
10.        JNEW=M12
11.        JLAST=M12
12.        ZNM=Z(M12)
13.        DO 40 J=M12,M-2
14.        DO 29 I=0,N-1
15.        DO 29 K=1,4
16.     29 V(I,K)=0.0
17.        ZNP = (ZN(J)+ZN(J+1))/2.
18.     30 ZOLDP=(Z(JNEW)+Z(JNEW+1))/2.
19.        IF(ZNP.GT.ZOLDP) THEN
20.        JNEW=JNEW+1
21.        IF(JNEW.EQ.M-1) THEN
22.        CALL STATM(-1,J,A,N,M,NM,RN,ZN,M12)
23.        GO TO 41
24.        END IF
25.        GO TO 30
26.        END IF
27.        Z2 = ZNM
28.        DEN = ZNP-ZNM
29.        DO 37 JJ=0,JNEW-JLAST
30.        Z1 = (Z(JLAST+JJ)+Z(JLAST+JJ+1))/2.
31.        IF(JJ.EQ.JNEW-JLAST) Z1=ZNP
32.        G=Z1-Z2
33.        DO 36 I=1,N-2
34.        DO 36 KK=1,4
35.     36 V(I,KK) = V(I,KK)+A((KK-1)*NM+I+(JLAST+JJ)*N)*G/DEN
36.        Z2 = Z1
37.     37 CONTINUE
38.        JLAST = JNEW
39.        ZNM = ZNP
40.        V(0,1)=V(1,1)
41.        V(0,2)=V(1,2)
42.        V(0,3)=V(1,3)
43.        V(0,4)=V(1,4)
44.        V(N-1 ,1) =V(N-2 ,1)
45.        V(N-1,2)=V(N-2,2)
46.        V(N-1,3)=V(N-2,3)
47.        V(N-1,4)=V(N-2,4)
48.        DO 38 I=0,N-1
49.        NODE=I+J*N
50.        A(NODE)=V(I,1)
51.        A(NM+NODE)=V(I,2)
52.        A(2*NM+NODE)=V(I,3)
53.        A(3*NM+NODE)=V(I,4)
```

115

```
54.         A(5*NM+NODE)=V(I,2)/V(I,1)
55.         A(6*NM+NODE)=V(I,3)/V(I,1)
56.         NUMVR=5*NM+NODE
57.         NUMVZ=6*NM+NODE
58.         E=(V(I,4)-(A(NUMVR)*A(NUMVR)+A(NUMVZ)*A(NUMVZ))/2.)/V(I,1)
59.         CALL GAS(V(I,1),E,1.293,GM1,1.E6)
60.         A(4*NM+NODE)=GM1*E*V(I,1)
61.      38 CONTINUE
62.      40 CONTINUE
63.      41 CONTINUE
64.         DO 42 J=M12+1,M-1
65.      42 Z(J)=ZN(J)
66.         RETURN
      C
      C     REZONE IN THE RADIAL DIRECTION
      C
67.      50 CONTINUE
68.         DO 51 I=1,N-1
69.      51 RN(I)=R(I)*1.11
70.         INEW=1
71.         ILAST=1
72.         RNM=(RN(0)+RN(1))/2.
73.         DO 65 I=1,N-2
74.         DO 54 J=0,M-1
75.         DO 54 K=1,4
76.      54 V(J,K)=0.0
77.         RNP=(RN(I)+RN(I+1))/2.
78.      55 ROLDP=(R(INEW)+R(INEW+1))/2.
79.         IF(RNP.GT.ROLDP) THEN
80.         INEW=INEW+1
81.         IF(INEW.EQ.N-1) THEN
82.         CALL STATM(0,I,A,N,M,NM,RN,Z ,M12)
83.         GO TO 66
84.         END IF
85.         GO TO 55
86.         END IF
87.         P2 = RNM
88.         DEN = RNP*RNP-RNM*RNM
89.         DO 62 II=0,INEW-ILAST
90.         R1 = (R(ILAST+II)+R(ILAST+II+1))/2.
91.         IF(II.EQ.INEW-ILAST) R1=RNP
92.         F=R1*R1-R2*R2
93.         DO 61 J=0,M-1
94.         DO 61 KK=1,4
95.      61 V(J,KK)=V(J,KK)+A((KK-1)*NM+(ILAST+II)+J*N)*F/DEN
96.         R2 = R1
97.      62 CONTINUE
98.         ILAST=INEW
99.         RNM=RNP
100.        DO 63 J=0,M-1
101.        NODE=I+J*N
102.        A(NODE)=V(J,1)
103.        A(NM+NODE)=V(J,2)
104.        A(2*NM+NODE)=V(J,3)
105.        A(3*NM+NODE)=V(J,4)
106.        A(5*NM+NODE)=V(J,2)/V(J,1)
107.        A(6*NM+NODE)=V(J,3)/V(J,1)
108.        NUMVR=5*NM+NODE
```

116

```
109.        NUMVZ=E*NM+NODE
110.        E=(V(J,4)-(A(NUMVR)*A(NUMVR)+A(NUMVZ)*A(NUMVZ))/2.)/V(J,1)
111.        CALL GAS(V(J,1),E,1.293,GM1,1.76)
112.        A(4*NM+NODE)=GM1*E*V(J,1)
113.     63 CONTINUE
114.     65 CONTINUE
115.     66 CONTINUE
116.        DO 67 I=1,N-1
117.     67 F(I) = RN(I)
118.        RETURN
      C
      C
      C  F.ZONE THE LOWER HALF OF THE MESH.
      C
119.     75 CONTINUE
120.        DO 76 J=1,M12
121.     76 ZN(M12-J)=Z(M12)-(Z(M12)-Z(M12-J))*1.11
122.        JNEW = M12
123.        JLAST=M12
124.        ZNM=Z(M12)
125.        DO 90 J=0,M12-2
126.        DO 79 I=0,N-1
127.        DO 79 K=1,4
128.     79 V(I,K) = 0.0
129.        ZNP = (ZN(M12-J)+ZN(M12-J-1))/2.
130.     80 ZOLDP = (Z(JNEW)+Z(JNEW-1))/2.
131.        IF(ZNP.LT.ZOLDP) THEN
132.        JNEW=JNEW-1
133.        IF(JNEW.EQ.0) THEN
134.        CALL STATM(1,J,A,N,M,NM,RN,ZN,M12)
135.        GO TO 91
136.        ENDIF
137.        GO TO 80
138.        ENDIF
139.        Z2 = ZNM
140.        DEN = ZNM-ZNP
141.        DO 87 JJ=0,JLAST-JNEW
142.        Z1 = (Z(JLAST-JJ)+Z(JLAST-JJ-1))/2.
143.        IF(JJ.EQ.JLAST-JNEW) Z1=ZNP
144.        G=Z2-Z1
145.        DO 86 I=1,N-2
146.        DO 86 KK=1,4
147.     86 V(I,KK)=V(I,KK)+A((KK-1)*NM+I+(JLAST-JJ)*N)*G/DEN
148.        Z2 = Z1
149.     87 CONTINUE
150.        JLAST=JNEW
151.        ZNM=ZNP
152.        V(0,1)=V(1,1)
153.        V(0,2)=V(1,2)
154.        V(0,3)=V(1,3)
155.        V(0,4)=V(1,4)
156.        V(N-1 ,1) =V(N-2 ,1)
157.        V(N-1,2)=V(N-2,2)
158.        V(N-1,3)=V(N-2,3)
159.        V(N-1,4)=V(N-2,4)
160.        DO 88 I=0,N-1
161.        NODE = I+(M12-J)*N
162.        A(NODE)=V(I,1)
163.        A(NM+NODE)=V(I,2)
```

117

```
164.        A(2*NM+NODE)=V(I,3)
165.        A(3*NM+NODE)=V(I,4)
166.        A(5*NM+NODE)=V(I,2)/V(I,1)
167.        A(6*NM+NODE)=V(I,3)/V(I,1)
168.        NUMVR=5*NM+NODE
169.        NUMV7=6*NM+NODE
170.        E=(V(I,4)-(A(NUMVR)*A(NUMVR)+A(NUMVZ)*A(NUMVZ))/2.)/V(I,1)
171.        CALL GAS(V(I,1),E,1.293,GM1,1.E6)
172.        A(4*NM+NODE)=GM1*E*V(I,1)
173.     88 CONTINUE
174.     90 CONTINUE
175.     91 CONTINUE
176.        DO 92 J=1,M12
177.     92 Z(M12-J) = ZN(M12-J)
178.        RETURN
179.        END
```

```
1.          SUBROUTINE STATM(IDIR,IJ,A,N,M,NM,R,Z,M12)
2.          DIMENSION A(0:7*NM-1),R(0:N-1),Z(0:M-1)
     C
3.          IF(IDIR) 25,50,75
     C
     C    MESH THE UPPER BOUNDARY FROM AXIAL NODE IJ TO M-1.
     C
4.       25 CONTINUE
5.          DO 30 J=IJ,M-1
6.          CALL PROP(Z(J),D,E,P)
7.          DO 30 I=0,N-1
8.          NODE=I+J*N
9.          A(NODE) = D
10.         A(NM+NODE)=0.0
11.         A(2*NM+NODE)=0.0
12.         A(3*NM+NODE) = E
13.         A(4*NM+NODE) = P
14.         A(5*NM+NODE)=0.0
15.         A(6*NM+NODE)=0.0
16.      30 CONTINUE
17.         RETURN
     C
     C    MESH THE RIGHT BOUNDARY FROM RADIAL NODE IJ TO N-1.
     C
18.      50 CONTINUE
19.         DO 55 I=IJ,N-1
20.         DO 55 J=0,M-1
21.         CALL PROP(Z(J),D,E,P)
22.         NODE=I+J*N
23.         A(NODE) = D
24.         A(NM+NODE)=0.0
25.         A(2*NM+NODE)=0.0
26.         A(3*NM+NODE) = E
27.         A(4*NM+NODE) = P
28.         A(5*NM+NODE)=0.0
29.         A(6*NM+NODE)=0.0
30.      55 CONTINUE
31.         RETURN
     C
     C    MESH THE LOWER BOUNDARY FROM AXIAL NODE IJ TO 0.
     C
32.      75 CONTINUE
33.         DO 80 J=IJ,M12
34.         CALL PROP(Z(M12-J),D,E,P)
35.         DO 80 I=0,N-1
36.         NODE = I+(M12-J)*N
37.         A(NODE) = D
38.         A(NM+NODE)=0.0
39.         A(2*NM+NODE)=0.0
40.         A(3*NM+NODE) = E
41.         A(4*NM+NODE) = P
42.         A(5*NM+NODE)=0.0
43.         A(6*NM+NODE)=0.0
44.      80 CONTINUE
45.         RETURN
46.         END
```

119

```
1.          SUBROUTINE PROP(ZM,D,E,PASCAL)
2.          DIMENSION Z(0:10),T(0:10),P(0:10)
3.          DATA Z/
    +0.              , .110000000E+02, .201000000E+02, .322000000E+02,
    + .474000000E+02, .515000000E+02, .720000000E+02, .860000000E+02,
    + .940000000E+02, .980000000E+02, .100000000E+03/
4.          DATA T/
    + .288150000E+03, .216774000E+03, .216650000E+03, .228756000E+03,
    + .270650000E+03, .270409000E+03, .214263000E+03, .186870000E+03,
    + .186740000E+03, .191720000E+03, .195080000E+03/
5.          DATA P/
    + .101325000E+07, .227026964E+06, .544626539E+05, .863909415E+04,
    + .110243380E+04, .662140402E+03, .384129611E+02, .373740480E+01,
    + .904559560E+00, .449637609E+00, .319224329E+00/
6.          PO = 6356.766
7.          GO = 9.80665
8.          R = 8.3143
9.          WTM = 28.9644
10.         ZKM = ZM*0.001
    C
    C
11.         DO 10 I=0,10
12.         IF(ZKM.LE.Z(I)) GO TO 11
13.      10 CONTINUE
14.      11 CONTINUE
15.         SLOPE = (T(I)-T(I-1)) / (Z(I)-Z(I-1))
16.         A = -GO*RO*RO*WTM/R/SLOPE/(RO+Z(I-1)-T(I-1)/SLOPE)
17.         B = (Z(I-1)-ZKM)/(RO+ZKM)/(RO+Z(I-1))
18.         C = ALOG((RO+ZKM)*T(I-1)/(RO+Z(I-1))/(T(I-1)+SLOPE*(ZKM-Z(I-1))))
19.         C = C/(RO+Z(I-1)-T(I-1)/SLOPE)
20.         POYNE = P(I-1)*EXP(A*(B-C))
21.         TEMP = T(I-1)+SLOPE*(ZKM-Z(I-1))
22.         PASCAL = POYNE*0.1
23.         D=PASCAL*WTM*0.001/R/TEMP
    C
    C
24.         EL = PASCAL/1.5/D
25.         EH = 4.5E6
26.         GM1P = 1.5
27.         NC = 1
28.      20 EINT = (EL+EH)/2.
29.         CALL GAS(D,EINT,1.293,GM1,1.E6)
30.         IF(ABS(GM1-GM1P).LT.1.E-9) GO TO 50
31.         IF(NC.GT.100) GO TO 50
32.         EP = PASCAL/D/GM1
33.         IF(EP.GT.EINT) EL=EINT
34.         IF(EP.LT.EINT) EH=EINT
35.         NC = NC+1
36.         GM1P = GM1
37.         GO TO 20
38.      50 E = EINT*D
    C
    C
39.         RETURN
40.         END
```

120

```
1.          SUBROUTINE RADIAT(A,N,M,NM,R,Z,TIME,DT)
2.          DIMENSION A(0:7*NM-1),R(0:N-1),Z(0:M-1),P(18),T(18)
3.          DATA P/.04,.278,.6,.84,1.,.878,.7,.41,.297,.192,.142,.115,.087,
       C   .072,.06,.053,.032,.022,.02/
4.          DATA T/0.,.25,.5,.75,1.,1.25,1.5,2.,2.25,2.5,2.75,3.,3.5,4.,4.5,
       C   5.,8.,10./
       C
       C   CALCULATE TOTAL FIREBALL ENERGY LOSS.
       C
5.          HOTSUM = 0.0
6.          DO 25 J=0,M-1
7.          DO 20 I=0,N-1
8.          NODE = I+J*N
9.          EINT = A(3*NM+NODE)/A(NODE) - (A(5*NM+NODE)*A(5*NM+NODE)+
       C                                   A(6*NM+NODE)*A(6*NM+NODE))/2.
10.         IF(EINT.LE.7.E5) GO TO 25
11.         VOL = 3.14159/6.*((R(I+1)+R(I))*(R(I+1)+R(I))-(R(I-1)+R(I))*
       C    (R(I-1)+R(I)))*(Z(J+1)-Z(J-1))
12.         HOTSUM = HOTSUM + A(NODE)*VOL*EINT*EINT*EINT
13.      20 CONTINUE
14.      25 CONTINUE
       C
       C   CALCULATE EACH ELEMENT'S ENERGY LOSS.
       C
15.         THAT = (TIME+DT/2.) / 0.039
16.         DO 30 I=2,19
17.         IF(T(I).GE.THAT) GO TO 31
18.      30 CONTINUE
19.      31 CONTINUE
20.         IF(I.LT.19) THEN
21.         PHAT = P(I)-(T(I)-THAT)*(P(I)-P(I-1))/(T(I)-T(I-1))
22.         ELSE
23.         PHAT = 0.02
24.         END IF
25.         PTOT = PHAT * 1.49E13
26.         DO 45 J=0,M-1
27.         DO 40 I=0,N-1
28.         NODE = I+J*N
29.         EINT = A(3*NM+NODE)/A(NODE) - (A(5*NM+NODE)*A(5*NM+NODE)+
       C                                   A(6*NM+NODE)*A(6*NM+NODE))/2.
30.         IF(EINT.LE.7.E5) GO TO 45
31.         Q = PTOT/HOTSUM*A(NODE)*EINT*EINT*EINT*DT
32.         A(3*NM+NODE) = A(3*NM+NODE)-Q
33.      40 CONTINUE
34.      45 CONTINUE
35.         RETURN
36.         END
```

121

```fortran
      1.          SUBROUTINE INDATA(A,N,M,NM,IOUT,JOUT,NROWS,NCOLS,V,TSTOP,
           C    NSTOP,NFITE,   DT,TIME,NSTEP,R,Z)
      2.          DIMENSION A(0:7*NM-1),IOUT(3),JOUT(3),V(0:N-1,4),R(0:N-1),Z(0:M-1
      3.          NSTEP = 0
      4.          READ(5,100) TSTOP,NSTOP,NFITE,NRS,NIT
      5.      100 FORMAT(E10.4,4I5)
      6.          READ(5,200)    TIME,NROWS,NCOLS
      7.          READ(5,300) (IOUT(I),I=1,NROWS),(JOUT(I),I=1,NCOLS)
      8.      200 FORMAT( E10.4,3I5)
      9.      300 FORMAT(6I5)
     10.          IF(NRS.EQ.1) GO TO 11
     11.          READ(8) TIME,NSTEP,DT
     12.          READ(8) (R(I),I=0,N-1),(Z(J),J=0,M-1)
     13.          DO 10 J=0,NM-1
     14.       10 READ(8) JC,(A(I*NM+J),I=0,6)
     15.          GO TO 20
     16.       11 CONTINUE
     17.       12 READ(8) TIME,NSTEP,DT
     18.          READ(8) (R(I),I=0,N-1),(Z(J),J=0,M-1)
     19.          DO 13 J=0,NM-1
     20.       13 READ(8) JC,(A(I*NM+J),I=0,6)
     21.          IF(NSTEP.NE.NST) GO TO 12
     22.       20 CONTINUE
     23.          DO 30 NODE = 0,N-1
     24.          DO 30 I=1,4
     25.       30 V(NODE,I) = A((I-1)*NM+NODE)
     26.          RETURN
     27.          END
```

```fortran
      1.          SUBROUTINE OUTDATA(A,N,M,NM,IOUT,JOUT,NROWS,NCOLS,DT,
     C       TIME,NSTEP,R,Z,ISTOP)
      2.          DIMENSION A(0:7*NM-1),IOUT(3),JOUT(3),R(0:N-1),Z(0:M-1)
      3.          WRITE(6,100) TIME,NSTEP,DT
      4.  100 FORMAT(///////,13X,*TIME=*,E10.4,5X,*NSTEP=*,I5,5X,*DT=*,E10.4)
      5.          WRITE(9,700) TIME,NSTEP,DT
      6.  700 FORMAT(E15.8,I10,E15.8)
      7.          DO 1 I=0,N-1
      8.    1 WRITE(9,800)   R(I)
      9.          DO 2 J=0,M-1
     10.    2 WRITE(9,800) Z(J)
     11.          DO 3 J=0,NM-1
     12.          DO 3 I=0,6
     13.    3 WRITE(9,800) A(I*NM+J)
     14.  800 FORMAT(E15.8)
     15.          DO 40 JO=1,NCOLS
     16.          WRITE(6,200) JOUT(JO)
     17.  200 FORMAT(10X,*COLUMN=*,I5)
     18.          WRITE(6,300)
     19.  300 FORMAT(//,5X,*J*,6X,*Z(J)*,11X,*RHO*,6X,*R-MOMENTUM*,3X,*Z-MOMENT
     C      UM*,4X,*ENERGY*,6X,*PRESSURE*,5X,*R-VELOCITY*,5X,*Z-VELOCITY*)
     20.          DO 15 J=0,M-1
     21.          ZHT=Z(J)-Z((M-1)/2)
     22.   15 WRITE(6,400) J,ZHT,(A(I*NM+JOUT(JO)+J*N),I=0,6)
     23.  400 FORMAT(3X,I3,8(3X,E10.4))
     24.   40 CONTINUE
     25.          DO 70 IO=1,NROWS
     26.          WRITE(6,500) IOUT(IO)
     27.  500 FORMAT(10X,*ROW=*,I5)
     28.          WRITE(6,600)
     29.  600 FORMAT(//,5X,*J*,6X,*E(J)*,11X,*RHO*,6X,*R-MOMENTUM*,3X,*Z-MOMENT
     C      UM*,4X,*ENERGY*,6X,*PRESSURE*,5X,*R-VELOCITY*,5X,*Z-VELOCITY*)
     30.          DO 45 I=0,N-1
     31.   45 WRITE(6,400) I,R(I),(A(J*NM+I+IOUT(IO)*N),J=0,6)
     32.   70 CONTINUE
     33.          IF(ISTOP.EQ.0) RETURN
     34.          WRITE(7) TIME,NSTEP,DT
     35.          WRITE(7) (R(I),I=0,N-1),(Z(J),J=0,M-1)
     36.          DO 90 J=0,NM-1
     37.   90 WRITE(7) J,(A(I*NM+J),I=0,6)
     38.          RETURN
     39.          END
```

```
1.          SUBROUTINE AIR(RHO,EX,RHOZ,GMONE,EZ,N,E1,E11,WS,FO,FON,BETA,
   C     FN,FE,E)
2.          DIMENSION RHO(0:N-1),EX(0:N-1),E(0:N-1),GMONE(0:N-1),E1(0:N-1),
   C     E11(0:N-1),WS(0:N-1),FO(0:N-1),FON(0:N-1),BETA(0:N-1),FN(0:N-1)
   C     ,FE(0:N-1)
C
C    SEMI-PHYSICAL FIT TO THE EQUATION OF STATE OF AIR
C    SUBROUTINE BY L.F. LOAN AND G.H. NICKEL.
C
C          TEMPERATURES FROM .025 TO 1.5 ELECTRON VOLTS.
C          DENSITIES FROM 10**(-7) NORMAL DENSITY.
C          PRESSURE * (GAMMA-1.)*RHO*E, WHERE GAMMA IS A FUNCTION OF
C             DENSITY AND ENERGY.
C    RHO = MATERIAL DENSITY.
C    RHOZ = 1.2935E MEGAGRAMS/CUBIC KILOMETER, IN THE UNITS OF THE
C             PROBLEM.
C    E = ENERGY/MASS
C    EZ = 1 JERK/MEGAGRAM, IN THE UNITS OF THE PROBLEM..
C    GMONE = (GAMMA - 1.)
C
3.          DO 1 I=0,N-1
4.        1 E(I)=EX(I)
5.          DO 2 I=0,N-1
6.        2 E(I) = ABS(E(I))/EZ
7.          DO 3 I=0,N-1
8.        3 E1(I)=(8.5-E(I))/0.975
9.          DO 5 I=0,N-1
10.         DE1=0.975*(RHO(I)/RHOZ)**0.05
11.         EE1=8.5+0.357*ALOG(RHO(I)/RHOZ)/2.3026
12.       5 E11(I)=(EE1-E(I))/DE1
13.         DO 10 I=0,N-1
14.      10 WS(I)=1./(EXP(-E11(I))+1.)
15.         DO 20 I=0,N-1
16.      20 WS(I)=CVMGT(0.,WS(I),E1(I).LE.-5.)
17.         DO 30 I=0,N-1
18.      30 WS(I)=CVMGT(1.,WS(I),E1(I).GT.5.)
19.         DO 40 I=0,N-1
20.         FO(I)=WS(I)*EXP(-E(I)/4.46)
21.      40 FON(I)=(1.-WS(I))*EXP(-E(I)/6.63)
C
C
22.         DO 50 I=0,N-1
23.      50 BETA(I)=(0.048*WS(I)+0.032*(1.-WS(I)))*ALOG(AMAX1(E(I),1.))
   C     /2.3026
24.         DO 60 I=0,N-1
25.         DE2=4.*(RHO(I)/RHOZ)**0.085
26.         EE2=45.*(RHO(I)/RHOZ)**0.0157
27.         E2=(E(I)-EE2)/DE2
28.      60 WS(I)=1./(EXP(-E2)+1.)
29.         DO 65 I=0,N-1
30.      65 E1(I)=(E(I)-40.)*0.33333333333333333333
31.         DO 70 I=0,N-1
32.      70 WS(I)=CVMGT(0.,WS(I),E1(I).LE.-5.)
33.         DO 80 I=0,N-1
34.      80 WS(I)=CVMGT(1.,WS(I),E1(I).GT.5.)
35.         DO 90 I=0,N-1
36.         FN(I)=WS(I)*EXP(-E(I)/25.5)
37.      90 BETA(I)=BETA(I)*(1.-WS(I))+0.045*WS(I)
```

124

```fortran
38.          DO 100 I=0,N-1
39.          E3=(E(I)-160.)/6.
40.     100  FE(I)=CVMGT(0.,1./(EXP(-E3)+1.),E3+5..LT.0.)
       C
       C
41.          DO 110 I=0,N-1
42.          RHOFAC=(RHO(I)/RHOZ)**BETA(I)
43.     110  GMONE(I)=(0.181+0.255*FO(I)+0.28*FON(I)+0.137*FN(I)+0.05*FE(I)
       C     )*RHOFAC
44.          RETURN
45.          END
```

```
1.          SUBROUTINE SHALTAZ(NM,V,I,A,N,M,ICOL,QPLUS,SPLUS,Z,FD,FT,VTD,
      C     DVTD,FC,R1,R2)
2.          DIMENSION A(0:7*NM-1),V(0:M-1),QPLUS(0:M-1),SPLUS(0:M-1),Z(0:M-1)
      C     ,FD(0:M-1),FT(0:M-1),VTD(0:M-1),DVTD(0:M-1),FC(0:M-1),
      C     R1(0:M-1),R2(0:M-1)
3.          INM = I * NM
4.          I1=INM+ICOL
5.          I2=I1+N
      C
      C    ADVANCE THE FLUID PROPERTIES I ONE TIME STEP IN THE AXIAL DIRECTION
      C    FOR COLUMN ICOL.   RETURN NEW VALUES IN V.
      C
      C       IF I = 0, DENSITY
      C                1, FACIAL MOMENTUM
      C                2, AXIAL MOMENTUM
      C                3, ENERGY
      C
      C
6.          V(0) = A(INM+ICOL)
7.          VTD(0)=0.0
8.          DO 5 J=1,M-4
9.          R1(J)=(Z(J)-Z(J-1))/(Z(J+1)-Z(J-1))
10.         R2(J)=(Z(J+1)-Z(J))/(Z(J+1)-Z(J-1))
11.       5 CONTINUE
      C
12.         FD(0)=0.0
13.         FT(0)=0.0
14.         DO 10 J=1,M-4
15.         FD(J)=0.25*(A(N*J+I1)-A(N*J+I2))
16.         FT(J)=(QPLUS(J)*QPLUS(J)-2.*QPLUS(J)+0.75)*A(N*J+I1)
      C       -(QPLUS(J)*QPLUS(J)-0.25)*A(N*J+I2)
17.      10 CONTINUE
      C
18.         DO 20 J=1,M-4
19.         VTD(J)=A(N*J+I1)+R1(J)*(FD(J-1)+FT(J-1))-R2(J)*(FD(J)+FT(J))
      C       -2.*R2(J)*QPLUS(J)*SPLUS(J)-2.*R1(J)*(1.-QPLUS(J-1))*SPLUS(J-1
20.      20 CONTINUE
21.         VTD(M-3)=VTD(M-4)
      C
22.         DVTD(0)=0.0
23.         DO 30 J=1,M-4
24.         DVTD(J)=VTD(J+1)-VTD(J)
25.      30 CONTINUE
26.         DVTD(M-3)=0.0
      C
27.         FC(0)=0.0
28.         DO 40 J=1,M-4
29.         S=SIGN(1.,DVTD(J))
30.         A1=AMIN1(S*DVTD(J-1)/R2(J)/2.,ABS(DVTD(J))*0.125,
      C       S*DVTD(J+1)/R2(J)/2.)
31.         FC(J)=S*AMAX1(0.,A1)
32.      40 CONTINUE
      C
33.         DO 50 J=1,M-4
34.         V(J)=VTD(J)+FC(J-1)*R1(J)*2.-FC(J)*R2(J)*2.
35.      50 CONTINUE
36.         V(M-3) = A(INM+ICOL+(M-3)*N)
37.         V(M-2) = A(INM+ICOL+(M-2)*N)
```

126

```
38.          V(M-1) = A(INM+ICOL+(M-1)*N)
39.          IF(I.EQ.1.AND.ICOL.EQ.0) THEN
40.          DO 60 J=0,M-1
41.     60   V(J)=0.
42.          END IF
43.          RETURN
44.          END
```

127

```
  1.         SUBROUTINE SHASTAR(NM,V,K,A,N,J,QPLUS,SPLUS,R,FD,FT,VTD,DVTD,
       C    FC,R1,F2,R3,F4)
  2.         DIMENSION A(0:7*NM-1),V(0:N-1),QPLUS(0:N-1),SPLUS(0:N-1),R(0:N-1
       C    ,FD(0:N-1),FT(0:N-1),VTD(0:N-1),DVTD(0:N-1),FC(0:N-1),
       C    R1(0:N-1),F2(0:N-1),R3(0:N-1),F4(0:N-1)
  3.         INM = K * NM
  4.         JN = J * N
  5.         I1=INM+JN
  6.         I2=I1+1
       C
       C    ADVANCE THE FLUID PROPERTY K ONE TIME STEP IN THE RADIAL DIRECTION
       C    FOW J.  RITURN THE NEW VALUES IN V.
       C       IF K=0, DENSITY IS ADVANCED
       C          1, RADIAL MOMENTUM
       C          2, AXIAL MOMENTUM
       C          3, ENERGY
       C
       C
  7.         DO 5 I=1,N-4
  8.         F1(I) = (R(I)+R(I-1))/2./R(I)
  9.         P2(I) = (R(I)+R(I+1))/2./R(I)
 10.         R3(I) = (R(I)-R(I-1))/    (R(I+1)-R(I-1))
 11.         F4(I) = (R(I+1)-R(I))/    (R(I+1)-R(I-1))
 12.      5 CONTINUE
       C
 13.         FD(0) = 0.C
 14.         FT(0) = 0.C
 15.         DO 10 I=1,N-4
 16.         FD(I)=0.25*(A(I+I1)-A(I+I2))
 17.         FT(I)=(QPLUS(I)*QPLUS(I)-2.*QPLUS(I)+0.75)*A(I+I1) -
       C    (QPLUS(I)*QPLUS(I)-0.25)*A(I+I2)
 18.     10 CONTINUE
       C
 19.         DO 20 I=1,N-4
 20.         VTD(I) = A(I+I1)+R1(I)*R3(I)*(FD(I-1)+FT(I-1)) -
       C    R2(I)*F4(I)*(FD(I)+FT(I)) - 2.*F4(I)*QPLUS(I)*SPLUS(I)
       C       -2.*F3(I)*(1.-QPLUS(I-1))*SPLUS(I-1)
 21.     20 CONTINUE
 22.         VTD(N-3)=VTD(N-4)
 23.         DVTD(0)=0.C
 24.         DO 30 I=1,N-4
 25.         DVTD(I) = VTD(I+1) - VTD(I)
 26.     30 CONTINUE
 27.         DVTD(N-3) = 0.0                                                    .
       C
 28.         FC(0) = 0.C
 29.         DO 40 I=1,N-4
 30.         S = SIGN(1.,DVTD(I))
 31.         A1 = AMIN1(S*DVTD(I-1)/R2(I)/F4(I)/2.,ABS(DVTD(I))*0.125,
       C    S*DVTD(I+1)/F2(I)/F4(I)/2.)
 32.         FC(I) = S*AMAX1(0.,A1)
 33.     40 CONTINUE
       C
 34.         DO 50 I=1,N-4
 35.         V(I) = VTD(I) + FC(I-1)*F1(I)*F3(I)*2. - FC(I)*R2(I)*R4(I)*2.
 36.     50 CONTINUE
 37.         V(0) = V(1)
 38.         IF(I.EQ.1) V(0) = 0.0
```

128

```
39.        V(N-3) = A(INM+N-3+JN)
40.        V(N-2) = A(INM+N-2+JN)
41.        V(N-1) = A(INM+N-1+JN)
42.        RETURN
43.        END
```

Bibliography

Bach, G.G., A.L. Kuhl, A.K. Oppenheim, "On Blast Waves in Exponential Atmospheres," J. Fluid Mechanics, 71 (1975), 105-122.

Boris, J.P. and D.L. Book, "Flux-Corrected Transport. I. SHASTA, A Fluid Transport Algorithm That Works," J. Computational Physics, 11, (1973), 38-69.

Book, D.L., J.P. Boris, and K. Hain, "Flux-Corrected Transport II: Generalizations of the Method," J. Computational Physics, 18, (1975), 248-283.

Boris, J.P. and D.L. Book, "Flux-Corrected Transport III. Minimal Error FCT Algorithms", J. Computational Physics, 20,(1976), 397-431.

Bridgman, C.J., Lecture Notes for AFIT Course NE 6.31, "Prompt Effects of Nuclear Weapons", Air Force Institute of Technology, Wright-Patterson Air Force Base, Ohio.

Brinkley, S.R., and Kirkwood, J.G., "Theory of the Propagation of Shock Waves", Phys. Review, 71 9, (1947), 606-611.

Courant, Friedrichs, and Lewy, "Uber die Partiellen Differenzengleichungen der Mathematischen Physik", Math. Ann., 100, (1928),32.

Doan, L.H., and Nickel, G.H., "A Subroutine for the Equation of State of Air", AFWL-TM-63-2, Air Force Weapons Laboratory, Kirtland Air Force Base, New Mexico, (1963).

Glasstone, S. and Dolan, P.J. (ed. s), The Effects of Nuclear Weapons (Third Edition), Dept. of Defense and Dept. of Energy, 1977.

Harlow, F.H., Amsden, A.A., "Fluid Dynamics", LA-4700, Los Alamos Scientific Laboratory, Los Alamos, New Mexico, (1971).

Hayes, W.D., "Self-Similar Strong Shocks in an Exponential Medium", J. Fluid Mech., 32, (1968a), 305-315.

Hayes, W.D., "The Propogation Upward of the Shock Wave from a Strong Explosion in the Atmosphere", J. Fluid Mech., 32, (1969b),317-332.

Laumbach, D.D., and Probstein, R.F., "A Point Explosion in a Cold Exponential Atmosphere", J. Fluid Mechanics, 35, 53-75.

Lax, P.D., and Wendroff, B., "System of Conservation", Comm. Pure Appl. Math., 13 (1960), 217-237.

Ledsham, F.C., and Pike, H.H.M., "The Effect of Atmosphere Varia-
tions on the Propagation of Blast Waves to High Altitudes", Re-
port No. 31/50, Armament Research Establishment, Fort Halstead,
Kent, England, January 1951.

Lutzky, M., and Lehto, D.L., "shock Propagation in Spherically
Symmertic Exponential Atmospheres", The Physics of Fluids, 11,
(1968), 1466-1472.

McNamara, W., Jordano, R.J., and Lewis, P.S., "Air Blast from a
One Kiloton Burst at 60 Meters Over an Ideal Surface", BRL-
CR-353, USA Ballistic Research Laboratory, Aberdeen Proving
Ground, Maryland, (1977).

Moulton, J.F., Ellis, P.A., Sachs, D.C., and Shahon, F.H., "Nu-
clear Weapons Blast Phenomena, Vol. I: Source and Development of
Blast Waves in Air", DASA-1200-1, Defense Atomic Support Agency,
1971. (S-RD)

Needham, C.E., Havens, M.L., and Knauth, C.S., "Nuclear Blast
Standard", AFWL-TR-73-55 (Rev), Air Force Weapons Laboratory,
Kirtland Air Force Base, New Mexico, (1975).

Richtmyer, R.D., and Morton, K.W., Difference Methods for
Initial-Value Problems (Second Edition), Interscience Publishers,
New York, 1967.

Roberts, K.V., and Weiss, N.O., "Convective Difference Schemes",
Math. Comp., 20 (1966), 272-299.

Sachdev, P.L., "Blast Wave Propagation in an Inhomogeneous Atmos-
phere", J. Fluid Mech., 50, (1971), 669-674.

Sachs, R.G., "The Dependence of Blast on Ambient Pressure and
Temperature", BRL Report 466, Ballistic Research Laboratory,
Aberdeen Proving Ground, Maryland, (1944).

Sedov, L.I., Similarity and Dimensional Methods in Mechanics,
Academic Press, 1959.

Sharp, A.L., and Dassow, W.R., "Systems Analysis Blast Environ-
ment Routine", AWFL-TR-70-85, Air Force Weapons Laboratory, Kirt-
land, New Mexico, (1970).

U.S. Standard Atmosphere, 1976, National Oceanic and Atmospheric
Adminstration, National Aeronautic and Space Adminstration, and
United States Air Force, Washington, D.C., October, 1976.

Von Neumann, J., and Richtmyer, R.D., "A Method for the Numerical
Calculation of Hydrodynamic Shocks", J. Appl. Phys., 21, (1950),
232-237.

Zel'dovich, Y.B., and Raizer, Y.P., Physics of Shock Waves and
High-Temeprature Hydrodynamic Phenomena, Vol. I:, Academic Press,
1966.

VITA

Michael Loyd Crawford was born ████████ ████████████████ ,
████████ He graduated from ████████████████████████████
████ ████████████████████████████████ . In 1973, he
received a Bachelor of Science degree with honors in Mechanical
Engineering as well as his commission as a distinguished graduate
of the Reserve Officer Training Corps. While on educational
delay from active duty, he completed his Master of Science degree
in Nuclear Engineering at the University of New Mexico. He entered
active duty in July 1975, and through May 1979 he was assigned to
the Air Force Weapons Laboratory's Technology Division (Space Nuclear
Power Branch) at Kirtland Air Force Base,NM. From June 1979 to
July 1982 he attended the resident School of Engineering at the Air
Force Institute of Technology at Wright-Patterson Air Force Base, OH.
He is presently an Instructor of Physics at the United States Air
Force Academy.